

PARTICLE INTERACTIONS IN COMPACT OBJECTS AND THE EARLY  
UNIVERSE

by

Faiz Khan, B.S.

THESIS

Presented to the Faculty of  
The University of Houston-Clear Lake  
In Partial Fulfillment  
Of the Requirements  
For the Degree

MASTER OF SCIENCE

in Physics

THE UNIVERSITY OF HOUSTON-CLEAR LAKE

DECEMBER, 2021

PARTICLE INTERACTIONS IN COMPACT OBJECTS AND THE EARLY  
UNIVERSE

by

Faiz Khan

APPROVED BY

---

Samina Masood, PhD, Chair

---

David Garrison, PhD, Member

---

Brandon Reddell, PhD, Member

APPROVED/RECEIVED BY THE COLLEGE OF SCIENCE AND ENGINEERING:

---

David Garrison, PhD, Associate Dean

---

Miguel A Gonzalez, PhD, Dean

## **Dedication**

This work is dedicated to my parents. Their undying love and support for me over the years has given me a well of strength to pull from; and allowed me to push through many moments of personal weakness that would have normally prevented me from achieving my goals. Without them this work would never have seen the light of day.

## Acknowledgments

I am most thankful and appreciative for the assistance of my advisor, Dr. Samina Masood, without which I would have surely been lost and meandering in the process of completing my thesis. Her guidance and approachability were a major factor in my ability to complete and comprehend the major ideas presented in this work.

Further, I would like to thank my committee, including Dr. Garrison and Dr. Reddell, for their willingness to listen and judge the quality of this work. I also would like to post-humorously acknowledge Dr. Mayes for his generous ability to converse and discuss topics not entirely in the scope of this work.

I would like to acknowledge the Physics department at University of Houston-Clear Lake for their support financially in various conferences, and Maria-Elena for her willingness and help in preparation for my thesis defense.

Finally, I would like to thank my parents and brother Yusuf, Emma, and my cats Lulu and Slate for their continual emotional support for me as I sculpted the document that sits before you today.

ABSTRACT  
PARTICLE INTERACTIONS IN COMPACT OBJECTS AND THE EARLY  
UNIVERSE

Faiz Khan

University of Houston-Clear Lake, 2021

Thesis Chair: Samina Masood, PhD

We show there is an effect of an extremely large magnetic field in highly dense media that has not been explored in prior work. We discuss the renormalizability of QED in such a medium. These extreme situations are found in the exotic environment of compact objects, especially neutron stars. It is found that the renormalization constants of QED are significantly modified in stellar media due to an additional  $B$  dependent term that appears due to the very high magnetic field in a highly dense star. The newly computed renormalization constants can be used as effective parameters of QED to study the particle processes in hot and dense stars with a strong magnetic field. We propose to use modified parameters to analyze astrophysical data and investigate the structure and composition of stars.

## TABLE OF CONTENTS

Chapter	Page
List of Tables . . . . .	viii
List of Figures . . . . .	ix
Introduction . . . . .	1
1. Stellar Dynamics . . . . .	4
1.1 Stellar Evolution . . . . .	4
1.2 Black Holes, White Dwarves and Neutron Stars . . . . .	8
1.2.1 Interior Structure of Neutron Stars . . . . .	9
1.3 Equations of State (EoS) . . . . .	15
1.3.1 Neutrinos and Stars . . . . .	17
1.3.2 Neutrino Emission via URCA/mURCA . . . . .	18
1.3.3 Constraints on the Equations of State . . . . .	19
1.3.4 Magnetars, Pulsars and Strange Quark Stars . . . . .	21
2. Mathematical Framework . . . . .	25
2.1 Introduction . . . . .	25
2.2 Phase Transitions and Distribution Functions . . . . .	26
2.2.1 Phase Transitions . . . . .	26
2.2.2 Distribution functions . . . . .	33
2.3 Lagrangian Formalism . . . . .	36
2.4 Quantum Field Theory . . . . .	39
2.4.1 Klein-Gordon equation . . . . .	39
2.4.2 Dirac equation . . . . .	41
2.4.3 Second Quantization . . . . .	42
2.4.4 Feynman Diagrams, Rules and Probabilities in QFT . . . . .	43
2.4.5 Renormalization . . . . .	46
3. Finite-Temperature Field Theory . . . . .	50
3.1 Finite Temperature and Density Statistical Corrections . . . . .	50
3.2 Real and Imaginary time propagators . . . . .	52
3.3 Electron Self-Energy and FTD Renormalization . . . . .	54
3.4 Incorporation of density effects . . . . .	60
3.5 Calculating $J_A$ . . . . .	65
3.5.1 Calculating $J_B$ and $J_B^0/E$ . . . . .	66
3.6 Renormalization at FTD with magnetic field B . . . . .	67

4. Calculation of Magnetic Field Contribution . . . . .	70
4.1 Electron mass in presence of magnetic field . . . . .	70
4.1.1 Taylor expansion of Masood's functions . . . . .	73
4.2 Evaluation at Limits . . . . .	74
4.2.1 Renormalization Constants . . . . .	76
4.3 Renormalization Constants for Various B Ranges . . . . .	77
4.4 Calculation of QED Renormalization Constants . . . . .	81
4.5 Results and Discussions . . . . .	85
4.6 Applications, Future Work and Conclusions . . . . .	95

LIST OF TABLES

Table	Page
2.1 Feynman rules for QED. . . . .	45

## LIST OF FIGURES

Figure	Page
1.1 Protostar evolution into zero-age main sequence (ZAMS) stars, 1 (left) and 60 solar masses (right). The time evolution begins on the right, as compression intensifies the protostar approximates the ZAMS lifecycle curve. Kippenhahn et al. [27] . . . . .	5
1.2 The amount of energy obtained from the burning of hydrogen in a zero-age main sequence star from the center of the star ( $m/M$ ). The left is the energy production at the core. The dot-dash line is a ZAMS star, dashed at $6.2 \times 10^9$ years, dotted at $8.2 \times 10^9$ years and $11.2 \times 10^9$ years for the solid line. Kippenhahn et al. [27] . . . . .	6
1.3 An Hertzsprung-Russell (HR) diagram that shows the typical evolution of a zero age main sequence star. We graph the temperature versus relative luminosity. A hotter star implies more nuclear fusion is occurring in the core. Kippenhahn et al. [27] . . . . .	7
1.4 Diagram that shows the interior structure of a neutron star. This diagram shows the interior contains several layers of varying intensity, the outer envelope, inner crust and so on. The interior structure of stars has implications regarding a stars dynamics and equation of state. Image taken from Haensel et al. [24] . . . . .	10
1.5 An equation of state graphed against exact values for the density versus pressure for a degenerate electron gas Haensel et al. [24] . . . . .	12
1.6 Graphs of density in relation to the center of a neutron star for different equations of state. The result shown here was obtained from the computational analysis and subsequent paper of Alvarez-Salazar [4].	16
1.7 Convergence of the Hulse-Taylor pulsar mass over time. The error bars are at the $2\sigma$ confidence interval. Notice that the bars virtually disappear around the year 2000. . . . .	20
1.8 An image of the Neutron star Interior Composition Explorer (NICER) Source: NASA . . . . .	21
2.1 Arrangement of N molecules in a 1-D lattice, otherwise known as an Ising chain. Image from Pathria Beale [5] . . . . .	28
2.2 Graph of Maxwell-Boltzmann distribution. Huang [25] . . . . .	33
2.3 Average number of particles per energy level in a Fermi-Dirac distribution. Huang [25] . . . . .	35
2.4 Average number of particles per energy level compared amongst all three distributions. Creative Commons . . . . .	36

2.5	Vacuum polarization Feynman diagram describing one loop self-interactions in QED. . . . .	45
2.6	A number of possible Feynman diagrams generated from the electron propagator at one loop. . . . .	47
3.1	Electron self-energy. Peskin and Schroeder [41] . . . . .	55
4.1	Renormalization constant $\delta m/m$ compared when (B=1.00E+14 T) $eB/m \gg m$ and (B=1.00E+10 T) $eB/m \sim m$ in the limit $\mu > T$ . In the $eB/m \sim m$ case there is a negligible change and the two graphs are overlaid thus B has almost no effect on electron mass. . . . .	89
4.2	Renormalization constant $\delta m/m$ compared when (B=1.00E+14 T) $eB/m \gg m$ and (B=1.00E+10 T) $eB/m \sim m$ in the limit $\mu > T$ . We graph chemical potential versus temperature versus the value of $\delta m/m$ . We observe a virtually identical result as in Figure 4.1. There is a negligible change for a typical neutron star magnetic field (B=1.00E+10 T) and the two graphs are overlaid thus B has almost no effect on electron mass. . . . .	90
4.3	Masood's abc functions compared when (B=1.00E+10 T) $eB/m \sim m$ in the limit $T > m$ . The functions <b>a</b> and <b>c</b> show almost no change, while <b>b</b> does change a small amount, by comparison. . . . .	91
4.4	Renormalization constants compared when (B=1.00E+10 T) $eB/m \sim m$ . In these graphs, there is a negligible change and the two graphs are virtually identical, and overlaid, in the limit $T > m$ . . . . .	92
4.5	Masood's abc functions compared when (B=1.00E+14 T) $eB/m \gg m$ in the limit $T > m$ . Compared with Figure 4.3, we see dramatic changes due to the magnetic field, and the contribution of all functions is reduced in this magnetic field. . . . .	93
4.6	Renormalization constants compared when (B=1.00E+14 T) $eB/m \gg m$ in the limit $T > m$ . Compared with Figure 4.4 we see dramatic differences as the high magnetic field reduces the renormalization constants $Z_2^{-1}$ and $Z_3$ while increasing $\delta m/m$ . . . . .	94

## INTRODUCTION

Since the dawn of time, humans have been fascinated and inspired by the movement of the heavens [17]. The amount of information coming from astrophysical phenomenon often leads us into a reformulation of our assumptions and knowledge to match the observations. This continues to be a source of inspiration for scientists. The nature of theory building is such that we can make a prediction about physical evolution, and then later build experiments in order to test and obtain proof for theoretical results. Scientifically, the interest we wish to demonstrate here is the unreasonable effectiveness of making predictions based on known data, in order to bring our understanding and theory building into the present environment.

Throughout this work stellar objects are treated essentially as laboratories [42]. Our goal is to predict and elaborate on the composition of stellar objects and explain how observations can eventually influence our theories. This is especially due to the limitations of working with such extremes on Earth. In many cases, the instruments that are within our engineering capacity on the planet are vastly more primitive in energy scales than what we can already find in nature. We briefly review the idea of compact stellar objects, our research interest in them and what we can gain from making predictions about these relatively unknown masses in the sky. With appropriate data we can generalize and make conclusions about observations that inform our future theories. Primarily our aim is to understand the interior regions of superdense stars with high magnetic fields.

Compact stellar objects such as black holes, neutron stars, white dwarfs and related stellar entities are those that have high mass relative to their total radius or the area and volume swept out by this radius, essentially equating them as extremely dense conglomerations of matter. With respect to a general understanding, these

entities are the remnants of stellar evolution, and found at the end of a regular star lifecycle. This provides a justification that the gravitational pressure exceeds the internal pressure from thermonuclear reactions causing a collapse of the stellar material into a very small area. This collapse causes stellar interiors to have very high temperature and density. Degeneracy pressure from nuclei is what sustains the radius of neutron stars and white dwarfs [50]. In the case of neutron stars, they are theorized to have a highly magnetic interior core, which has not been studied in the context of particle propagation.

This may seem archaic at first glance, but it is absolutely relevant to our discussion. At a broad generalization, we must probe physics at the fringe of our understanding to develop more accurate theories.

The interiors of these stars have a great deal of scientific value in the form of theory. Knowing the dynamics of compact stars, we can safely admit that we understand particle behavior at an extreme place in the universe. For example, particle accelerators are specified and built every 30 to 50 years [21] in hopes of achieving greater and greater energies in the cross-section or collision area between particles. Given there already exists a laboratory in the early universe that contains these particle interactions, and there are measurements we are able to make about this laboratory, it makes sense that we might look to the skies in order to understand more of our world from what we see in the sky.

Specifically, the compressed nature of these objects implies that all four of the fundamental interactions are at work within the interiors of these stars. The energies involved in the interactions, as this is a stellar remnant, means not only are they energies frankly unattainable on Earth but also so enormous as to possibly giving us clues regarding the state of the early universe and unified theories of interaction as

well. This, predominantly, is our motivation for researching this particular extreme of the stars.

We will find that, with the help of our high powered telescopes located on Earth and in orbit, we know a few properties of compact stellar objects, such as luminosity, temperature, and the magnetic field at the surface. It is our job as scientists to make predictions about what we cannot yet observe, such as the interior properties, in order to better understand the nature of how these objects form and evolve over time. We note that our understanding of these objects is still limited, due to our ability to obtain observations or having a dearth of scientific equipment readily available to observe their properties. For this reason it is instructive to develop theories of interior dynamics based on current findings in the hope that future observations will readily verify theoretical results.

We show that the temperature, chemical potential and strong magnetic field of a star have a significant effect on the properties of propagating particles in the star. We utilize finite temperature field theory (FTD) in order to develop an understanding of renormalization constants in such extreme media. Simulations are run to suggest that not only is this change significant but may explain future observations of compact objects that report very high magnetic fields, such as neutron stars [12]. We discuss first the dynamics of stars in Chapter 1. After the introduction of mathematical techniques of phase transitions, statistical mechanics and quantum field theories in Chapter 2, we discuss the finite temperature and density formalism in Chapter 3, and then the renormalization of quantum electrodynamics in this formalism. In Chapter 4 we calculate the effect of magnetic fields on quantum electrodynamics parameters and then study the application of these results in compact stars.

# CHAPTER 1

## STELLAR DYNAMICS

### 1.1 Stellar Evolution

There is not much that can be discussed about compact objects without a description of stellar evolution, which can give us an understanding of how these objects start and end up in the state they are in.

According to Kippenhahn et al. [27], an initially homogeneous compressible gas larger than the Jeans instability radius is gravitationally unstable. The Jeans instability is a change away from equilibrium of internal gas pressure and gravitational forces of the stellar material, such that a gravitational collapse occurs. At these scales the gas is modeled as free-fall collapse of a homogeneous sphere, a classical calculation. This results in a hydrostatic core which is externally buffered by a still-collapsing region. As temperature and pressure continue to increase in the core of the gas, the hydrostatic core becomes unstable and the core itself begins to collapse. This generally is when the gas cloud is referred to as a protostar, with a large reduction in radius and increase in temperature.

If the star has not yet reached the temperature for nuclear reactions, collapse continues in the core until nuclear reactions dominate. This protostar then eventually undergoes nucleosynthesis and is called a zero-age main sequence star (ZAMS), and the Carbon-Nitrogen-Oxygen (CNO) and proton-proton (p-p) chain reactions (ppI, ppII, ppIII) follow in this environment.

The proton-proton or PP chain is a reaction between hydrogen atoms (protons) into deuterium and then a following reaction where the deuterium reacts with another hydrogen atom to form helium and some energy released as a photon. Originally

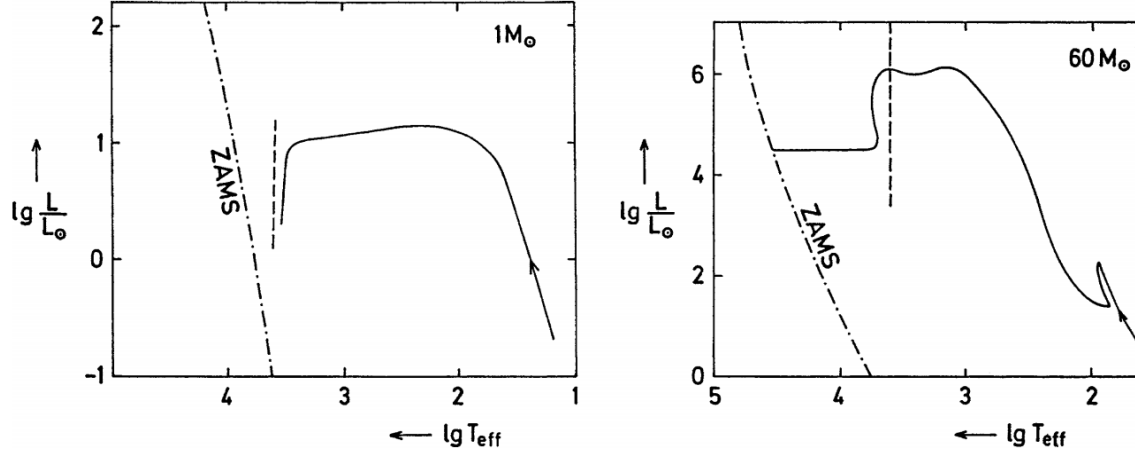


**Figure 1.1.** Protostar evolution into zero-age main sequence (ZAMS) stars, 1 (left) and 60 solar masses (right). The time evolution begins on the right, as compression intensifies the protostar approximates the ZAMS lifecycle curve. Kippenhahn et al. [27]

calculated by Hans Bethe in 1939, he won the Nobel Prize for his discovery of the ppII branch that one of the foundational reactions in the processes underlying stellar nucleosynthesis [7] [8].



The processes called pp1, pp2, pp3 generate other isotopes of helium and further energy in the form of neutrinos and photons.

The CNO cycle is the other dominant process in stars, that have different by-products but release varying amounts of energy. The kinds of processes occurring in stars can be determined from the observed energy spectrum. Generally this will result in the PP chain being a regular process at lower temperatures ( $T \sim 10^7 K$ ) and the CNO cycle being the more widespread process up to the order of  $T \sim 10^7 K$ . While we have covered hydrogen burning reactions, it is worth noting that both carbon burning and helium burning also contribute to the energy, however it is not pertinent to our

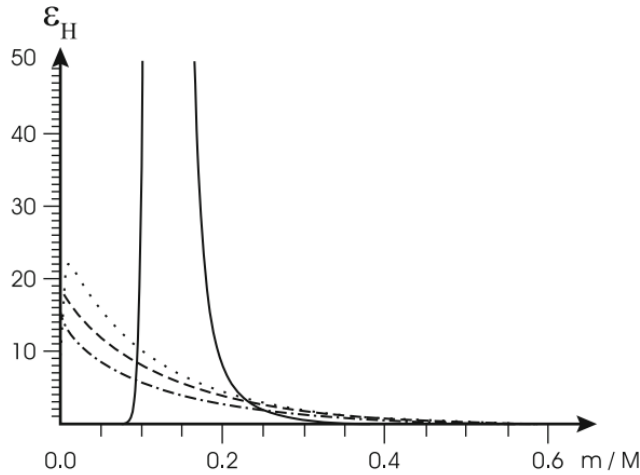


**Figure 1.2.** The amount of energy obtained from the burning of hydrogen in a zero-age main sequence star from the center of the star ( $m/M$ ). The left is the energy production at the core. The dot-dash line is a ZAMS star, dashed at  $6.2 \times 10^9$  years, dotted at  $8.2 \times 10^9$  years and  $11.2 \times 10^9$  years for the solid line. Kippenhahn et al. [27]

work. The dynamics of a main sequence star generally occur from the loss of hydrogen as the various burning processes take place in the star. The energy generation changes as less hydrogen is available over time, and with it the mass and radius of the star.

An HR diagram (Hertzsprung-Russell) [45] can very clearly show the evolution of a star. A star's luminosity is graphed against its surface temperature, based on observations. As more hydrogen is consumed the star becomes brighter, thus the HR diagram also serves as a window into understanding the stellar evolution of stars. The main sequence line on an HR diagram allows us to estimate where a star is in its lifecycle.

Further burn cycles are completed for helium, carbon, oxygen and other by-products of hydrogen burning processes in a cyclical way until our understanding is dominated entirely by computer models of stellar evolution and observation instead of theory. Computer models suggest that as heavy elements build up in the

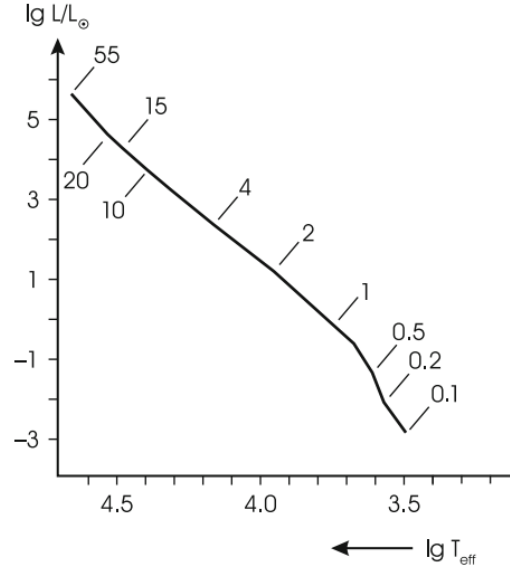


**Figure 1.3.** An Hertzsprung-Russell (HR) diagram that shows the typical evolution of a zero age main sequence star. We graph the temperature versus relative luminosity. A hotter star implies more nuclear fusion is occurring in the core. Kippenhahn et al. [27]

core, electron capture occurs and the heavy elemental core contracts. Stellar evolution allows stars to move from the main sequence by affecting size, and density. The chains of thermonuclear reactions and heavy element production are related to the density of matter under pressure. Neutrinos that are opaque to the outer shell begin to add pressure resulting in a supernova explosion which can cause the star to explode, leaving behind a black hole or a compact object such as a neutron star.

From this we should begin to understand why and how it is important to study stellar objects, and not only that but how it leads us to more accurate, physical theories. Our specific goals imply that we want to study how various properties change, such as charge or mass, as well as the properties of propagating particles in the interior of the star, in order to better apply our findings and our understanding of the lifecycle of stars.

## 1.2 Black Holes, White Dwarves and Neutron Stars

White dwarves are one of the end products of main sequence stars with masses of the order of our Sun and radii of the order of the Earth. They are made of electrons that exert a degeneracy pressure from the Pauli exclusion principle, which states that no particles with half-integer spin can occupy the same quantum state, in order to maintain their size, and radiate energy left over from the supernova that created it.

Since white dwarves are supported by the pressure of electrons obeying the Pauli exclusion principle, Chandrasekhar was able to obtain a mass-radius relationship by solving an hydrostatic equation using a white dwarf equation of state and show that a very specific limit exists, later named after Chandrasekhar himself. The Chandrasekhar limit,  $M_{Ch} \leq 1.4M_{\odot}$  [13] is an important discovery in the study of compact objects. It is the theoretical limit of the mass of a white dwarf that, when exceeded, can result in gravitational instability leading to a collapse into a black hole or neutron star. The exact equation for the Chandrasekhar limit was originally derived by Subrahmanyan Chandrasekhar in 1930 and is given by [13]

$$M_{Ch} = 2.018 \frac{\sqrt{6}}{8\pi} \left( \frac{hc}{G} \right)^{3/2} \frac{1}{m_H^2 m_w^2} \quad (1.3)$$

Where  $G$  is the gravitational constant,  $m_H$  is the hydrogen mass,  $h$  is the Planck constant,  $c$  is the speed of light, and  $m_w$  is the average mass of the star in units of electron mass.

Both neutron stars and white dwarves can become unstable if they accrete too much mass due to the Chandrasekhar limit, and when this happens the gravitational energy increases. General relativity tells us this can sustain itself cyclically such that at some point the cycle is inverted and nothing can escape the area inside a region called the Schwartzchild radius [50]. These are called black holes. Black holes can also produce relativistic jets as matter accretes [37] around the Schwartzchild radius

and "falls" inwards. As the matter falls into the black hole, it loses energy in the form of high energy particles. Black holes have enormous masses several times larger than the mass of our sun generally.

Neutron stars were proposed initially by Lev Landau in 1932 (although there is some debate [55] on those records), anticipating their existence as a transition from a main sequence star to a neutron-dominant star through a supernova explosion. Generally neutron stars are of the order of the solar mass,  $M_{\odot}$  where the mass is compressed into a sphere of radius around 10km, which is little more than 6 miles. This is an extreme level of compression and density, which provides physicists with an enormous opportunity experimentally and theoretically to understand the physics of these extremely compact objects. We intend to treat neutron stars as our stellar laboratories for the duration of the work for the reasons outlined above. As mentioned, neutron stars are created during stellar evolution, normally at the end of several stages of stellar collapse [10] [8]. Similar to white dwarves, degeneracy pressure from neutrons is the pressure that sustains the structure of the star. Generally, neutron stars are considered to be structured in four layers and an atmosphere, which do not have clear boundaries but rather blend into one another. The exact density profile, that is, the composition and ratios of particles in the core of neutron stars, is currently unknown. Despite this, there are still theoretical models that have been proposed, one of them is shown in Figure 1.4, from Haensel et al.

### **1.2.1 Interior Structure of Neutron Stars**

While the nucleons of a neutron star come from iron imparted to the star in the supernova explosion, the atmosphere of a neutron star is composed of a plasma envelope [24]. With a surface temperature of  $\approx 10^6 K$ , the structure of a neutron star

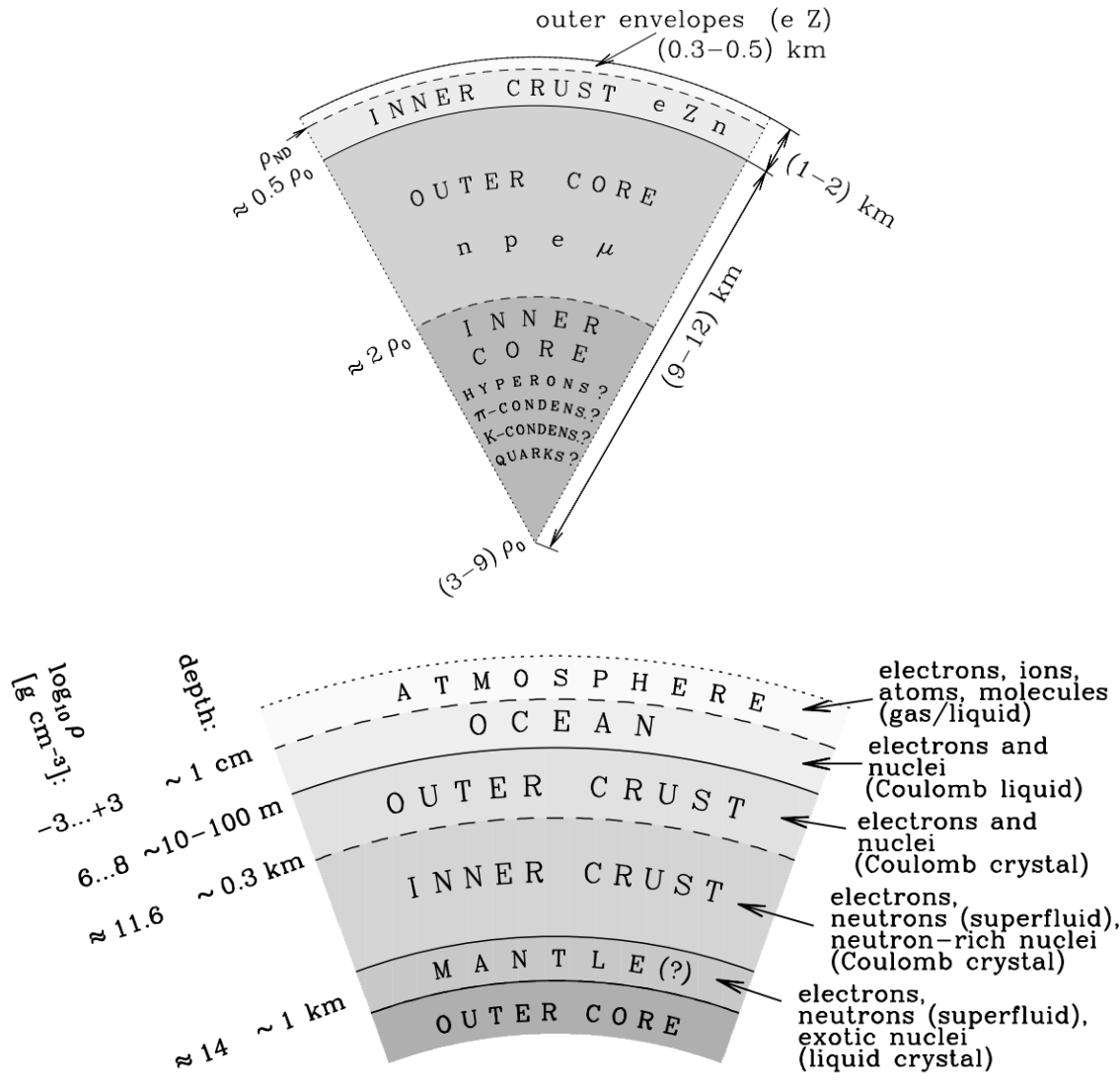


**Figure 1.4.** Diagram that shows the interior structure of a neutron star. This diagram shows the interior contains several layers of varying intensity, the outer envelope, inner crust and so on. The interior structure of stars has implications regarding a stars dynamics and equation of state. Image taken from Haensel et al. [24]

envelope is expected to have layers in depth and density as shown in Figure 1.4, beneath which are the outer and inner crusts of the star. A plasma is considered as a fluid where a major fraction of the fluid is ionized and the electrons are free in the mixture. This normally happens when a sufficient temperature is reached, considering a regular example of excessive heating of a fluid in a tube. Plasma is also considered an additional phase of matter apart from solid, liquid and gas, due to its high conductivity and peculiar interactions with electromagnetic fields.

One of the key functions of this outer envelope is thermal insulation, which can be modified in the presence of a strong magnetic field greater than  $10^{11}$  Gauss. An electron-positron plasma has a phase which is used to calculate properties of the material, such as baryon number density, Coulomb interaction strength, and polarization  $\epsilon$  of the gas. The ions that compose the envelope are non-relativistic in the atmosphere. So, according to plasma physics we treat this layer as a fully ionized dense plasma [24]. The pressure of this gas can be shown to be responsible through the effect of electron degeneracy pressure.

Relativistic electrons in thermodynamic equilibrium are described using Fermi-Dirac statistics

$$f(E - \mu_e, T) = \frac{1}{\exp((E - \mu_e)/kT) + 1} \quad (1.4)$$

$$= \sum_{n=0}^{\infty} (-1)^n \exp\{-n\beta(E - \mu_e)\} \quad (1.5)$$

while they are moving with relativistic energies. Here and throughout this work,  $\beta = 1/kT$ . The number density can then be computed by integrating over phase

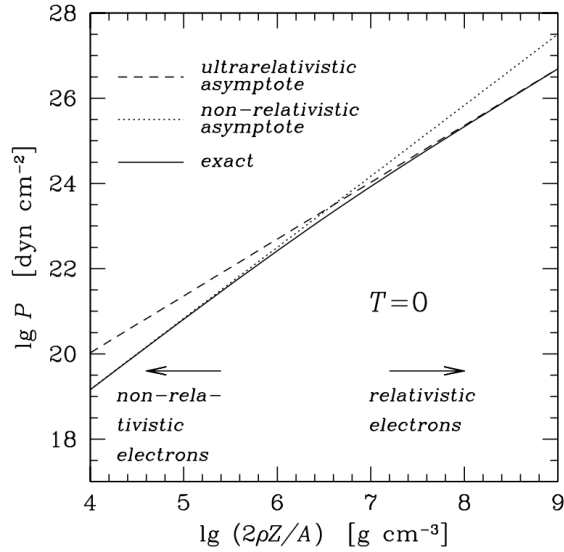


**Figure 1.5.** An equation of state graphed against exact values for the density versus pressure for a degenerate electron gas Haensel et al. [24]

space

$$n_e = 2 \int f(E - \mu_e, T) \frac{d^3p}{(2\pi)^3} \quad (1.6)$$

$$= 2 \int \sum_{n=0}^{\infty} (-1)^n \exp\{-n\beta(E - \mu_e)\} \frac{d^3p}{(2\pi)^3} \quad (1.7)$$

For strongly degenerate electron gases an accurate approximation for the pressure can be found by setting  $T=0$ , and the description for white dwarves and neutron star envelopes can be regarded as being dominated by the effects of strongly degenerate matter, as can be seen in Figure 1.5. For ultra relativistic and non-relativistic limits the pressure is given by [24]

$$P = K\rho^{1+1/n} \quad (1.8)$$

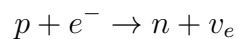
where  $K$  is a constant and  $n$  is the polytropic index,  $n = (1 - \gamma)K + \gamma$ , where  $\gamma$  is the ratio of heat capacities at constant volume and constant pressure. This is also the equation of state plotted in Figure 1.5. While there are intermediate areas of

the plasma where the density is far less than the fully dense case, computational techniques have allowed for the interpolation of the dense equation of state in order to predict the effects and properties of the plasma at lower densities.

The outer crust is an area where heavy elements are found, normally expected in a structure resembling a crystal or lattice. The equation of state is based on a pure neutron gas at very high density. Neutron drip, where a structure of heavy nuclei is disfavored over a neutron superfluid is between the inner and outer crusts. Further than that we expect the superfluid to be dominating the interior structure, and many equations of state and neutron star models have hypothesized what could lie at the innermost core of the star [11].

Neutron drip is an important concept as we move closer to the core, as mentioned [11]. In general, when a particle process between nuclei such as protons and neutrons take place, energy is either required or released in order for the reaction to be energetically viable. There are certain combination numbers of nucleons (that is, neutrons and protons) that when another nucleon is acquired, it immediately decays. The number of nucleons required before such a spontaneous emission occurs is called either the neutron or proton drip line. This "drip line" is a boundary where immediate emission of a proton or neutron takes place, in some sense the limit of stability of an atomic nucleus to take on another proton or neutron.

In neutron star cores, this becomes important, as the process of inverse beta decay takes hold and relativistic electrons combine with protons to produce a neutron and electron antineutrino



If this process did not occur, nuclei would get infinitely large, however, due to strong Coulomb interactions between nuclei, fission occurs at a mass number  $A=56$  (total

number of protons and neutrons) [50]. Because of relativistic electrons and inverse beta decay, more neutrons exist than protons in these nuclei and the strong Coulomb interactions play less of a role (due to the lack of charge). At a critical density where Coulomb interactions become less dominant due to the neutron to proton ratio,  $\sim 4 \times 10^{11} g cm^{-3}$ , neutron drip occurs and neutrons leak out of the nuclei due to instability of the particle interaction [50]. This causes free neutrons to exist with electrons and nuclei as we move closer to the center, and the pressure of the system at higher density occurs from these neutrons obtaining their lowest energy level from the Pauli exclusion principle.

### 1.2.1.1 Superfluidity

Superfluidity is a quantum phenomena that occurs in fluids causing them to have frictionless flow. This can result in infinitely rotating vortices in the fluid and generally complex quantum behavior. Regarding superfluids, due to the energies involved in neutron star interiors, neutrons and protons exist in a superfluid state as mentioned. This can lead to some interesting physical phenomena such as neutron vortices which can affect for example, pulsar timing and indeed may be an explanation for pulsar glitches. Superconductivity, where fermions carry electric current with little to no resistivity under a critical temperature is also a phenomena related to superfluidity.

Near neutron drip we find that the fluid of free electrons forms into a superfluid by forming Cooper pairs [49]. Since the total spin of a Cooper pair is 0 or 1, and integral, the Pauli Exclusion principle need not be obeyed and the system becomes bosonic. The neutron pairs that condense into the ground state is what composes the superfluid in the neutron star [11] [44]. In this state quantum hydrodynamics must be used in order to understand the dynamics of the vortices produced. Quantum hydrodynamics is the study of quantum systems using an alternative formulation of

Schrodinger's equation, using hydrodynamic quantities such as flow velocity and mass density. Further complexifying the issue is the possibility of strong magnetic fields. At this stage we will defer to the existing literature [44] [38] [39] which includes a detailed discussion of magnetohydrodynamics for those interested, as the area is a very interesting area of research however not especially pertinent to our discussion.

### 1.3 Equations of State (EoS)

There is a lot of theoretical work in search of correct equations of state for compact objects. An accurate equation of state can yield a mass-radius relation using general relativity. We use equations of state in order to understand the relationship between density and pressure inside white dwarves and neutron stars. These equations of state are guided by experiment but are developed theoretically. One of the first studies in this direction was the derivation of the equation of hydrostatic equilibrium for a neutron star by Tolman, Oppenheimer and Volkoff [40]. After this research headed towards finding an EoS for dense nuclear matter that included nuclear and baryonic interactions, with an eye towards different possibilities such as the case of neutron stars that are composed of different phases of nuclear matter.

Since there is some uncertainty in the density profiles of neutron stars, it allows researchers to speculate on possible physical processes taking place inside neutron stars, which is discussed by Alvarez-Salazar and Quimbay [4]. Alvarez-Salazar et al. analyzed various density profiles from different equations of state and applied cooling models in order to better understand the physical processes going on inside the stars. Specifically, they numerically calculated the neutrino and photon luminosities based on cooling models, compared them to experiment and drew conclusions about the dominant processes in neutron stars.

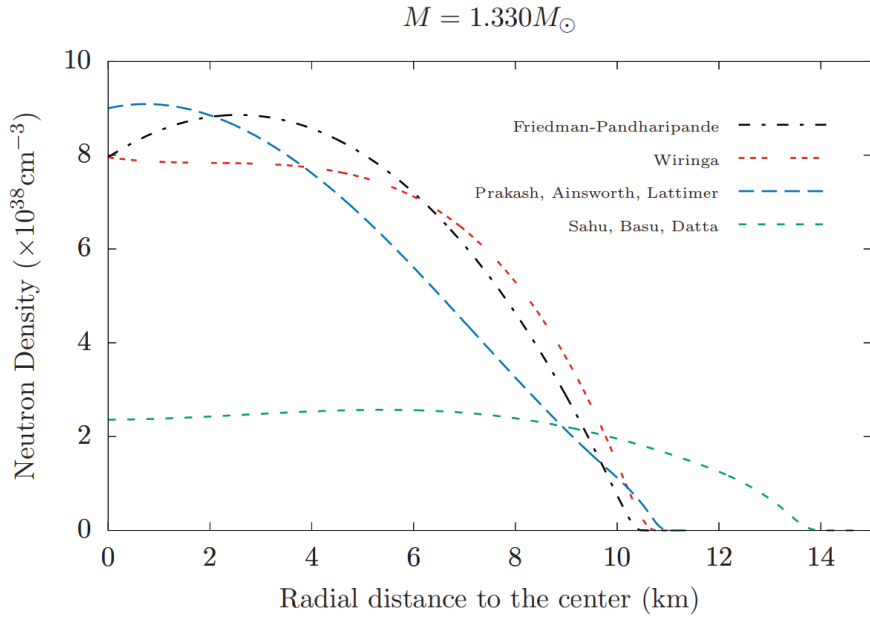
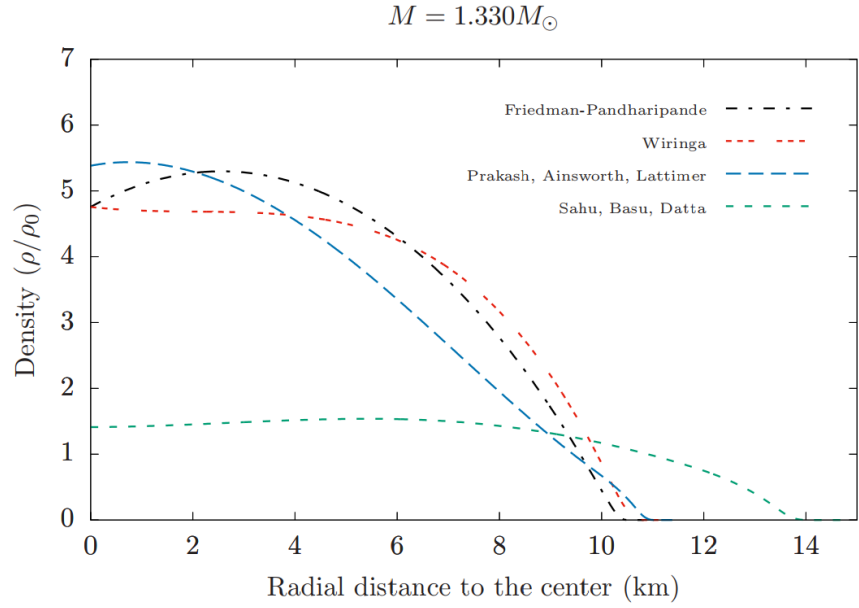


**Figure 1.6.** Graphs of density in relation to the center of a neutron star for different equations of state. The result shown here was obtained from the computational analysis and subsequent paper of Alvarez-Salazar [4].

### 1.3.1 Neutrinos and Stars

In the 1930s, Wolfgang Pauli postulated that a massless particle needed to exist to conserve lepton number and momentum, he called it the "neutrino". Hans Bethe had theorized that neutrinos were produced in the Sun during their thermonuclear reactions. The Homestake experiment in the 1960s really was the first to give birth to neutrino astronomy and of course detect neutrinos from the Sun as well. This in turn allowed for scientists to determine the specifics of fusion processes which in turn allowed major developments in stellar evolution theory to occur. The observed neutrinos during experiment differed by a significant fraction, and to account for this explanation of neutrino oscillation was proposed.

In beta decay, neutral fermionic particles called neutrinos are needed to conserve lepton number, momentum and energy. While originally proposed as massless, we now understand neutrinos have a small nonzero mass. Additionally, neutrinos come in three flavors, or species, the electron neutrino, muon neutrino and tau neutrino. It is also known that neutrinos created with a specific flavor may oscillate or transform into another flavor spontaneously. Neutrinos have antiparticles called antineutrinos, which are the right-handed chirality partners in the electroweak theory of the regular neutrinos, which are left-handed massless neutrinos. Neutrinos interact with the weak interaction only and belong to a class of particles called lepton.

Neutrino oscillation is the process that allows for one flavor of neutrino to change into another mid-flight, and there is currently much research focused on this phenomena. Despite there being a suitable explanation for this discrepancy, it cannot be accommodated in the standard electroweak model of particle physics described as  $SU(2) \times U(1)$ , and thus extensions have been proposed to the Standard Model in order to find a way to converge experiment with theory. Since neutrinos do not

interact strongly with matter or the electromagnetic field, they give us a large amount of information of the source, and where to find large concentrations of high energy particles.

### 1.3.2 Neutrino Emission via URCA/mURCA

It is well established that after a supernova explosion and during the birth of a neutron star, very quickly a neutron star will cool through the emission of neutrinos that are produced in the star by various leptonic processes and nuclear reactions.

The neutrino emission processes depend on the composition and location in the star, but generally  $e^-e^+$  annihilation, plasmon decay and electron synchrotron all contribute to the neutron star cooling from neutrino emission [22]. There are two major types of cooling scenarios for neutron stars, enhanced and standard scenarios. For each, there is a respective Urca process that is theorized as the main source of energy loss, the Modified Urca (MUrca) and direct Urca (DUrca) processes. In the neutron star core, the Urca reactions are considered to be much more dominant in terms of emissivity than on the crust. The Urca reaction proceeds by the semi-leptonic decays or scattering processes caused by the weak decay are,

$$\mathcal{B}_1 \rightarrow \mathcal{B}_2 + e^- + \bar{\nu}_e \quad (1.9)$$

$$\mathcal{B}_2 + e^- \rightarrow \mathcal{B}_1 + \nu_e \quad (1.10)$$

where  $\mathcal{B}_1$  and  $\mathcal{B}_2$  are baryons (usually neutrons or protons),  $e^-$  the electron and  $\nu_e$  the electron-neutrino, corresponding to beta decay and is the most common process in the case of the neutron star. This is a charged weak current interaction [44]. There

is another important reaction called the modified Urca process

$$\mathcal{B}_1 + \mathcal{C} \rightarrow \mathcal{B}_2 + \mathcal{C} + e^- + \bar{\nu}_e \quad (1.11)$$

$$\mathcal{B}_2 + \mathcal{C} + e^- \rightarrow \mathcal{B}_1 + \mathcal{C} + \nu_e \quad (1.12)$$

As the process involves the neutrino, this is a weak interaction process, as the neutrino only interacts weakly. The weak interaction in general is involved in nuclear decay processes, and the range of the weak force is generally limited to subatomic distances less than the diameter of a proton. Particles that obey the Pauli exclusion principle such as electrons and neutrinos are involved in the weak interaction and exchange force-carrying intermediate vector bosons, the charged W and neutral Z particles. The W boson is involved in charged current interactions and the Z boson is involved in neutral current interactions [46]. The modified Urca process is not a higher order process but one that becomes dominant in stars with lower densities, specifically in superfluid outer crusts. Both reactions radiate energy away from the star via neutrino emission. Density profiles are used to numerically estimate various properties of the neutron star and neutrino emissivities.

Similarly, while we know neutrinos play a role in cooling, we do not know the exact matter composition and thermodynamic properties of neutron stars, which is why equations of state are needed to express the relationship between pressure and density. Neutrino emissivity needs to be calculated for each equation of state for every region, so techniques needed to be developed in order to estimate the amount of cooling based on possible emissivity rates.

### 1.3.3 Constraints on the Equations of State

Due to the nearly unlimited theoretical models that can be constructed, the very fundamental way to construct valid equations of state is by using observational state

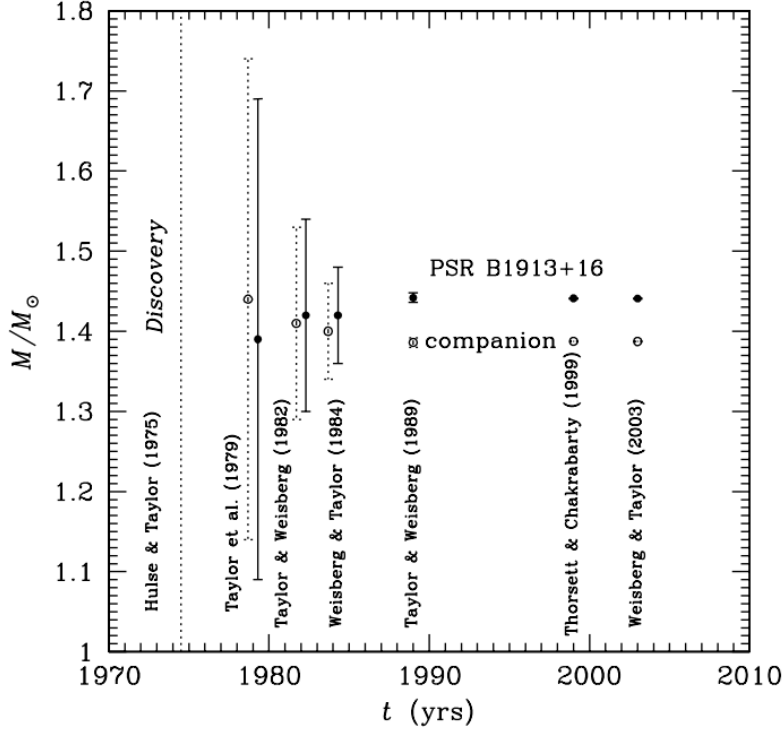


**Figure 1.7.** Convergence of the Hulse-Taylor pulsar mass over time. The error bars are at the  $2\sigma$  confidence interval. Notice that the bars virtually disappear around the year 2000.

from various methods [36]. Most of the techniques employed today are focused on reducing the uncertainty in the mass and radius of neutron stars, otherwise known as the mass-radius relation.

In a binary system such as a neutron star and white dwarf binary, we can obtain accurate results for the masses due to general relativity. The effect from the star spinning is also incorporated if one of the stars is a pulsar for even greater accuracy.

For isolated neutron stars thermal emission from X-rays remains the best way to determine the radii of neutron stars. NICER, the Neutron star Interior Composition Explorer, is a NASA project that seeks to generate precision measurements of neutron stars, in order to put limits on their mass and radii. The project determines the size of a star using X-ray timing and lightcurve analysis, as well as X-ray beam properties.

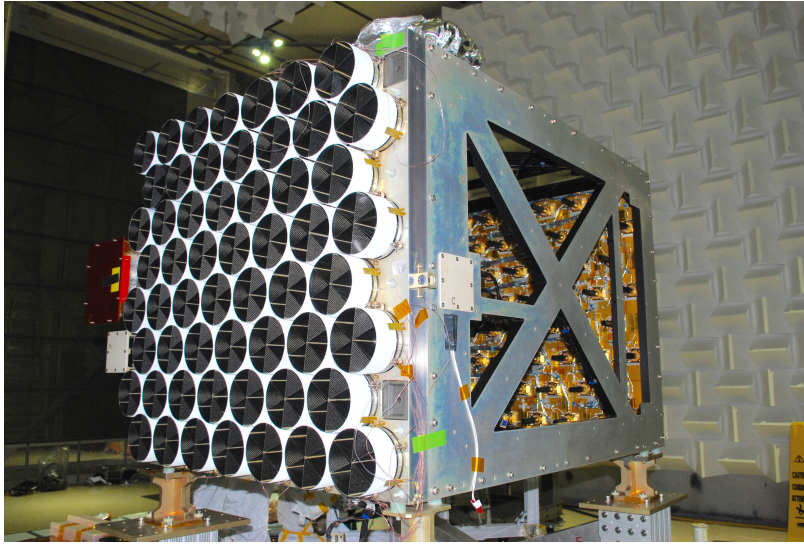


**Figure 1.8.** An image of the Neutron star Interior Composition Explorer (NICER)  
Source: NASA

This method is more complicated than using a neutron star in a binary, but it remains possible using computational techniques to infer the mass-radius relation.

In addition to the above equations of state are constrained by observation of short and long pulsar timing, including submillisecond pulsars, the observation of burst neutrinos from Supernova 1987A and pulsar glitches, which are long and short disturbances in pulsar timing.

### 1.3.4 Magnetars, Pulsars and Strange Quark Stars

Pulsars are rotating neutron stars that give off electromagnetic signals at timed intervals, detected first in 1967 and originally predicted to exist in the 1930s. Depending on the type of radiation, pulsars may emit radio, X-ray or gamma rays. Due to the complex interactions in the atmospheric plasma, a magnetosphere that is present above the atmosphere can produce and emit electromagnetic radiation as particles from the underlying plasma are accelerated in the magnetic fields. This is thought to

be the mechanism of the electromagnetic emissions from at least some type of pulsars. Most known neutron stars are radio pulsars [24], and radiowave emission from these stars are captured by radio telescopes with high precision allowing a pulsar's period to be established with very high accuracy.

As discussed, the atmospheric plasma allows for rich dynamics of the magnetosphere to take place. Generally these surface fields are strong, on the order of (on the surface)  $10^{11} - 10^{13}$  Gauss. Magnetars are neutron stars with a super-strong rotating magnetic field on the order of  $B \sim 10^{14} - 10^{15}$  Gauss. Currently, not too much is known about the cause of these neutron stars with super-strong magnetic fields, but observations have linked X-ray pulsars that are not in a binary system to neutron stars that emit irregular short gamma ray bursts (soft gamma repeaters, or SGRs) as potentially the same class of object as their magnetic fields should be of the same order of magnitude [24].

A theorized type of compact star called a Quark star has been proposed as a possible end product of stellar evolution as well. In general, quarks are a fundamental, bound particle combined to form composite particles such as protons and neutrons, which are considered very stable, as baryonic matter is part of the everyday experience. For example, the neutron has a lifetime around 10 minutes, and the possibility of proton decay is still under theoretical investigation. The neutron and proton consist of up and down quarks, however there are other quarks such as the strange, charm, top and bottom quark that compose other, relatively unstable particles. As discussed, after neutron star cores have been under sufficient pressure, the individual neutrons will go through a phase transition from hadronic matter into a quark-gluon plasma (QGP), a phase where the quarks are asymptotically free [43] under very high density and pressure due to gravitational forces. In this state of matter, via the weak-interaction, a significant portion of the down quarks in the QGP turn into strange

quarks, which at sufficient density and pressure is more stable than regular baryonic matter at temperatures and densities near our everyday experience. This "strange matter" is hypothesized to exist at some or all neutron star cores, and currently is only theoretical, as there has not been any observable evidence yet for the existence of strange quark or strange matter, at any temperature or density [24].

As can be seen, the various aspects of compact stellar objects implies that we will need some mathematical formalism in order to use theory to understand and interpret experimental data and make predictions about unknowns. To that measure we will employ many body field theory techniques in order to make various estimates for neutron star interiors in conditions that were explained, that is, at the very dense and high temperature regimes. Without question we would anticipate the predictions made will lead us onto a more accurate equation of state for inner core of the star, which in turn will provide us with a way to verify our results using measurement techniques defined earlier. Although the instrumentation may not currently exist to verify the results, further development of methodology will allow us to either experimentally favor or disfavor the hypothesis that our predictions support. The following chapter intends to elaborate on the mathematical techniques that are used in the development of our predictions. The results that then follow may clarify the dynamics of compact stellar cores and give rise to more certainty in correct models of the equation of state of neutron stars.

In the rest of this work we elaborate on mathematical preliminaries and study the propagation of particles in stellar media. We use the renormalization parameters of quantum electrodynamics (QED) in order to do this in hot and dense media with strong magnetic fields. Neutron stars allow us to investigate this regime and the properties of charged leptons in this medium. The next two chapters develop the

necessary mathematical framework to understand these calculations to, especially, find properties of electrons in neutron stars.

## CHAPTER 2

### MATHEMATICAL FRAMEWORK

#### 2.1 Introduction

As we continue to ask the question of how we intend to obtain predictions of highly condensed states, it makes sense to discuss the mathematical framework which helps to make such predictions. We deal with, in the case of neutron stars, a highly compressed and condensed form of matter where countably many baryons are smashed so tightly the densities in this space rivals the densities found in an atomic nucleus. These extremes, like we have mentioned, will require us to move outside the typical toolset a researcher is familiar with, and many-body physics techniques which are commonly used in condensed matter theory and applications will become very useful in order to tackle problems of prediction in the case of equations of state of these compact stellar objects.

Many Body Physics (MBP) deals with finding the dynamics of bodies more than two [14] [15]. As is well understood, certain three body problems can be reduced to a two body problem, especially gravitationally. The nature of the system under study implies that we will need to apply a consistent framework that also adheres to the principles of quantum mechanics, as the objects under study are individual particles like baryons and leptons. Additionally there is no real upper bound on the number of bodies that need to be modeled, so it is fair to say we are not restricted to search for methods of just a three or four body solution, but in fact a very large number. Because of this we rely heavily on statistical methods, the understanding of phase transitions and spin statistics. Many of the methods thus inevitably share some features with statistical mechanics, and may be familiar. The difference in our case is

normally the inclusion of quantum mechanics and relativity since we deal with high energy due to extremely high temperatures and pressures due to gravitational forces. This approach is what we intend to use throughout this work, and specifically theories of the field under finite temperature and density (FTD), which will be elaborated on in the next chapter.

In general we seek to apply many body theory to stellar systems in order to find equations of state of the physical system that fit observational results. As mentioned, we wish to incorporate the effects of spin statistics, field theories and phase transitions in order to find physically valid results. It is worth noting that there are non-relativistic methods (Bethe-Brueckner-Goldstone expansion) to solving nucleon-nucleon interactions, which involve a perturbation around the ground state at low energies, but since the relativistic effects are assumed to be important to us we will neglect a proper treatment of non-relativistic methods and merely acknowledge them here [44].

## **2.2 Phase Transitions and Distribution Functions**

In this section we will elaborate, at a high level, upon a general model of phase transitions, the Ising model, and the exact solutions of the model developed by Ernst Ising, to apply these ideas in neutron stars [5] [51] [28].

### **2.2.1 Phase Transitions**

A general problem in thermodynamic functions is the problem of phase transitions. Normally, at some given point (called a critical point) for one of the dynamical variables, we encounter singularities or infinities and the thermodynamic functions "blow

up". There are many examples of phase transitions, such as condensation of gases, ferromagnetism and superconductivity in materials, etc. which give ample motivation towards finding a possible model to develop a framework to understand these phenomena, especially common in dense stars such as neutron stars, which we have been discussing.

Generally, we primarily deal with systems where we neglect interactions between particles for simplicity. The study of phase transitions however requires that we dispense with that simplification, since many transitions, such as condensation or ferromagnetism, emerge from the basis of inter-particle cooperation, meaning particles of a system cooperate to exhibit transitions between states. It is reasonable to say, that in an  $N$ -particle system, the number of interactions will grow very large, and assumptions must be made in order to solve the problem.

Primarily, we assume that the most significant inter-particle interactions emerge from a particles' nearest neighbors, and the contribution from further neighbors is not very significant. From this assumption we can use a set of lattice points to represent our system, only taking into account the interparticle interactions of a particles' nearest neighbors. This model can describe many different phase transitions, and one of the first developed was for ferromagnetism called the Ising model, and is described below.

**The Ising Model** Let us assume there exists a lattice of  $N$  molecules each having a magnetic moment  $\mu$  and is able to take on two different orientations in space. Such a system can attain  $2^N$  possible configurations. If we immerse our lattice within a magnetic field  $B$  then the possible total energy  $E$  will be based on the intermolecular interactions of the lattice and the lattice's interactions with the magnetic field. If we use statistical theory we can find a partition function, which will then allow us to

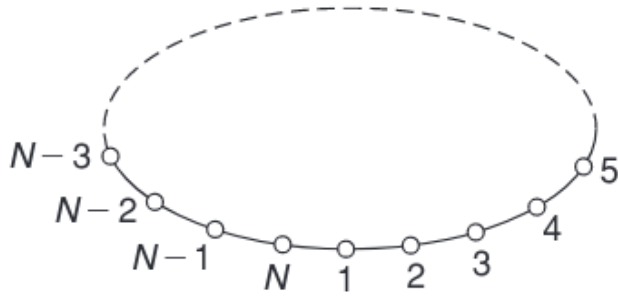


**Figure 2.1.** Arrangement of  $N$  molecules in a 1-D lattice, otherwise known as an Ising chain. Image from Pathria Beale [5]

obtain the expectation value of the magnetization of the lattice  $\bar{M}(B, T)$  as a function of the magnetic field and temperature. In the absence of magnetic fields, we might find a non-zero magnetization for certain critical temperatures, and in that case we would say that our model exhibits spontaneous magnetic phase transitions, which is what the Ising model hopes to show. Our model must also account for the interactions between neighboring particles, we do this by assuming a certain inter-particle energy  $K_{ij} \pm J_{ij}$  where  $K_{ij}$  is the Coloumb interaction energy between spins and  $J_{ij}$  is the exchange energy (a purely quantum mechanical effect resulting from the symmetric exchange of particles with same spin). The difference between the energy of a pair of parallel and antiparallel spins is  $\epsilon(\uparrow\uparrow) - \epsilon(\uparrow\downarrow) = -2J_{ij}$ . This implies that  $\epsilon(\uparrow\uparrow)$  is energetically favored if  $J_{ij} > 0$ , and  $\epsilon(\uparrow\downarrow)$  is favored if  $J_{ij} < 0$ . The former allows for ferromagnetism, and the latter antiferromagnetism.

This allows us to write the total interaction energy as

$$E = \text{constant} - J \sum \sigma_i \sigma_j$$

where  $\sigma$  denotes the spin of the particle (being +1 or -1) and the sum is over all nearest neighbors of a particle,  $i < j$  to avoid double counting in neighbor interactions. In

practice we write the Hamiltonian of this system as

$$H\{\sigma_i\} = -J \sum_{n_i n_j} \sigma_i \sigma_j - \mu \mathbf{B} \sum_i \sigma_i$$

This equation says the Hamiltonian of the set of particles  $\sigma_i$  is equal to the exchange energy plus (minus) the interaction of the particle with an external field  $\mathbf{B}$ . Developing the Hamiltonian allows us to write the partition function of the system

$$Q_N(B, T) = \sum_{\sigma_1} \sum_{\sigma_2} \dots \sum_{\sigma_N} \exp(-\beta H\{\sigma_i\})$$

The rest of the thermodynamics of the system follows:

$$\begin{aligned} A(B, T) &= -kT \ln(Q_N) \\ U(B, T) &= kT^2 \frac{\partial}{\partial T} \ln(Q_N) \\ C(B, T) &= \frac{\partial U}{\partial T} \\ \bar{M}(B, T) &= -\left(\frac{\partial A}{\partial B}\right)_T \end{aligned}$$

Where  $\bar{M}(0, T)$  would allow us to determine whether the system has a spontaneous net magnetization. If this is nonzero at some critical temperature  $T_c$  then the system would be ferromagnetic at  $T < T_c$  and anti-ferromagnetic for  $T > T_c$ .

**Exact Solution in 1D** We now investigate solutions of the Ising model in one dimension. The reason for this simple treatment is two-fold, first, this was the model that Ising himself solved in 1925, and second, there are certain physical phenomena that this simple model applies to such as adsorption on a protein chain, so it is instructive and physical to examine the model in 1D. The approach we will use is not what Ising used but instead we will utilize matrix methods in order to obtain the final solution. We begin by replacing the particle lattice discussed in the last section with a closed endless structure, essentially a loop with particles dotted along

the chain, as shown below. This structure is beneficial as it automatically allows for easier computation of the nearest neighbors and removes the effect of particles at the 'edge' of the lattice.

We write our Hamiltonian in the same manner as previously discussed, except our sum over nearest neighbors instead is a sum from 1 to N, and spin interactions are calculated only for the particle immediately in front of the current particle:

$$H_N\{\sigma_i\} = -J \sum_{i=1}^N \sigma_i \sigma_{i+1} - \frac{1}{2} \mu B \sum_{i=1}^N (\sigma_i + \sigma_{i+1})$$

Where  $\sigma_{N+1} = \sigma_1$ . Lets say we can write the partition function as a sum over spins of some product of matrices:

$$\begin{aligned} Q_N(B, T) &= \sum_{\sigma_1=\pm 1} \dots \sum_{\sigma_N=\pm 1} \\ &\langle \sigma_1 | \hat{P} | \sigma_2 \rangle \langle \sigma_2 | \hat{P} | \sigma_3 \rangle \dots \\ &\langle \sigma_{N-1} | \hat{P} | \sigma_N \rangle \langle \sigma_N | \hat{P} | \sigma_1 \rangle \end{aligned}$$

Where  $\hat{P}$  is an operator defined as

$$\hat{P} = \begin{pmatrix} e^{\beta(J+\mu B)} & e^{-\beta J} \\ e^{-\beta J} & e^{\beta(J-\mu B)} \end{pmatrix}$$

Due to the continuous completeness relation  $\int |\sigma_i\rangle \langle \sigma_i| = 1$ , the summations in  $Q_N$  collapse to give a very simple relation, which we can further simplify using the rules of matrix algebra:

$$\begin{aligned} Q_N(B, T) &= \sum_{\sigma_1=\pm 1} \langle \sigma_1 | \hat{P}^N | \sigma_1 \rangle \\ &= \text{Tr}(\hat{P}^N) \\ &= \lambda_1^N + \lambda_2^N \end{aligned}$$

We see that the formulation of the Ising model in matrix mechanics allows for a very simple expression of the partition function, namely that the partition function is equal to the trace of the operator matrix to the Nth power. This yields two eigenvalues raised to the Nth degree, as we expect.

We can find these eigenvalues by solving the eigenvalue equation which is obtained from the determinant:

$$|\hat{P}| = \begin{vmatrix} e^{\beta(J+\mu B)} - \lambda & e^{-\beta J} \\ e^{-\beta J} & e^{\beta(J-\mu B)} - \lambda \end{vmatrix} = 0$$

We obtain the following characteristic quadratic equation:

$$\lambda^2 - 2\lambda e^{\beta J} \cosh(\beta\mu B) + 2 \sinh(2\beta J) = 0$$

which can be solved easily to give us the eigenvalues of the operator matrix:

$$\begin{pmatrix} \lambda_1 \\ \lambda_2 \end{pmatrix} = \begin{pmatrix} e^{\beta J} \cosh(\beta\mu B) + \{e^{-2\beta J} + e^{2\beta J} \sinh^2(\beta\mu B)\}^{1/2} \\ e^{\beta J} \cosh(\beta\mu B) - \{e^{-2\beta J} + e^{2\beta J} \sinh^2(\beta\mu B)\}^{1/2} \end{pmatrix}$$

Which is a standard result in statistical mechanics. We can assume that  $\lambda_2$  will be less than  $\lambda_1$ , since the second term in  $\lambda_2$  is subtracted, so as N gets large the contribution to the partition function  $Q_N$  for large N is  $\approx \lambda_1^N$ . Thus we can conclude

$$\begin{aligned} \ln(Q_N(B, T)) &\approx N \ln(\lambda_1) \\ &= N \ln e^{\beta J} \cosh(\beta\mu B) \pm \\ &\quad \{e^{-2\beta J} + e^{2\beta J} \sinh^2(\beta\mu B)\}^{1/2} \end{aligned}$$

The rest of the thermodynamics can be derived from the Helmholtz free energy,

$$\begin{aligned} A(B, T) &= -NJ - NkT \ln \cosh(\beta\mu B) \\ &\quad + e^{-4\beta J} + \sinh^2(\beta\mu B)^{1/2} \end{aligned}$$

Such as the average energy and magnetization

$$\begin{aligned}
 U(B, T) &= -T^2 \frac{\partial}{\partial T} \left( \frac{A}{T} \right) \\
 &= -NJ - \frac{N\mu B \sinh(\beta\mu B)^{1/2}}{e^{-4\beta J} \sinh^2(\beta\mu B)} + \\
 &\quad \frac{2NJ e^{-4\beta J}}{[\cosh(\beta\mu B) + e^{-4\beta J} + \sinh^2(\beta\mu B)^{1/2}] \{e^{-4\beta J} + \sinh^2(\beta\mu B)\}^{1/2}} \\
 \bar{M}(B, T) &= - \left( \frac{\partial A}{\partial B} \right)_T = \frac{N\mu \sinh(\beta\mu B)}{\{e^{-4\beta J} + \sinh^2(\beta\mu B)\}^{1/2}}
 \end{aligned}$$

We can see from this that as  $B$  approaches 0,  $\bar{M}$  also approaches 0, showing that spontaneous magnetization is not possible for finite  $T$ . However, at  $T=0$ ,  $\sinh(\infty) = 1$  and  $\bar{M} = N\mu$  which shows there is a theoretical phase transition at  $T_c = 0$  and a spontaneous magnetization occurs for the system at this temperature. Despite this, the phase transition at  $T_c = 0$  is only theoretical, as an actual temperature this is not attainable by any system.

The last section presented an exact solution to the Ising model in broad terms in one dimension. The model has been extended to two and three dimensions, however the techniques used to solve the three dimensional case are not exact and instead numerical techniques are used to obtain a solution. While we do not go into detail here about the solution of the Ising model in 2-D, we note the derivation involves the assumption of the existence of a square lattice (as opposed to an infinite chain), graph theory to enumerate the lattice, and dual transformations in order to obtain a model where the limit between high and low temperature lattices meet.

The subject of the Ising model and phase transitions generally is more involved mathematically and exact analytical solutions are almost impossible. Therefore, the majority of solutions in the modern day use numerical methods such as Monte Carlo,

instead of seeking exact solutions. Most of the analysis (which we omitted) of the 1-D model involves mean-field theory which is inaccurate [5].

### 2.2.2 Distribution functions

Much has been said about the dependence of our results in the high temperature and density regimes, which will include later discussion on propagators modified by spin statistics functions,  $n_F$  and  $n_B$ , Fermi-Dirac and Bose-Einstein statistics. Thus it may be worthwhile to present a brief review to understand the significance in the context of statistical mechanics. The kinetic theory of gases, where particles in a

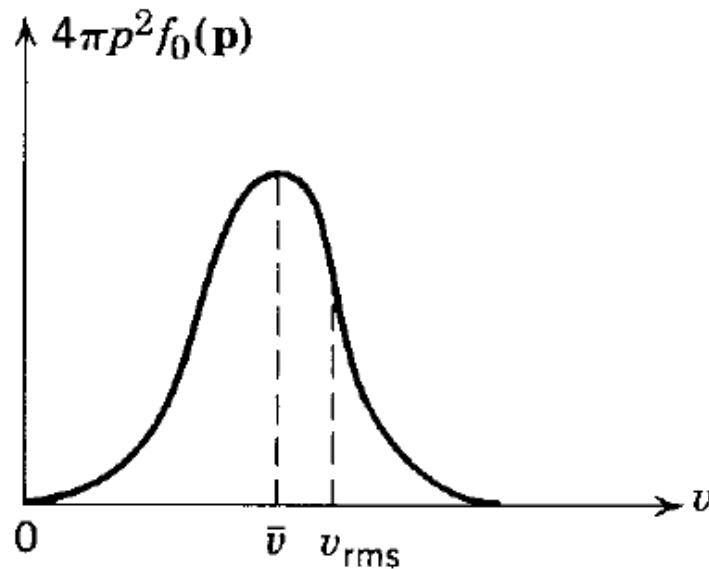


**Figure 2.2.** Graph of Maxwell-Boltzmann distribution. Huang [25]

gas are much smaller than the volume in which they are contained, non-interacting amongst themselves, and there are a large number of them to justify a statistical treatment, gives classical results that we are familiar with, such as the ideal gas law,  $PV = NT$  (and  $k_B = 1$ ), where pressure  $P$ , volume  $V$ , the number of molecules  $N$  and temperature  $T$  are related (it can also be written in terms of the gas constant

R and moles  $n$ ,  $PV = nRT$ ). It is relevant to ask given the fundamental equation of thermodynamics,  $E = TS - PV + \mu N$ , where  $S$  is the entropy,  $\mu$  is the chemical potential, if there is a distribution that encapsulates the probability of each particle in a particular energy state.

Maxwell-Boltzmann (MB) statistics allows us to calculate the expected value of the number of particles  $N$  in a particular energy microstate  $E_i$ . Derived from classical statistical mechanics, the expression is

$$\bar{N}_m = g_i e^{\beta(\mu - E_i)} \quad (2.1)$$

Where  $g_i$  is the number of states that have a particular energy level  $E_i$ , to account for degeneracy, and  $\beta = 1/T$ . As this is classically derived, there is no attempt to treat particles as indistinguishable, as quantum mechanics tells us. In fact the assumption of these statistics is such that switching two particles is a new, unique configuration, which is a classical idea inherently. It is worth noting that there is no way to account for spin in the statistics, so there is no real hope of extending this idea into quantum mechanics. The distribution function for Maxwell Boltzman statistics is a probability distribution of the various energies of particles of the system, is usually written as a function of average velocity or momentum  $\langle p \rangle$

$$f(\vec{p}) = \left(\frac{1}{2\pi mT}\right)^{3/2} e^{-\frac{\vec{p}^2}{2mT}} \quad (2.2)$$

is called the Maxwell-Boltzmann distribution. In the grand canonical ensemble, which is a statistical model that assumes a system is in equilibrium with a heat bath and particle reservoir such that the system can exchange energy and the number of particles, we can derive quantum statistics of indistinguishable particles. There are two basic forms of spin statistics. Bosons can accumulate in any number of particle energy states without limit, in contrast to fermions, which may only occupy one energy state

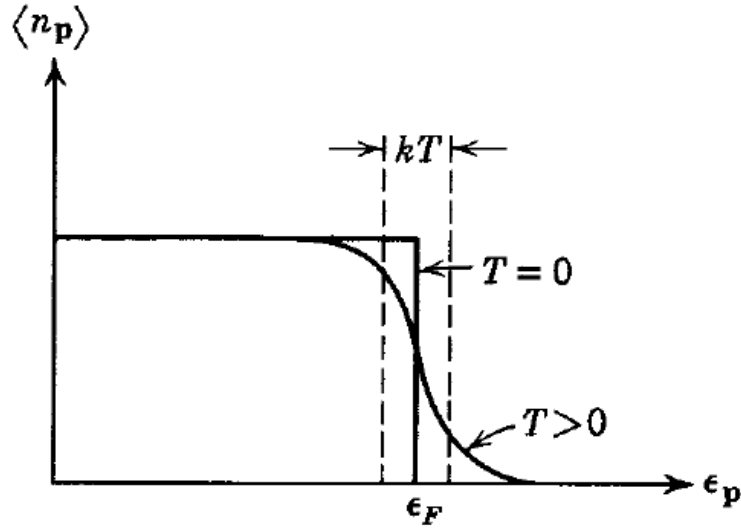


**Figure 2.3.** Average number of particles per energy level in a Fermi-Dirac distribution. Huang [25]

per particle. Bose-Einstein statistics are given as

$$\bar{N}_b = \frac{g_i}{e^{\beta(E_i - \mu)} - 1} \quad (2.3)$$

And the Fermi-Dirac statistics for fermions as

$$\bar{N}_f = \frac{1}{e^{\beta(E_i - \mu)} + 1} \quad (2.4)$$

Where  $g_i$  is set to 1 since only one particle can be assigned one energy state as a fermion (obeying the Pauli exclusion principle). As temperature increases and particle density decreases, both the Fermi-Dirac and Bose-Einstein statistics recover the classical Maxwell-Boltzmann distribution.

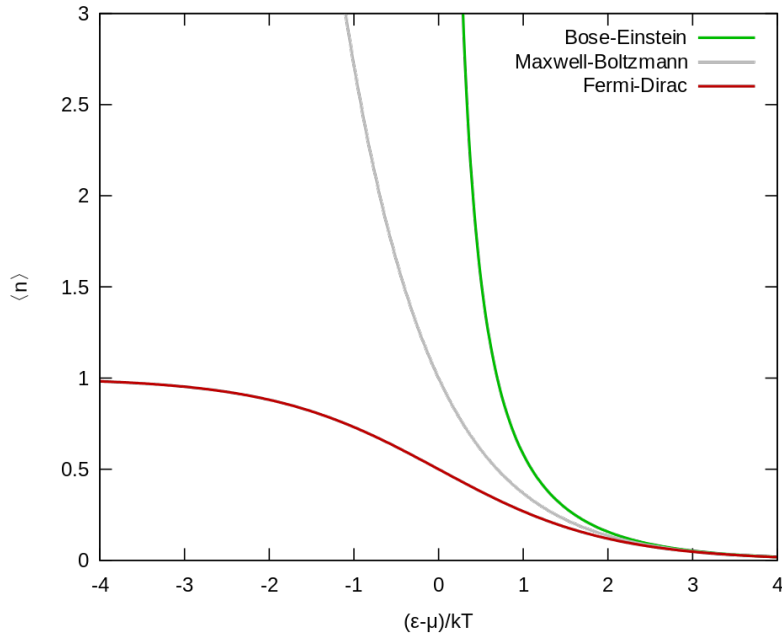


**Figure 2.4.** Average number of particles per energy level compared amongst all three distributions. Creative Commons

## 2.3 Lagrangian Formalism

Our Lagrangian density is represented as  $\mathcal{L} = \mathcal{L}(\phi, \nabla\phi, \frac{d\phi}{dt}, \vec{x}, t)$ , depending on a scalar field  $\phi = \phi(\vec{x}, t)$ , the position coordinate  $\vec{x}$ , time  $t$  and the derivatives of  $\phi$  with respect to the time and position.

Hamilton's Principle states that for monogenic systems the variation in the total action integrated from  $t_1 \rightarrow t_2$  is zero, or stationary value, for the motion. We can restate Hamilton's Principle for this continuous system as:

$$\delta I = \delta \int_{t_1}^{t_2} \int \mathcal{L} d^3x dt = 0$$

Where we vary only  $\phi$  and its derivatives similar to a discrete system. The variation of  $\phi$  at the endpoints is zero at  $t_1$  and  $t_2$ . and the corresponding Euler-Lagrange

equations are derived from Hamilton's principle as

$$\frac{\partial \mathcal{L}}{\partial \phi} - \frac{d}{dx_\mu} \left( \frac{\partial \mathcal{L}}{\partial \frac{\partial \phi}{\partial x_\mu}} \right) - \frac{d}{dt} \left( \frac{\partial \mathcal{L}}{\partial \frac{\partial \phi}{\partial t}} \right) = 0$$

Where we sum over  $\mu = 1...4$ , which is used as a dummy index. This Lagrangian formalism for vector fields in four dimensional space is a straightforward generalization of the above Lagrangian theory, with more use of tensor notation for simplicity. We can use summation to describe the vector field  $\phi_\rho$  as  $\rho$  indicates the component of the field. In electromagnetism, components of a 4-vector field, where the derivative of  $\phi_\rho$  with respect to the continuous coordinates is noted with a comma and another subscript, and  $\rho = 1...4$  can be expressed as:

$$\eta_{\rho,\nu} \equiv \frac{d\eta_\rho}{dx^\nu}$$

$$\eta_{i,\mu\nu} = \frac{d^2\eta_i}{dx^\mu dx^\nu}$$

Using this notation our Lagrangian density is a function of the vector field, and the derivatives of the field with respect to the continuous coordinates:

$$\mathcal{L} = \mathcal{L}(\eta_\rho, \eta_{\rho,\nu}, x^\nu)$$

Where Hamilton's principle can be written as an integral over four dimensional space, also known as 'minimizing the action':

$$\delta I = \delta \int \mathcal{L} dx^\mu = 0$$

The variation of the  $\phi_\rho$  at the boundary of the surface is zero, and we define a parameterized  $\phi_\rho$  such that  $\phi_\rho(x^\nu; \alpha) = \phi_\rho(x^\nu; 0) + \alpha \xi(x^\nu)$  where  $\xi$  is well behaved and go to zero at the boundary of the surface. We set the derivative of  $\frac{dI}{d\alpha}$  to zero to get the extremum:

$$\frac{dI}{d\alpha} = \int \frac{\partial \mathcal{L}}{\partial \phi_\rho} \frac{\partial \phi_\rho}{\partial \alpha} + \frac{\partial \mathcal{L}}{\partial \phi_{\rho,\nu}} \frac{\partial \phi_{\rho,\nu}}{\partial \alpha} dx^\mu = 0$$

And then integration by parts is used again to obtain

$$\begin{aligned} \frac{dI}{d\alpha} &= \int \left[ \frac{\partial \mathcal{L}}{\partial \phi_\rho} - \frac{d}{dx^\mu} \left( \frac{\partial \mathcal{L}}{\partial \phi_{\rho,\nu}} \right) \right] \frac{\partial \phi_\rho}{\partial \alpha} dx^\mu + \\ &\int \frac{d}{dx^\mu} \left( \frac{\partial \mathcal{L}}{\partial \phi_{\rho,\nu}} \frac{\partial \phi_\rho}{\partial \alpha} \right) dx^\mu = 0 \end{aligned}$$

Where the last integral goes to zero since it can be transformed by a divergence theorem into an integral over a bounding surface, which is zero by our assumption that the variation is zero at the boundary of the surface.

$$\frac{dI}{d\alpha} = \int \left[ \frac{\partial \mathcal{L}}{\partial \phi_\rho} - \frac{d}{dx^\mu} \left( \frac{\partial \mathcal{L}}{\partial \phi_{\rho,\nu}} \right) \right] \frac{\partial \phi_\rho}{\partial \alpha} dx^\mu = 0$$

Thus we are only left with the term in brackets, and since the variation is arbitrary the coefficient must be equal to zero:

$$\frac{d}{dx^\mu} \left( \frac{\partial \mathcal{L}}{\partial \phi_{\rho,\nu}} \right) - \frac{\partial \mathcal{L}}{\partial \phi_\rho} = 0$$

These are the generalized Euler-Lagrange equations for vector fields in four dimensional space. The index  $\mu, \rho$  runs over  $\mu, \nu = 1, 2, 3, 4$  [23]. Thus, for a given Lagrangian, such as the electromagnetic Lagrangian density,

$$\mathcal{L} = \frac{-1}{16\pi} F_{\alpha\beta} F^{\alpha\beta} - J_\alpha A^\alpha \quad (2.5)$$

We may use the Euler-Lagrange equations to obtain the equations of motion for electromagnetism,

$$\frac{1}{4\pi} \partial^\beta F_{\beta\alpha} = J_\alpha \quad (2.6)$$

Where  $F_{\alpha\beta} = \partial_\alpha A_\beta - \partial_\beta A_\alpha$  is the electromagnetic tensor,  $J_\alpha = (\rho, \vec{j})$  is the four-current with  $J_0$  being the charge density and  $J_i$  over  $i = 1, 2, 3$  being the current density and the components of  $A_\alpha = (\phi, \vec{A})$  are the electric potential  $\phi$  and vector potential  $\vec{A}$ . Historically, the theory of electromagnetism was developed as a theory

of fields, as elastic disturbances of some invisible medium. Now we have recreated the formulation used in a terse way, with the assistance of tensor notation and the Euler-Lagrange equations. While these fields are not stressed much in the development of classical electrodynamics [26] [56], the formulation has wide application in quantum theories, as will be discussed.

## 2.4 Quantum Field Theory

Originally, dynamical interactions in quantum mechanical processes were described in terms of electron fields, with positrons being the holes created due to the absence at some part of the electron field . Richard Feynman was able to show in several landmark papers that we may be able to treat this problem using Greens functions as solutions of the relativistic form of Schrodinger's equation. His clever intuition paved the way for a graphical description of quantum processes that we use today. The contributions of Feynman and many other physicists developed into some of the most accurate predictions of any physical theory, the theory of quantum fields, and modern quantum electrodynamics (QED). Here we describe some of the most relevant points in order to motivate our continuing discussion.

### 2.4.1 Klein-Gordon equation

Relativity in quantum mechanics was included by developing the Schrodinger's equation in 4-dimensional space. Oskar Klein and Walter Gordon published their Klein-Gordon equation describing spinless relativistic particles, and the possibility of a relativistic equation describing particles with spin begun to emerge. To obtain the Klein-Gordon equation, which is a relativistic equation, we start with the non-relativistic

equation for the energy of a free particle (it should be noted from here we take  $\hbar = c = k = 1$ )

$$H = KE + PE = \frac{\mathbf{p}^2}{2m} + V$$

First quantization leads us to the Schrodinger's equation, from non-relativistic quantum mechanics

$$\hat{H}\psi = \hat{E}\psi = \frac{\hat{\mathbf{p}}^2}{2m}\psi \quad (2.7)$$

As a note, time dependence is accounted for via the energy operator:

$$\hat{E} = i\frac{\partial}{\partial t} \quad (2.8)$$

and the momentum operator is proportional to the del operator

$$\hat{\mathbf{p}} = -i\vec{\nabla} \quad (2.9)$$

The Schrodinger's equation is not relativistically invariant, so the natural place to start this process is the energy-momentum relation and substitute the first quantized quantities for momentum and energy:

$$E^2 = p^2 + m^2 \rightarrow E = \pm\sqrt{p^2 + m^2} \quad (2.10)$$

$$E\psi = \pm\sqrt{p^2 + m^2}\psi \quad (2.11)$$

$$i\frac{\partial\psi}{\partial t} = \pm\sqrt{(-i\nabla)^2 + m^2}\psi \quad (2.12)$$

Using the square of the energy,  $E^2 = p^2 + m^2$  as the operator we wish to work with instead, we obtain a slightly different relation for energy conservation

$$\left(\frac{\partial^2}{\partial t^2} - \nabla^2\right)\psi + m^2\psi = 0 \quad (2.13)$$

This equation is applicable to both real and complex fields. Finally, by using the d'Alembert operator,  $\square \equiv \frac{1}{c^2}\frac{\partial^2}{\partial t^2} - \nabla^2$ , we can rewrite the Schrodinger's equation into

the Klein Gordon equation,

$$(\square + m^2)\psi = 0 \tag{2.14}$$

Solutions to the KG equation are covariant, however include negative and positive energies, which are interpreted as particle and antiparticle solutions. The probability density of the KG equation can be both positive and negative, something that is corrected by Paul Dirac in 1928.

### 2.4.2 Dirac equation

In the 1920s, there was a search to find a way to include spin-statistics in the relativistic Schrodinger's equation while still describing all the behavior understood from experiment at the time, such as the model of the hydrogen atom, including such phenomena such as fine splitting. Dirac was interested in finding an equation that was first order in space and time, in order to correct the issue of negative probabilities from the KG equation.

His search concluded with the equation named after him, the Dirac equation, a relativistic equation describing the Fermi statistics of spin-1/2 particles such as the electron as well as accounting for all of the known phenomena of the hydrogen atom, such as fine splitting, as well as having a positive definite probability density.

Dirac rewrote the D'Alembertian as a product of two, four-termed equations, each term having a coefficient that was a matrix. In this way Dirac was able to see it was possible to have the Schrodinger equation that was first order in space and time. The realization that a set of matrices satisfy this equation was the key insight into determining the usual form of the Schrodinger's equation that not only incorporated relativistic effects, but also spin. The Dirac equation is written using

Einstein notation as

$$i\gamma^\mu \partial_\mu \psi - m\psi = 0 \quad (2.15)$$

Where  $\gamma^\mu$  are known as the *gamma matrices*, and are written as follows:

$$\gamma^0 = \begin{bmatrix} 1 & 0 & 0 & 0 \\ 0 & 1 & 0 & 0 \\ 0 & 0 & -1 & 0 \\ 0 & 0 & 0 & -1 \end{bmatrix} \quad i\gamma^1 = \begin{bmatrix} 0 & 0 & 0 & 1 \\ 0 & 0 & 1 & 0 \\ 0 & -1 & 0 & 0 \\ -1 & 0 & 0 & 0 \end{bmatrix} \quad (2.16)$$

$$i\gamma^2 = \begin{bmatrix} 0 & 0 & 0 & 1 \\ 0 & 0 & -1 & 0 \\ 0 & -1 & 0 & 0 \\ 1 & 0 & 0 & 0 \end{bmatrix} \quad i\gamma^3 = \begin{bmatrix} 0 & 0 & i & 0 \\ 0 & 0 & 0 & -i \\ -i & 0 & 0 & 0 \\ 0 & i & 0 & 0 \end{bmatrix} \quad (2.17)$$

It is worth noting the Dirac equation has positive definite probability density and its solutions are written in matrix notation, called Dirac spinors.

### 2.4.3 Second Quantization

To connect the dots we note that the KG equation for massless fields  $\square\psi = 0$  is satisfied by the general solution

$$\psi(x, t) = \int \frac{d^3p}{(2\pi)^3} (a_p(t)e^{-i\vec{p}\cdot\vec{x}} + a_p^*(t)e^{i\vec{p}\cdot\vec{x}}) \quad (2.18)$$

With the  $a_p(t)$  satisfying the equation of motion for a harmonic oscillator,

$$(\partial_t^2 + \vec{p} \cdot \vec{p})a_p(t) = 0$$

From non-relativistic quantum mechanics we know the analysis of the quantum harmonic oscillator is easiest by using annihilation and creation operators. Similarly, by

promoting the  $a_p(t)$  and  $a_p(t)^*$  to operators and integrating we obtain the Hamiltonian of the theory as

$$H = \int \frac{d^3p}{(2\pi)^3} |\vec{p}| \left( a_p^\dagger a_p + \frac{1}{2} \right) \quad (2.19)$$

The commutation relations of the theory being similar to the quantum harmonic oscillator ( $[a, a^\dagger] = 1$ )

$$[a_k, a_p^\dagger] = (2\pi)^3 \delta^3(\vec{p} - \vec{k}) \quad (2.20)$$

where the  $2\pi$  factors are conventional. The creation operator  $a_p^\dagger$  creates particles with momentum  $p$  from the vacuum

$$a_p^\dagger |0\rangle = \frac{1}{\sqrt{2|\vec{p}|}} |\vec{p}\rangle \quad (2.21)$$

The inner product of two separate one-particle states, and identity operator, are

$$\langle p|k\rangle = 2|\vec{p}|(2\pi)^3 \delta^3(\vec{p} - \vec{k}) \quad (2.22)$$

$$\int \frac{d^3p}{(2\pi)^3} \frac{1}{2|\vec{p}|} |\vec{p}\rangle \langle \vec{p}| = 1 \quad (2.23)$$

With the factors  $(2\pi)^3$  and  $\frac{1}{2|\vec{p}|}$  added by convention. We can check this,

$$|k\rangle = \int \frac{d^3p}{(2\pi)^3} \frac{1}{2|\vec{p}|} |p\rangle \langle p|k\rangle = \int d^3p |\vec{p}\rangle \delta^3(\vec{p} - \vec{k}) = |k\rangle \quad (2.24)$$

In this way we have quantized the fields leading to the naming of this process second quantization. Our quantum field solution to the massless KG equation is now operator-valued and written as [47]

$$\psi(x) = \int \frac{d^3p}{(2\pi)^3} \frac{1}{\sqrt{2|\vec{p}|}} (a_p e^{-i\vec{p}\vec{x}} + a_p^\dagger e^{i\vec{p}\vec{x}}) \quad (2.25)$$

#### 2.4.4 Feynman Diagrams, Rules and Probabilities in QFT

There is a somewhat substantial change in notation as we move from Classical Fields to Quantum Fields, as is required when analyzing phenomena from condensed matter

systems such as neutron stars. The main quantities we analyze under these theories are scattering cross sections, otherwise known as the rate at which particles are produced in the same cross-sectional area. The nature of inclusion of relativistic effects implies that not only do particles scatter, but particles may be created or destroyed at certain energies due to the exchange of energy in any collision.

The differential cross section  $\frac{d\sigma}{d\Omega}$  can be given in terms of a parameter called the scattering amplitude,  $f(\theta, \phi)$ , and is defined as the number of particles that are scattered in an area swept by the solid angle  $d\Omega$ . This is made clear when defining  $J_{inc}$  as the incident flux or incident particle current density. The scattering amplitude  $f(\theta, \phi)$  is the probability amplitude of the scattered spherical wave in the scattering process. The wave function in the scattering process is given by  $\psi(\vec{r}) = e^{i\vec{k}_0 \cdot \vec{r}} + f(\theta, \phi)e^{ikr}/r$ , with  $f$  again being the scattering amplitude, also known as the form factor or structure function. Thus, the differential cross section can be written as:

$$\frac{d\sigma(\theta, \phi)}{d\Omega} = \frac{1}{J_{inc}} \frac{dN(\theta, \phi)}{d\Omega} = |f(\theta, \psi)|^2 \quad (2.26)$$

We will frequently be attempting to determine quantities related to the differential cross section, including  $\mathcal{M}$ , a dimensionless quantity that is an amplitude proportional to the scattering amplitude (eg.  $\frac{d\sigma}{d\Omega} \sim |\mathcal{M}|^2$ ).

For all QED processes, we cannot exactly determine  $\mathcal{M}$ , instead, we sum a perturbation series and cutoff the series at some appropriate term that is small enough to be ignored in order to obtain a result. The method of obtaining these series is through the summing of various possible orders of perturbative expansions of virtual loops.

These terms in the expansion can be given a pictorial representation, commonly known as *Feynman diagrams*, invented by Richard Feynman in a series of papers on

quantum electrodynamical interactions. These diagrams make complex perturbative interactions much easier to describe, visually, as well as making the resulting notation especially compact and intuitive.

Diagrams such as these are thus the description of a particle exchange, and our sought-after quantity  $\mathcal{M}$  is composed of the addition of several of these exchanges. The exact rules for constructing Feynman diagrams vary with the theory, and these rules allow for one to read the terms in each diagram, which in turn allows for an approximation of  $\mathcal{M}$ .

Fermion propagator		$\frac{i(\not{p}+m)}{p^2-m^2+i\epsilon}$
Boson propagator		$\frac{-ig_{\mu\nu}}{p^2+i\epsilon}$
Vertex		$iQe\gamma^\mu$
External Leg Fermions		incoming $u^s(p)$ , outgoing $\bar{u}^s(p)$
External Leg anti-Fermions		incoming $\nu^s(p)$ , outgoing $\bar{\nu}^s(p)$
External Photons		incoming $\epsilon_\mu(p)$ , outgoing $\epsilon_\mu^*(p)$

**Table 2.1.** Feynman rules for QED.

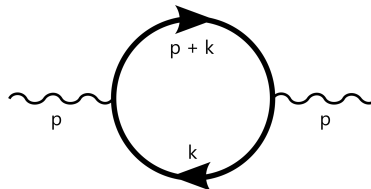


**Figure 2.5.** Vacuum polarization Feynman diagram describing one loop self-interactions in QED.

Feynman diagrams represent a transition from an initial state to a final state due to an interaction. In Figure 2.5, electron positron pairs are created on very short timescales as the photon propagates through the vacuum. The photons are represented by the wavy external lines, and the electron-positron pairs are represented by the middle loop. The interaction probability  $\mathcal{M}$  can be read from the diagram using the Feynman rules of QED [47]:

$$i\mathcal{M} = e^2 \epsilon_\mu^{2*} \epsilon_\nu^1 \int \frac{d^4k}{(2\pi)^4} \text{tr} \left[ \gamma^\mu \frac{i(\not{p} + \not{k} + m)}{(p+k)^2 - m^2 + i\epsilon} \gamma^\nu \frac{i(\not{k} + m)}{k^2 - m^2 + i\epsilon} \right] \quad (2.27)$$

Where we integrate over all momenta and take the trace to sum over possible spin states.

We may now discuss some of the Feynman rules in QED, listed in Table 2.1. For wavy photon lines, our propagator is represented using  $\frac{-ig_{\mu\nu}}{p^2+i\epsilon}$ , where  $g_{\mu\nu}$  is the Minkowski metric tensor. The internal loop lines representing the spin-1/2 particles are represented by the fermion propagator  $\frac{i(\not{p}+m)}{p^2-m^2+i\epsilon}$ . The square of the matrix element  $\mathcal{M}^2$  represents the interaction probability. In this way we can compute such quantities as the effect of vacuum polarization in QED [6] [9].

## 2.4.5 Renormalization

Renormalization is an essential part of an acceptable quantum field theory and cancellation of infinities is required to find measurable parameters of the theory [3] [2]. Broadly, renormalization is the process of removing infinities so that a finite quantity may be established and the theory is meaningful. A related idea is regularization, which allows us to control infinities by introducing a cutoff parameter into the theory. The idea of introducing a cutoff was not always well-accepted, and historically it has been viewed with some skepticism [48].

**Regularization** From classical physics, we have the mass-energy of the electromagnetic field

$$m_{em} = \int \frac{1}{2} E^2 dV \quad (2.28)$$

This integral evaluates to  $q^2/(8\pi r)$ , however it is clear that as  $r \rightarrow 0$  the quantity becomes quickly infinite. The mass-energy for the electromagnetic field becomes the electron mass for  $r_e \approx 2.8 \times 10^{-15}$  m, which informs us that the theory lacked some kind of intuition to allow the electron to become a point particle. Restricting the theory to a finite, non-zero radius is thus one kind of regularization. It hides our ignorance about scales of physics we do not fully comprehend, and yet still gives us the opportunity to use the theory practically.

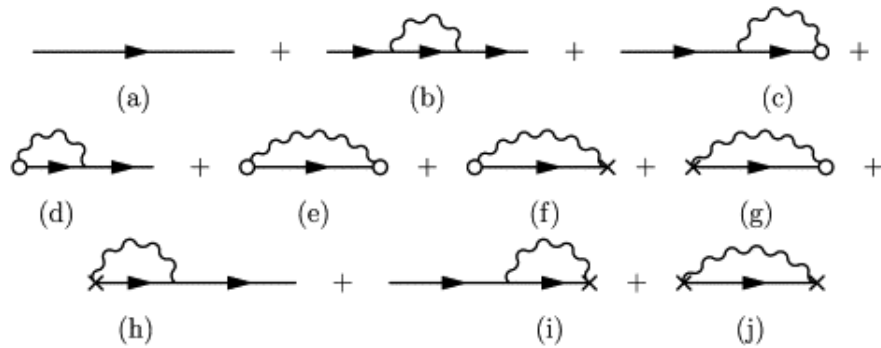


**Figure 2.6.** A number of possible Feynman diagrams generated from the electron propagator at one loop.

Renormalization is required in quantum field theory (QFT) in order to obtain finite quantities from integrals where interaction probabilities are calculated, as stated earlier. Early physicists noted that there were many divergences in the calculation of perturbation series' of various processes in quantum electrodynamics (QED).

For example, in the electron's propagation, it may interact with radiation virtually and gives self-energy corrections. These produce "loops" in Feynman diagrams, and to calculate the outcomes of this process one has to integrate over all possi-

ble combinations of interactions, including radiative corrections at different orders of the perturbation series. These Feynman diagrams (which are terms in a perturbation series) usually diverge, and a new prescription had to be developed to tame the infinities.

As an example of how these infinities might arise, for meson-meson scattering, we have a matrix element proportional to

$$\mathcal{M} \propto \int_0^\infty \frac{d^4k}{(2\pi)^4} \frac{1}{k^2 - m^2 + i\epsilon} \frac{1}{(K - k)^2 - m^2 + i\epsilon} \quad (2.29)$$

$$\propto \int_0^\infty \frac{d^4k}{k^4} \quad (2.30)$$

Which is very clearly a source of a logarithmic divergence. In quantum electrodynamics, infinities tend to come up in the mass and charge of the electron, as well as the normalization factor of the field,  $Z_2^{-1}$ . Since we could observe these quantities and observe finite values, the solution was to separate the Lagrangian of the theory into finite contributing terms and divergent terms, and then collect and integrate such that the divergent terms would cancel each other out.

There are many techniques for the regularization of singularities that lead to renormalization of the theory. We will only discuss one of the most common techniques, called dimensional regularization [57] as an effective process to remove singularities in vacuum theories.

## Dimensional Regularization

The idea behind this regularization scheme is to perform a Wick rotation and then evaluate the integral in  $d$  dimensions. Consider a divergent integral like above,

$$I = \int \frac{d^4k}{(2\pi)^4} \frac{1}{(k^2 - c^2 + i\epsilon)^2}$$

Now rotating by substitution  $t = i\tau$  into Euclidean space and evaluating the integral in  $d$  dimensions,

$$\begin{aligned}
I(d) &= i \int \frac{d_E^d k}{(2\pi)^d} \frac{1}{(k^2 + c^2)^2} \\
&\propto \int_0^\infty \frac{dk k^{d-1}}{(k^2 + c^2)^2} \\
&\propto \frac{1}{2} c^{d-4} \int_0^1 dx (1-x)^{d/2-1} x^{1-d/2} \\
&\propto \Gamma\left(\frac{4-d}{2}\right)
\end{aligned}$$

Where in the second to last step we use the substitution  $k^2 + c^2 = c^2/x$  and in the last step we recognized the integral is in the form of a Beta function, thus can be easily evaluated.

As we approach  $d \rightarrow 4$  we see the result approaches infinity, but now our integral is parameterized by a regulation variable  $d$ . This technique can be combined with renormalization such that the regulation parameter cancels out of the final result. In this way the objective is to parameterize infinite quantities, we have succeeded, and the process of regularization is complete [57].

$$I = \frac{i}{(4\pi)^2} \left[ \frac{2}{4-d} - \log(c^2) + \log(4\pi) - \gamma + O(d-4) \right] \quad (2.31)$$

This process, while initially not fully understood as being mathematically rigorous, had produced results but caused the physics community to be skeptical of the validity of such approaches. It was not much later, until Wilson [54], that renormalization techniques were proven to be mathematically consistent, and quantum field theories became accepted as rigorous.

CHAPTER 3  
FINITE-TEMPERATURE FIELD THEORY

### 3.1 Finite Temperature and Density Statistical Corrections

We have previously developed quantum electrodynamics in a vacuum. Now we incorporate the statistical properties of the medium to study the properties of propagating particles. Statistical effects from a medium such as temperature and density could have significant effects from vacuum theories and this is something we wish to prove.

Specifically, in the early universe, it is assumed the hot and dense media is effectively a heat bath as a statistical medium of stars. In order to understand particle propagation in astrophysical environments, we should consider that particle properties are modified due to extreme conditions, and extend quantum field theories to incorporate statistical effects, thereby including high temperature and chemical potential [32].

By incorporating statistical effects in quantum electrodynamics, we should be able to model particle propagation in a heat bath, which resembles the state of the early universe or the cores of some of the most compact objects that inhabit the current universe, such as neutron stars. The heat bath, as a reminder, is essentially a closed, large pool of hot and dense particles at thermodynamic equilibrium.

Unfortunately, there is a difficulty with straightforward generalization of quantum electrodynamics to finite temperature and density, and that is the problem of the heat bath. By choosing the rest frame of the heat bath, we break Lorentz invariance in the theory [20] and work to re-establish the co-variance. The imaginary-time formalism is a 4-dimensional generalization of quantum field theory described in Euclidean space where time is imaginary and spatial coordinates are real. We can include the effect of

temperature and chemical potential of the heat bath on the propagating particles in a medium. However this formalism has the side-effect of giving infinities for certain temperatures. An alternate formalism, the real-time formalism, has certain advantages that helps to prove order-by-order cancellation of divergences and allows us to obtain finite quantities [53]. So we cannot leave out a discussion of the advantages and disadvantages of either formalism.

Additionally, after deriving the theory in the real-time formalism, we must undergo a renormalization scheme in order to obtain finite quantities from the integration of matrix elements. This is necessary in order to obtain propagators that are finite and thus finite interaction probabilities. The program of quantum electrodynamics at finite temperature is at this point basically complete and we can begin to establish and discuss quantities such as the fermion self-energy.

Two obvious limits are elected for discussion,  $T \gg m_e$ , and  $T \ll m_e$ . Since the temperature in neutron star cores are of the order  $T \sim m_e \sim 10^{10}K$  and the center of a typical hot star is on the order of  $T \sim 10^6 - 10^7K$  [20], the  $T \ll m_e$  case seems relevant for most of the universe except for extreme media, such as the quark-gluon plasma of the early universe or the centers of the most compact stellar objects, an area which previously discussed is quite unknown. In that sense the  $T \gg m_e$  case should be considered not only relevant but extremely interesting from the perspective of particle propagation.

However, for extremely dense systems, the inclusion of density effects and chemical potential of particles is required, and the treatment follows lines similarly to the above for the limits  $T \gg \mu$  and  $T \ll \mu$ .

## 3.2 Real and Imaginary time propagators

As we have established the utility of the real time formalism, we present the results of real-time formalism that we use for the rest of this paper, and also the results of the imaginary time formalism for comparison.

The spinless Greens function at finite temperature for the photon in imaginary time is given by Dolan and Jackiw [16] [20],

$$D_{\mu\nu}(x) = \frac{2}{\beta} \sum_n \int \frac{d^3k}{(2\pi)^3} e^{-i(k_n t + \vec{k} \cdot \vec{x})} D_\beta(k) \quad (3.1)$$

Where the sum is over discrete  $n = 0, \pm 1, \pm 2, \dots \pm \infty$ . For a non-interacting field,

$$D_{\mu\nu}(k) = \frac{-ig_{\mu\nu}}{k_n^2 - \vec{k}^2} \quad (3.2)$$

With  $k^\mu = (k_n, \vec{k})$  and  $k_n = \frac{2\pi n}{-i\beta}$  and  $\beta = 1/T$ . We can see here the time component  $k^0 = iT2\pi n$  is imaginary, as expected. It is worth noting that in Equation 3.1 we have a sum over an infinite number of k-modes. This sum is what is problematic, and which we will soon see, is not present in the real-time formalism. The transformation from the imaginary to real time boson propagator is an application of Wick's rotation and analytically continuing the periodic boundary conditions of the imaginary time propagator to obtain the real-time propagator

$$\tilde{D}_{\mu\nu}(k) = -g_{\mu\nu} \left( \frac{i}{k^2 + i\epsilon} + \frac{2\pi}{e^{\beta E} - 1} \delta(k^2) \right) \quad (3.3)$$

$$= -g_{\mu\nu} \left( \frac{i}{k^2 + i\epsilon} + n_B 2\pi \delta(k^2) \right) \quad (3.4)$$

Where  $E = (\vec{k}^2 + m^2)^{1/2}$  and  $k_n = \frac{2\pi n}{\beta}$ . The important difference is not only that the summation over  $n$  is removed, but the additional term in the propagator which incorporates the effects of Bose-Einstein statistics ( $n_B$ ) explicitly. This additional

term is another one of the nice properties of the real time formalism. We now present the results for fermions. In imaginary time the Greens function is given as

$$S_\beta(x) = \frac{1}{-i\beta} \sum_n \int \frac{d^3p}{(2\pi)^3} e^{-ikx} S_\beta(p) \quad (3.5)$$

With the definitions the same as above except,  $k_n = \frac{(2n+1)\pi}{-i\beta}$ . Here we have the imaginary-time fermion propagator as

$$S_\beta(p) = \frac{i}{\not{p} - m} = \frac{i(\not{p} - m)}{p^2 - m^2} \quad (3.6)$$

Where  $\not{p} = \gamma^\mu p_\mu$ , and the fermion propagator in real-time is

$$\tilde{S}_\beta(x) = \frac{i}{\not{p} - m} - \frac{2\pi}{e^{\beta E} + 1} (\not{p} + m + i\epsilon) \delta(p^2 - m^2) \quad (3.7)$$

$$= \frac{i}{\not{p} - m} - n_F 2\pi (\not{p} + m + i\epsilon) \delta(p^2 - m^2) \quad (3.8)$$

We have not yet included the effects of density, but the dependence on temperature and particle distribution is now apparent in both cases, as Equation 3.4 and 3.8 depend on the distribution functions  $n_B$  and  $n_F$  respectively. The Feynman rules for QED at finite temperature will stay the same, apart from these propagators. For those interested the derivation of these results, Dolan and Jackiw [16] is recommended for the calculational details.

**Real Time versus Imaginary time** Finite temperature and density effects are two parallel approaches to incorporate statistical background effects, both having their own advantages and disadvantages. The most obvious difference which was discussed earlier with the most relevance for finite temperature theory is [53] the covariance of the real-time approach at finite T and the removal of infinities due to the lack of infinite sums in the real-time formalism. Additionally, the imaginary time

formalism has periodic boundary conditions which restricts its temperature range. This restriction is not present in the real-time formalism. Another briefly touched upon advantage of the real-time approach is the separation of terms in the propagator into a zero and non-zero temperature component [19]. This can make comparison of quantities and subsequent analysis between  $T = 0$  and  $T \neq 0$  cases relatively straightforward. For these reasons we intend to utilize the real-time formalism for the rest of this work.

These results help us understand contextually how it is possible to obtain a quantum field theory at finite temperature, the link due to Wick's rotation and analytic continuation makes such theories possible [57][47]. From this point renormalization techniques are applied, Feynman diagrams and their associated rules can be developed, and our theory is complete. The details of this prescription are summed up in [29] [52] [20] [16]. We will build upon this foundation in order to make our contribution to QFT at FTD by incorporating the effect of strong magnetic fields in the subsequent chapter.

### **3.3 Electron Self-Energy and FTD Renormalization**

With the basics of the theory established, we can continue to calculating quantities of interest. The electron interacts with itself as it propagates through the vacuum, causing divergent Feynman diagrams to be generated at  $T=0$ . In order to re-calculate the effect of the electron self-energy at  $T \neq 0$ , we follow a similar process but utilize the modified propagators to determine the matrix element, renormalize the theory and calculate the renormalized mass, wavefunction and electron charge constants. We begin with the electron self-energy (Figure 3.1) at zero-temperature. The Lagrangian

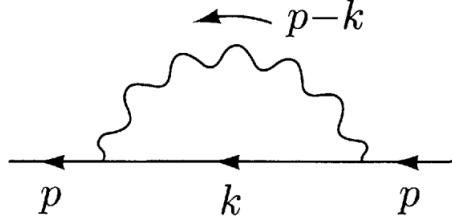


**Figure 3.1.** Electron self-energy. Peskin and Schroeder [41]

of this theory [20] is

$$\mathcal{L} = \bar{\psi}_0(x)(i\not{\nabla} - m_0)\psi_0(x) \quad (3.9)$$

Where  $m_0$  is our un-renormalized electron mass. Using our Feynman rules from standard QED given in Table 2.1, the matrix element of the self-interaction is determined from the diagram as

$$\Sigma(p) = ie^2 \int \frac{d^4k}{(2\pi)^4} \frac{g^{\mu\nu}}{k^2} \frac{\gamma_\mu(\not{p} - \not{k} + m)\gamma^\nu}{k^2 - 2p \cdot k + p^2 - m^2} \quad (3.10)$$

Evaluation is done using dimensional integration in order to obtain a result parameterized by  $1/\epsilon$

$$\Sigma(p) = \frac{-\alpha}{4\pi} [m_0 - (\not{p} - m_0)] \left( \frac{3}{\epsilon} - 4 \right) + \dots \quad (3.11)$$

$$\frac{1}{\epsilon} = \frac{2}{d-4} + \gamma - \ln(4\pi) + \ln(m^2) \quad (3.12)$$

and  $d$  is the number of dimensions,  $\gamma$  is the Euler-Mascheroni constant. The propagator  $\frac{1}{\not{p} - m_0 - \Sigma(p)}$  is redefined in such a way to cancel any infinities after regularization, by introducing a constant  $Z_2$  depending on the regularization parameter  $1/\epsilon$ . This

parameter will drop out of the final result,

$$G(p) = \frac{Z_2}{\not{p} - m_0 - \delta m_0} \quad (3.13)$$

$$\delta m_0 = \frac{-\alpha}{4\pi} \left( \frac{3}{\epsilon} - 4 \right) m_R \quad (3.14)$$

$$Z_2 = \left( 1 - \frac{\alpha}{4\pi} \left( \frac{3}{\epsilon} - 4 \right) \right)^{-1} \quad (3.15)$$

Our Lagrangian can now be rewritten using these renormalization constants  $\delta m_0$  and  $Z_2$ ,

$$\mathcal{L} = Z_2(\psi_R^\dagger(x)(i\not{\nabla} - m_R)\psi_R(x) + \psi_R^\dagger(x)\delta m_0\psi_R(x)) \quad (3.16)$$

$$\psi_R(x) = Z_2^{-1/2}\psi_0(x) \quad (3.17)$$

Where  $m_R = m_0 + \delta m$  is the observed or renormalized mass of the electron,  $\psi_R(x)$  is the renormalized wavefunction,  $d_m$  is the mass renormalization constant, and  $Z_2$  is the wavefunction renormalization constant. This standard treatment of the self-energy will be modified when incorporating the effect of the heat bath. The photon propagator is modified in a heat bath to be

$$D_{\mu\nu}(k) = g_{\mu\nu} \left( \frac{-i}{k^2 + i\epsilon} - 2\pi\delta(k^2)n_B(k) \right) \quad (3.18)$$

Where  $n_B(k) = \frac{1}{e^{\beta k} - 1}$ , the Bose-Einstein distribution function. If we re-calculate the self-energy using the modified propagator we see the benefit of the real-time formalism

$$\Sigma(E, \vec{p}) = \Sigma_{T=0}(E, \vec{p}) + \Sigma_\beta(E, \vec{p}) \quad (3.19)$$

As the self-energy is split into a  $T = 0$  term and  $\beta$  or non-zero  $T$  term.  $\Sigma_{T=0}$  is given above. The second term is found to be

$$\Sigma_\beta(E, \vec{p}) = \frac{\alpha}{4\pi^2} [I_A(\not{p} - m_R) + \quad (3.20)$$

$$I|_{\not{p}=m_R} + I|_{\not{p}=m_R} (p^2 - m_R^2) + \dots] + O(\exp(-m/T)) \quad (3.21)$$

$$I_A = 8\pi \int \frac{dk}{k} n_B(k) \quad (3.22)$$

$$I_\mu = 2 \int \frac{d^3k}{k_0} n_B(k) \frac{(k_0, \vec{k})}{E_p k_0 - \vec{p} \cdot \vec{k}} \quad (3.23)$$

$$L_\mu = -\frac{1}{E_p} \int d^3k n_B(k) \frac{(k_0, \vec{k})}{(E_p k_0 - \vec{p} \cdot \vec{k})^2} \quad (3.24)$$

$$E_p = \sqrt{p^2 + m_R^2} \quad (3.25)$$

Where in the low-temperature case ( $T \ll m_e$ ) the rest of the series is suppressed on the order  $\exp(-m/T)$ . The mass shift in this limit is found to be

$$\delta m_\beta = \frac{\pi\alpha T^2}{3m} \quad (3.26)$$

The details of this result are found in [19]. For the  $T \gg m$  case the renormalized fermion propagator must be included in the self-energy calculations. The full expression for the renormalized mass for all  $T$  is given as

$$m_{phys}^2 = m^2 + \frac{2\pi\alpha T^2}{3} + \frac{\alpha}{2\pi^2} m^2 J_A(p) + \frac{4\alpha}{\pi} \int_0^\infty \frac{l^2 dl}{E_l} n_F(E_l) \quad (3.27)$$

$$J_A = \int \frac{d^3l}{E_l} n_F(E_l) \left[ \frac{1}{E_p E_l + m^2 - \vec{p} \cdot \vec{l}} - \frac{1}{E_p E_l - m^2 + \vec{p} \cdot \vec{l}} \right] \quad (3.28)$$

Where  $n_F(E) = \frac{1}{e^{\beta E} + 1}$ . It is important to note the energy dependence in the last two terms of Equation 3.27, which drop out for low  $T$ . The renormalization constant of

the wave function is found to be

$$Z_2^{-1} = Z_2^{-1}(T = 0) - \frac{2\alpha}{\pi} \int \frac{dk}{k} n_B(k) + \frac{\alpha\pi T^2}{3E^2} + J_A - \frac{J_B^0}{E} \quad (3.29)$$

$$J_B^\mu = \int \frac{d^3l}{E_l} n_F(E_l) \left[ \frac{(E_p + E_l, \vec{p} + \vec{l})}{E_p E_l + m^2 - \vec{p} \cdot \vec{l}} - \frac{(E_p - E_l, \vec{p} + \vec{l})}{E_p E_l - m^2 + \vec{p} \cdot \vec{l}} \right] \quad (3.30)$$

The full calculations of which are included in [20] [19]. The constants  $m_{phys}^2$  and  $Z_2^{-1}$  can also be written in terms of Masood's abc functions in the limit  $T \gg m$ ,

$$m_{phys}^2 = m^2 \left( 1 + \frac{6\alpha}{\pi} b(m\beta) \right) + \frac{4\alpha}{\pi} m T a(m\beta) + \frac{2\alpha\pi T^2}{3} \left( 1 - \frac{6}{\pi^2} c(m\beta) \right) \quad (3.31)$$

$$Z_2^{-1} = Z_2^{-1}(T = 0) - \frac{2\alpha}{\pi} \int \frac{dk}{k} n_B(k) + \quad (3.32)$$

$$\frac{\alpha\pi T^2}{3E^2} \left( 1 - c(m\beta) + m\beta a(m\beta) \right) - \frac{5\alpha}{\pi} b(m\beta) \quad (3.33)$$

Where Masood's abc functions in the limit  $T \gg m$  only are,

$$a(m\beta) = \ln(1 + e^{-m\beta}) \quad (3.34)$$

$$b(m\beta) = \sum_{n=1}^{\infty} (-1)^n Ei(-nm\beta) \quad (3.35)$$

$$c(m\beta) = \sum_{n=1}^{\infty} \frac{(-1)^n}{n^2} e^{-nm\beta} \quad (3.36)$$

Where  $Ei(x)$  is the exponential integral, again. When discussing the limit  $T \ll m$  Masood's abc functions are very small due to the exponential and we have, approximately in this limit [2],

$$m_{phys}^2 \simeq m^2 + \frac{2\pi\alpha T^2}{3} \quad (3.37)$$

$$Z_2^{-1} \simeq Z_2^{-1}(T = 0) - \frac{2\alpha}{\pi} \int \frac{dk}{k} n_B(k) + \frac{\alpha\pi T^2}{3E^2} \quad (3.38)$$

To compute the renormalization of the QED vertex, we must calculate the vacuum polarization matrix element to first order (See Figure 2.5 where we have taken the upper internal leg momentum as  $k - p$ ) and dimensionally regularize,

$$i\Pi_{\mu\nu}(p) = ie^2 \int \frac{d^4k}{(2\pi)^4} \text{tr} \left[ \gamma_\mu \frac{(\not{k} - \not{p} + m)}{(k-p)^2 - m^2 + \epsilon} \gamma_\nu \frac{i(\not{k} + m)}{k^2 - m^2 + i\epsilon} \right] \quad (3.39)$$

$$= \frac{\alpha}{\pi} (-p^2 g_{\mu\nu} + p_\mu p_\nu) \frac{1}{3\epsilon} + \dots \quad (3.40)$$

Where again  $\frac{1}{\epsilon}$  is our regularization parameter. The vertex correction also requires contributions from other diagrams, the results of those corresponding computations are simply stated (details can be found within [20]) as

$$M_\mu^{total}(T=0) = Z_2^{-1} Z_3^{-1/2} (M_\mu^{(0)} + M_\mu^{SE} + M_\mu^{CT} + M_\mu^V + M_\mu^{VP}) \quad (3.41)$$

$$= -e_R \bar{u}(p') \left( \gamma_\mu - i \frac{\alpha}{2\pi} \sigma_{\mu\nu} q^\nu \frac{1}{2m_R} \right) u(p) \quad (3.42)$$

Where the renormalized electron charge is defined  $e_R = e_0 Z_3^{1/2} \approx (1 - \frac{\alpha}{6\pi\epsilon})$  for  $T=0$ . Renormalization at  $T \ll m$  gives us the same result, so there is no significant contribution to charge renormalization at low temperature [20]. At high temperature  $T \gg m$ , we find that

$$Z_3 = 1 + \frac{e^2}{6} \frac{1}{m^2 \beta^2} \quad (3.43)$$

Thus the constant scales as  $\frac{T^2}{m^2}$ . This of course implies the possibility of significant modifications to observables at high enough temperatures, such as the early universe or compact stellar interiors. For the exact calculations we refer to Ahmed and Masood [1].

It is worth it to mention why these specific cases  $T \gg m$  and  $T \ll m$  are examined. This scenario for  $T \ll m$  corresponds to the temperatures of the early universe around 1 second after the Big Bang. Additionally, this regime is important because most of

the current universe exists in this regime, such as stellar cores. Conversely, there are some stars which are very hot, as well as the very early universe that require us to calculate  $T \gg m$  in order to fully understand the complete dynamics of the universe. For that reason we have to explore both limits. However, that does not yet incorporate the effects of density and particle exchange. For a thorough analysis of the early universe and stellar interiors, we will need to understand how the effects of density play a role, which is the subject of the next section.

### 3.4 Incorporation of density effects

In our analysis we neglected to include the effects of a dense medium, which is necessary for the understanding of environments such as compact stellar media or the early universe. If we wish to incorporate density effects, and then subsequently check the limits where  $T \gg \mu$  and  $T \ll \mu$ , we can modify the distribution functions to incorporate this effect. Density implies some kind of mass per unit volume, and for QED our intermediary particle is the photon which is massless, the Bose-Einstein distribution function remains unmodified as

$$n_B(k) = \frac{1}{e^{\beta k_0} - 1} \quad (3.44)$$

Where again  $\beta = 1/T$ . The positron(+) and electron(-) Fermi-Dirac distribution functions are modified with a chemical potential  $\mu$

$$n_F(E \pm \mu) = \frac{1}{e^{\beta(E \pm \mu)} + 1} \quad (3.45)$$

Recalculation of the renormalized constants gives us modifications due to density effects, which are written in terms of the  $I$ ,  $\mathcal{J}$  integrals, which are given in terms of the  $a'b'c'd'$  and  $a''b''c''d''$  functions, relevant only in the limit of temperature and

chemical potential  $\mu > T$

$$m_{phys}^2(T, \pm\mu) = m_0^2(T = \mu = 0) + \frac{2\pi\alpha T^2}{3} + \quad (3.46)$$

$$\frac{4\alpha}{\pi^2} m^2 \int_m^\infty \frac{dE_l}{E_l} n_F(E_l \pm \mu) + \frac{4\alpha}{\pi} \int_0^\infty \frac{l^2 dl}{E_l} n_F(E_l \pm \mu) \quad (3.47)$$

$$Z_2^{-1}(T, \mu) = Z_2^{-1}(T = \mu = 0) - \quad (3.48)$$

$$\frac{\alpha}{4\pi} \left[ I_A - \frac{I^0}{E} - \frac{4\pi}{E^2} I_1 - 12\pi I_2 - \frac{\pi E^2}{2} I_3 \right] \quad (3.49)$$

$$Z_3(T, \mu) \cong 1 + \frac{2e^2}{m^2\pi^2} \left[ \mathcal{J}_1 + \frac{1}{4} \left[ m^2 + \frac{\omega^2}{3} \right] \mathcal{J}_2 - \frac{1}{4} m^4 \mathcal{J}_3 \right] \quad (3.50)$$

Where for  $Z_2^{-1}$  we use either  $I'_1, I'_2, I'_3$  for the electron,

$$I'_1(T, \mu) = \int_m^\infty E dE n_F(E - \mu) = \frac{\mu^2}{2} \left( 1 - \frac{m^2}{\mu^2} \right) - \frac{a'(m\beta, \mu)}{\beta} - \frac{c'(m\beta, \mu)}{\beta^2} \quad (3.51)$$

$$I'_2(T, \mu) = \int_m^\infty \frac{dE}{E} n_F(E - \mu) = \ln \frac{\mu}{m} + b'(m\beta, \mu) \quad (3.52)$$

$$I'_3(T, \mu) = \int_m^\infty \frac{dE}{E^3} n_F(E - \mu) = \frac{1}{2m^2} \left( 1 - \frac{m^2}{\mu^2} \right) - \frac{1}{4\mu^2} + \frac{n_F(\mu - m)}{m^2} + \quad (3.53)$$

$$\frac{\beta}{m} \frac{e^{-\beta(\mu-m)}}{(1 + e^{-\beta(\mu-m)})^2} + d'(m\beta, \mu) \quad (3.54)$$

The corresponding  $a'b'c'd'$  functions in this limit are given as

$$a'(m\beta, \mu) = \mu \ln 2 - m \ln 1 + e^{-\beta(\mu-m)} \quad (3.55)$$

$$b'(m\beta, \mu) = \sum_{n=1}^{\infty} (-1)^n e^{-n\beta\mu} Ei(nm\beta) \quad (3.56)$$

$$c'(m\beta, \mu) = \frac{\pi^2}{12} + \sum_{n=1}^{\infty} (-1)^n e^{-n\beta(\mu-m)} \quad (3.57)$$

$$d'(m\beta, \mu) = \sum_{n=1}^{\infty} (-1)^n \frac{(n\beta)^2}{2} \left( \ln \frac{\mu}{m} - \frac{1}{2n\beta\mu} + Ei(nm\beta) \right) \quad (3.58)$$

and  $I_1, I_2, I_3$  for the positron,

$$I_1(T, \mu) = \int_m^\infty E dE n_F(E + \mu) = \frac{a''(m\beta, \mu)}{\beta} - \frac{c''(m\beta, \mu)}{\beta^2} \quad (3.59)$$

$$I_2(T, \mu) = \int_m^\infty \frac{dE}{E} n_F(E + \mu) = b''(m\beta, \mu) \quad (3.60)$$

$$I_3(T, \mu) = \int_m^\infty \frac{dE}{E^3} n_F(E + \mu) = \frac{n_F(\mu - m)}{m^2} + \quad (3.61)$$

$$\frac{\beta}{m} \frac{e^{-\beta(\mu+m)}}{(1 + e^{-\beta(\mu+m)})^2} + d''(m\beta, \mu) \quad (3.62)$$

The corresponding  $a''b''c''d''$  functions in this limit are given as

$$a''(m\beta, \mu) = m \ln 1 + e^{-\beta(\mu+m)} \quad (3.63)$$

$$b''(m\beta, \mu) = \sum_{n=1}^{\infty} (-1)^n e^{-n\beta\mu} Ei(-nm\beta) \quad (3.64)$$

$$c''(m\beta, \mu) = \sum_{n=1}^{\infty} (-1)^n e^{-n\beta(\mu+m)} \quad (3.65)$$

$$d''(m\beta, \mu) = \sum_{n=1}^{\infty} (-1)^n \frac{(n\beta)^2}{2} e^{-n\beta\mu} Ei(-nm\beta) \quad (3.66)$$

Where  $Ei(x)$  is the exponential integral,  $Ei(x) = \int_{-\infty}^x \frac{dt e^{-t}}{t}$ .

For  $Z_3$  the  $\mathcal{J}_i$  are averaged over the distribution function for both  $\pm\mu$  thus we have the same function for both positrons and electrons,

$$\mathcal{J}_1(T, \mu) = \frac{1}{2} \int_m^\infty E dE [n_F(E + \mu) + n_F(E - \mu)] \quad (3.67)$$

$$= \frac{1}{2} \left[ \frac{\mu^2}{2} \left( 1 - \frac{m^2}{\mu^2} \right) - \frac{a(m\beta, \mu) + a'(m\beta, \mu)}{\beta} - \frac{c(m\beta, \mu) + c'(m\beta, \mu)}{\beta^2} \right] \quad (3.68)$$

$$\mathcal{J}_2(T, \mu) = \frac{1}{2} \int_m^\infty \frac{dE}{E} [n_F(E + \mu) + n_F(E - \mu)] \quad (3.69)$$

$$= \frac{1}{2} \left[ \ln \frac{\mu}{m} + b(m\beta, \mu) + b'(m\beta, \mu) \right] \quad (3.70)$$

$$\mathcal{J}_3(T, \mu) = \frac{1}{2} \int_m^\infty \frac{dE}{E^3} [n_F(E + \mu) + n_F(E - \mu)] \quad (3.71)$$

$$= \frac{1}{2} \left[ \frac{1}{2m^2} \left( 1 - \frac{m^2}{\mu^2} \right) - \frac{1}{4\mu^2} + \frac{n_F(\mu + m) + n_F(\mu - m)}{m^2} + \right. \quad (3.72)$$

$$\left. \frac{\beta}{m} \left[ \frac{e^{-\beta(\mu-m)}}{(1 + e^{-\beta(\mu-m)})^2} + \frac{e^{-\beta(\mu+m)}}{(1 + e^{-\beta(\mu+m)})^2} \right] + d'(m\beta, \mu) + d(m\beta, \mu) \right] \quad (3.73)$$

It is worth a second mention that the primed integrals are for the electron only, and the unprimed integrals for the positron. The full details of obtaining these quantities can be found in [35]. As mentioned earlier, the main significance is of the limit  $\mu > T > m$ , since this is the limit in which superdense media like neutron stars exist at. In the case of  $\mu \gg m \gg T$  we recover the classical limit, with the primed and double-primed abc functions going to zero, and the positron  $I$  integrals as well.

### 3.5 Calculating $J_A$

To give a flavor for the calculational details, we can show the result of  $J_A$  using some simple integration techniques. Starting from [2] Eq 2.2,

$$J_A = \int \frac{d^3l}{E_l} n_F^\pm \left[ \frac{1}{E_p E_l + m^2 - \vec{p} \cdot \vec{l}} - \frac{1}{E_p E_l - m^2 + \vec{p} \cdot \vec{l}} \right] \quad (3.74)$$

$$= \int_0^{2\pi} d\phi \int_0^\infty \int_{-1}^1 \frac{l^2 dl}{E_l} \frac{d\mu}{1} n_F^\pm \left[ \frac{1}{E_p E_l + m^2 - pl\mu} - \frac{1}{E_p E_l - m^2 + pl\mu} \right] \quad (3.75)$$

$$= \frac{-2\pi}{p} \int_0^\infty \frac{l dl}{E_l} n_F^\pm \left( \ln \left[ \frac{E_p E_l + m^2 - pl}{E_p E_l + m^2 + pl} \right] + \ln \left[ \frac{E_p E_l - m^2 + pl}{E_p E_l - m^2 - pl} \right] \right) \quad (3.76)$$

$$= \frac{-2\pi}{p} \int_0^\infty dE_l n_F^\pm \left( \ln \left[ \frac{1 + \frac{2m^2 p}{m^2 E_l}}{1 - \frac{2m^2 p}{m^2 E_l}} \right] \right) \quad (3.77)$$

$$\approx \frac{-2\pi}{p} \int_0^\infty dE_l n_F^\pm \left( \frac{4m^2 p}{m^2 E_l} \right) \quad (3.78)$$

$$\approx -8\pi \int_0^\infty \frac{dE_l}{E_l} n_F^\pm \quad (3.79)$$

Where we use the assumption that  $E_l \gg m$  and  $l dl \approx E_l dE_l$  to first order. We use  $\cos(\theta) = \mu$  as an integration variable in the second step, Taylor expand  $\ln(1+x)$  in powers of  $\frac{m}{E}$ , and the integral identity

$$\int_{-1}^1 \frac{dx}{A+Bx} = \frac{1}{B} \ln \left( \frac{A+B}{A-B} \right) \quad (3.80)$$

for evaluation in the next one. The approximation (for  $E_l \gg m$ ) is also used,

$$l = (m^2 - E_l^2)^{1/2} \simeq E_l \left( 1 - \frac{m^2}{2E_l^2} \right) \quad (3.81)$$

### 3.5.1 Calculating $J_B$ and $J_B^0/E$

Similarly, We can use related techniques to find  $J_B^0/E_p$ , another integral used in these FTD calculations. For example, in [2] we have the parts of the self energy calculations,

$$\Sigma(p) = A(p)E\gamma_0 - B(p)\mathbf{p} \cdot \boldsymbol{\gamma} - C(p) \quad (3.82)$$

$$A(p) = \frac{\alpha}{4\pi^2}(I^A + I^0/E - J_A + J_B^0/E) \quad (3.83)$$

$$B(p) = \frac{\alpha}{4\pi^2}(I^A + \mathbf{I} \cdot \mathbf{p}/p^2 - J_A + \mathbf{J}_B \cdot \mathbf{p}/p^2) \quad (3.84)$$

$$C(p) = \frac{\alpha}{4\pi} m(I^A - 2J^A) \quad (3.85)$$

where  $J_B$  is given in Donoghue et al. [20] as

$$\vec{J}_B^\mu = \int \frac{d^3l}{E_l} n_F \left[ \frac{(E_p + E_l, \vec{p} + \vec{l})}{E_p E_l + m^2 - \vec{p} \cdot \vec{l}} - \frac{(E_p - E_l, \vec{p} + \vec{l})}{E_p E_l - m^2 + \vec{p} \cdot \vec{l}} \right] \quad (3.86)$$

If we are attempting to compute  $A(p)$  then we will need  $J_A$ ,  $I^A$ ,  $I^0$  and  $J_B^0/E$ . Now we compute the latter quantity,

$$J_B^0/E_p = \frac{1}{E_p} \int \frac{d^3l}{E_l} n_F(E_l) \left[ \frac{E_p + E_l}{E_p E_l + m^2 - \vec{p} \cdot \vec{l}} - \frac{E_p - E_l}{E_p E_l - m^2 + \vec{p} \cdot \vec{l}} \right] \quad (3.87)$$

$$= \frac{2\pi}{E_p} \int \frac{l^2 dl}{E_l} n_F(E_l) \int_{-1}^1 d\mu \left[ \frac{E_p + E_l}{E_p E_l + m^2 - pl\mu} - \frac{E_p - E_l}{E_p E_l - m^2 + pl\mu} \right] \quad (3.88)$$

$$= \frac{2\pi}{E_p} \int \frac{l^2 dl}{E_l} n_F(E_l) \left[ \frac{E_p + E_l}{-pl} \ln \left[ \frac{E_p E_l + m^2 - pl}{E_p E_l + m^2 + pl} \right] - \frac{E_p - E_l}{pl} \ln \left[ \frac{E_p E_l - m^2 + pl}{E_p E_l - m^2 - pl} \right] \right] \quad (3.89)$$

$$\approx -8\pi b + \frac{8\pi T^2}{E_p^2} c + \frac{8\pi T \mathcal{M}}{E_p^2} a \quad (3.90)$$

In this calculation we use  $l dl \approx E_l dE_l$ , integrals from Appendix A in [34], and the integral

$$\int_{-1}^1 d\mu \left[ \frac{A_+}{B_+ + C_- \mu} - \frac{A_-}{B_- + C_+ \mu} \right] = \quad (3.91)$$

$$= \frac{A_+}{C_-} \ln \left( \frac{B_+ + C_-}{B_+ - C_-} \right) - \frac{A_-}{C_+} \ln \left( \frac{B_- + C_+}{B_- - C_+} \right) \quad (3.92)$$

where  $A_{\pm} = E_p \pm E_l$ ,  $B_{\pm} = E_p E_l \pm m^2$  and  $C_{\pm} = \pm pl$ . The approximation (for  $E_l \gg m$ ) is also used,

$$l = (m^2 - E_l^2)^{1/2} \simeq E_l \left( 1 - \frac{\mathcal{M}^2}{2E_l^2} \right) \quad (3.93)$$

### 3.6 Renormalization at FTD with magnetic field B

Finally, we are prepared to move on to the contribution of magnetic field properties in such media. Considering that it is accounted by observation that the highest magnetic fields have been noted in neutron stars (and especially magnetars) we should find it worthwhile to consider the analysis of particle propagation under finite temperature and density with a magnetic field. This treatment will cover cases  $\frac{eB}{m} > m > T$  and  $\frac{eB}{m} > T > m$  in order to determine the properties of such stellar media extensively.

To give an example, let us say we wish to integrate contributions from a magnetic field B into a quantum field theory at finite temperature and density [30] [31] for a certain observable such as the electron mass. The results can then be applied to equations of state for compact objects such as neutron stars in order to make predictions of a star's structure.

First we acknowledge that electrons obey Fermi-Dirac statistics (Section 2.2.2) which allow us to model the energy distribution of a system of electrons, where the

number of electrons in a given energy level  $l$  is given by

$$n_F(E_l) = \frac{1}{e^{(E_l - \mu)/kT} + 1} \quad (3.94)$$

Next we make a substitution of  $E_l = \sqrt{m^2 + eB(2l + 1)}$  where we've added a magnetic field contribution to the energy from a quantization of charged particles in a magnetic field, otherwise known as Landau levels.

Recall that the renormalization constant for the electron mass is given by [18] [2]

$$m_{phys}^2 = m^2 + \frac{2\pi\alpha T^2}{3} + \frac{\alpha}{2\pi^2} m^2 J_A(p) + \frac{4\alpha}{\pi} \int_0^\infty \frac{l^2 dl}{E_l} n_F(E_l) \quad (3.95)$$

Where the  $J_A$  integrand is another term proportional to  $E^n$ . Evaluating the integrals approximately we find a solution and can obtain a renormalized mass in the presence of a magnetic field at finite temperature and density.

$$\int_0^\infty \frac{l^2 dl}{E_l} n_F = \int_0^\infty \frac{l^2 dl}{E_l} \frac{1}{e^{(E_l - \mu)/kT} + 1} \quad (3.96)$$

$$= \int_0^\infty \frac{l^2 dl}{\sqrt{m^2 + eB(2l + 1)}} \frac{1}{e^{(\sqrt{m^2 + eB(2l + 1)} - \mu)/kT} + 1} \quad (3.97)$$

$$\approx -\frac{eB + m^2}{(eB/kT)^3} + \dots \quad (3.98)$$

In leading order we see a sign change in the result due to the magnetic field, which might imply a renormalized mass that is lighter instead of heavier under these circumstances. By using a slightly different notation,

$$m_{phys} \simeq m \left( 1 + \frac{\delta m}{m} \right) \quad (3.99)$$

$$\frac{\delta m}{m} \simeq -\frac{2\alpha}{\pi m^2} \frac{eB + m^2}{(eB/kT)^3} + \frac{\pi\alpha T^2}{3m^2} + \frac{\alpha}{4\pi^2} J_A(p) + \dots \quad (3.100)$$

To first order, we can see that the renormalized mass now depends on the magnetic field  $B$ . This gives some idea that the magnetic field might produce changes in renor-

malization constants at some intensity of the magnetic field. We will investigate this situation more fully in the next chapter.

## CHAPTER 4

### CALCULATION OF MAGNETIC FIELD CONTRIBUTION

During the computation of perturbative corrections to the QED parameters, integrals over the energy play a crucial role in the computation of background effects. Here we elaborate on the computational details as well as present our own work as an investigation of the magnetic field effects at finite temperature and density.

#### 4.1 Electron mass in presence of magnetic field

One of the self energy integrals for the electron shows up as a correction to the electron mass,

$$\int p^2 dp \frac{n_F}{E} \quad (4.1)$$

which was originally evaluated in [2]. In order to add a correction to the self energy due to the presence of a magnetic field, we modify the evaluation of this integral. Specifically, we make a transformation such that  $E^2$  is defined as

$$E^2 = p^2 + m^2 + eB(2k + 1)$$

Where we have included a magnetic field contribution to the energy of the electron,  $eB(2k + 1)$ , where  $k$  corresponds to the Landau level here. This modifies the fermion distribution function  $n_F^\pm(E, \pm\mu)$  through its dependence on the particle energy  $E$

$$n_F^\pm(E, \pm\mu) = \frac{1}{e^{\beta(E \pm \mu)} + 1} \quad (4.2)$$

$$= \sum_{n=0}^{\infty} (-1)^n e^{n\beta(E \pm \mu)} \quad (4.3)$$

where  $\beta = 1/T$ , and  $\mu$  is the chemical potential, as before. We expanded  $n_F$  as a geometric series in the last step.

We borrow the integrals directly from Masood [32] to evaluate Equation 4.1. For a simple case of  $k = 0$ , our electron energy becomes

$$E^2 = p^2 + m^2 + eB \quad (4.4)$$

$$= p^2 + \mathcal{M}^2 \quad (4.5)$$

with the use of a substitution  $\mathcal{M}^2 = m^2 + eB$ . By rewriting the integrand totally in terms of the energy, we can solve the integral, Equation 4.1, by a substitution of variables  $p \rightarrow E$  and get

$$\int p^2 dp \frac{n_F}{E} = \int E \left(1 - \frac{\mathcal{M}^2}{E}\right)^{1/2} n_F^\pm(E, \pm\mu) dE \quad (4.6)$$

We now have a series written entirely in terms of energy, where we utilize the binomial theorem and discard higher order terms in the infinite series giving

$$\int p^2 dp \frac{n_F}{E} = \int E_p \left(1 - \frac{\mathcal{M}^2}{E}\right)^{1/2} n_F^\pm(E, \pm\mu) dE \quad (4.7)$$

$$= \int E dE n_F^\pm - \frac{\mathcal{M}^2}{2} \int \frac{dE}{E} n_F^\pm + \frac{3\mathcal{M}^4}{8} \int \frac{dE}{E^3} n_F^\pm + \dots \quad (4.8)$$

Making the substitution  $\mathcal{M}^2 = m^2 + eB$  in those integrals from [32] we find,

$$\int E dE n_F^\pm = \frac{c(\mathcal{M}\beta, \pm\mu)}{\beta^2} + \frac{\mathcal{M}}{\beta} a(\mathcal{M}\beta, \pm\mu) \quad (4.9)$$

$$\int \frac{dE}{E} n_F^\pm = b(\mathcal{M}\beta, \pm\mu) \quad (4.10)$$

$$\int \frac{dE}{E^3} n_F^\pm = \beta^2 h(\mathcal{M}\beta, \pm\mu) \quad (4.11)$$

Given that the abc functions modified to incorporate a magnetic field are

$$a(\mathcal{M}\beta, \pm\mu) = \ln(1 + e^{-\beta(\mathcal{M}\pm\mu)}) \quad (4.12)$$

$$b(\mathcal{M}\beta, \pm\mu) = \sum_{n=1}^{\infty} (-1)^n e^{\mp n\beta\mu} Ei(-n\beta\mathcal{M}) \quad (4.13)$$

$$c(\mathcal{M}\beta, \pm\mu) = \sum_{n=1}^{\infty} \frac{(-1)^n}{n^2} e^{-n\beta(\mathcal{M}\pm\mu)} \quad (4.14)$$

$$h(\mathcal{M}\beta, \pm\mu) = - \sum_{n=1}^{\infty} (-1)^n \left[ \frac{\beta^2 n^2}{2} Ei(-n\beta\mathcal{M}) + n\beta \frac{e^{-n\beta\mathcal{M}}}{\mathcal{M}} \right] e^{\mp n\beta\mu} \quad (4.15)$$

We can substitute back into 4.8 to find that

$$\int p^2 dp \frac{n_F}{E_p} = \int E_p dE_p n_F^{\pm} - \frac{\mathcal{M}^2}{2} \int \frac{dE_p}{E_p} n_F^{\pm} + \frac{3\mathcal{M}^4}{8} \int \frac{dE_p}{E_p^3} n_F^{\pm} \quad (4.16)$$

$$= \frac{c(\beta\mathcal{M}, \pm\mu)}{\beta^2} + \frac{\mathcal{M}}{\beta} a(\beta\mathcal{M}, \pm\mu) \quad (4.17)$$

$$- \frac{m^2 + eB}{2} b(\beta\mathcal{M}, \pm\mu) + \frac{3(m^2 + eB)^2}{8} \beta^2 h(\beta\mathcal{M}, \pm\mu) \quad (4.18)$$

These results are valid for  $T > \mu$ . This puts us in a nice position to calculate the limit where  $\frac{eB}{m} > T > m > \mu$  and  $T > \mu > m > \frac{eB}{m}$ . Our final solution to the integral being

$$\int p^2 dp \frac{n_F}{E_p} = \frac{1}{\beta^2} \sum_{n=1}^{\infty} \frac{(-1)^n}{n^2} e^{-n\beta(\mathcal{M}\pm\mu)} + \frac{\mathcal{M}}{\beta} \ln(1 + e^{-\beta(\mathcal{M}\pm\mu)}) \quad (4.19)$$

$$- \frac{\mathcal{M}^2}{2} \sum_{n=1}^{\infty} (-1)^n e^{\mp n\beta\mu} Ei(-n\beta\mathcal{M}) \quad (4.20)$$

$$- \frac{3\mathcal{M}^4}{8} \beta^2 \sum_{n=1}^{\infty} (-1)^n \left[ \frac{\beta^2 n^2}{2} Ei(-n\beta\mathcal{M}) + n\beta \frac{e^{-n\beta\mathcal{M}}}{\mathcal{M}} \right] e^{\mp n\beta\mu} \quad (4.21)$$

Plugging this result back into the renormalized mass [2],

$$m_{phys}^2 = m^2 + \frac{2}{3}\alpha\pi T^2 + \frac{\alpha^2}{2\pi^2}\mathcal{M}^2 J_A(p) + \frac{4\alpha}{\pi} \int_0^\infty p^2 dl \frac{n_F}{E} \quad (4.22)$$

$$= m^2 + \frac{2}{3}\alpha\pi T^2 - \frac{\alpha^2}{2\pi^2}\mathcal{M}^2 8\pi b(\beta\mathcal{M}, \pm\mu) \quad (4.23)$$

$$+ \frac{4\alpha}{\pi} \left[ \frac{c(\beta\mathcal{M}, \pm\mu)}{\beta^2} + \frac{\mathcal{M}}{\beta} a(\beta\mathcal{M}, \pm\mu) \right] \quad (4.24)$$

$$\left. - \frac{m^2 + eB}{2} b(\beta\mathcal{M}, \pm\mu) + \frac{3(m^2 + eB)^2}{8} \beta^2 h(\beta\mathcal{M}, \pm\mu) \right] \quad (4.25)$$

Where  $J_A \approx -8\pi \frac{\mathcal{M}^2}{m^2} b(\beta\mathcal{M}, \pm\mu)$  [32].

#### 4.1.1 Taylor expansion of Masood's functions

It is worthwhile to show the direct dependence on a magnetic field B of Masood's abc functions through a Taylor expansion. Given  $\mathcal{M} = \sqrt{m^2 + eB(2k+1)}$ , to first order, we can show the dependence on a magnetic field B,

$$\begin{aligned} a(\beta\mathcal{M}, \pm\mu) &= \ln(1 + e^{-\beta(\mathcal{M}\pm\mu)}) \\ &= e^{-\beta(\mathcal{M}\pm\mu)} - \frac{e^{-2\beta(\mathcal{M}\pm\mu)}}{2} + \frac{e^{-3\beta(\mathcal{M}\pm\mu)}}{3} - \dots \\ &\approx 1 - \beta \left( m \left( 1 + \frac{eB(2k+1)}{2m^2} \right) \pm \mu \right) \\ &= 1 - \frac{e\beta B(2k+1)}{2m} - \beta m \mp \beta\mu \end{aligned}$$

Similarly,

$$\begin{aligned} c(\beta\mathcal{M}, \pm\mu) &= \sum_{n=1}^{\infty} \frac{(-1)^n}{n^2} \exp \left\{ -n\beta \left( m \sqrt{1 + \frac{eB(2k+1)}{m^2}} \pm \mu \right) \right\} \\ &\approx \sum_{n=1}^{\infty} \frac{(-1)^n}{n^2} \left[ 1 - \frac{ne\beta B(2k+1)}{2m} - n\beta m \mp n\beta\mu \right] \end{aligned}$$

Where we have used the expansions,

$$\begin{aligned}\ln(1+x) &= x - \frac{x^2}{2} + \frac{x^3}{3} - \dots \\ e^x &= 1 + \frac{x}{1!} + \frac{x^2}{2!} + \frac{x^3}{3!} + \dots \\ \sqrt{1+x} &= 1 + \frac{x}{2} - \frac{x^2}{8} + \frac{x^3}{16} + \dots\end{aligned}$$

It is worth mentioning that the B-dependent term in the final result requires multiplication by certain factors in order for the overall quantity to remain unit-less. Now, we wish to discuss some of the relevant limits to the regime of neutron stars.

## 4.2 Evaluation at Limits

By factoring out  $m$  from  $\mathcal{M} = \sqrt{m^2 + eB}$  we obtain an expression that is useful for evaluation of the limits,  $\mathcal{M} = m\sqrt{1 + \frac{eB}{m^2}}$ , where we evaluate the electron mass when  $eB \ll m^2$  and  $eB \gg m^2$ , where comparisons here are made in the unit  $\text{MeV}^2$ . Of course, when B is very small,  $\frac{eB}{m^2} \ll 1$ , and we have  $m\sqrt{1 + \frac{eB}{m^2}} \simeq m$  and  $m_{phys}^2$  and the existing results are all reproduced (for all Landau levels) as  $m\sqrt{1 + \frac{eB}{m^2}(2k+1)} \simeq m$  in the limit  $\frac{eB}{m^2} \ll 1$ . The most relevant limits for neutron stars are when  $eB \gg m^2$  and  $\mu > T$ , to be further discussed. For  $eB \gg m^2$  a significant correction to the electron mass occurs, since  $\frac{eB}{m^2} \gg 1$ , we have, by the binomial theorem and the neglect of higher order terms,

$$\mathcal{M} = m\sqrt{1 + \frac{eB}{m^2}} \simeq m\left(1 + \frac{1}{2}\frac{eB}{m^2} + \frac{3}{8}\frac{(eB)^2}{m^4} + \dots\right) \quad (4.26)$$

$$\simeq m\left(1 + \frac{1}{2}\frac{eB}{m^2}\right) \quad (4.27)$$

$$\simeq \frac{1}{2}\frac{eB}{m} \quad (4.28)$$

Replacing this we find that  $m_{phys}^2$  is modified to become, with higher order corrections included and a Landau level  $k = 0$  as,

$$m_{phys}^2 = m^2 + \frac{2}{3}\alpha\pi T^2 - \frac{\alpha^2}{2\pi^2} \frac{(eB)^2}{4m^2} 8\pi b\left(\frac{\beta eB}{2m}, \pm\mu\right) \quad (4.29)$$

$$+ \frac{4\alpha}{\pi} \left[ \frac{c\left(\frac{\beta eB}{2m}, \pm\mu\right)}{\beta^2} + \frac{eB}{2m\beta} a\left(\frac{\beta eB}{2m}, \pm\mu\right) \right] \quad (4.30)$$

$$- \frac{(eB)^2}{8m^2} b\left(\frac{\beta eB}{2m}, \pm\mu\right) + \frac{3(eB)^4}{2^7 m^4} \beta^2 h\left(\frac{\beta eB}{2m}, \pm\mu\right) \quad (4.31)$$

To extend our results across all Landau levels for  $eB \gg m^2$ , we simply restore  $k$  in the substitution  $\frac{eB}{m^2} \rightarrow \frac{eB}{m^2}(2k+1)$ . This leaves the  $eB \ll m^2$  case unchanged, while the  $eB \gg m^2$  case is now,

$$\mathcal{M} = m\sqrt{1 + \frac{eB}{m^2}(2k+1)} \simeq \frac{1}{2} \frac{eB}{m}(2k+1) \quad (4.32)$$

Giving us a  $m_{phys}^2$  result for all Landau levels when  $\frac{eB}{m^2} \gg 1$ ,

$$m_{phys}^2 = m^2 + \frac{2}{3}\alpha\pi T^2 - \frac{\alpha^2}{2\pi^2} \frac{(eB(2k+1))^2}{4m^2} 8\pi b\left(\frac{\beta eB}{2m}(2k+1), \mp\mu\right) \quad (4.33)$$

$$+ \frac{4\alpha}{\pi} \left[ \frac{c\left(\frac{\beta eB}{2m}(2k+1), \mp\mu\right)}{\beta^2} + \frac{eB(2k+1)}{2m\beta} a\left(\frac{\beta eB}{2m}(2k+1), \mp\mu\right) \right] \quad (4.34)$$

$$- \frac{(eB(2k+1))^2}{8m^2} b\left(\frac{\beta eB}{2m}(2k+1), \mp\mu\right) \quad (4.35)$$

$$+ \frac{3(eB(2k+1))^4}{2^7 m^4} \beta^2 h\left(\frac{\beta eB}{2m}(2k+1), \mp\mu\right) \quad (4.36)$$

We can see from this expression that the renormalized electron mass now depends clearly on  $B$ , the magnetic field. Simulation will suggest to us whether this dependence is significant. To conclude, in the limit  $\frac{eB}{m} > T > m > \mu$  we see a dependence on the magnetic field arise, and in the limit  $T > \mu > m > \frac{eB}{m}$  we see existing results reproduced Masood [2].

## 4.2.1 Renormalization Constants

We are now in a position to give the renormalization constants with magnetic field modifications. As  $\frac{eB}{m} \ll m$  reproduces existing results we will only need to discuss the case where  $\frac{eB}{m} \gg m$ . By defining  $m_{phys} = m(1 + \frac{\delta m}{m})$  we substitute the results from above to obtain the mass renormalization constant,

$$\frac{\delta m}{m} = \frac{\alpha\pi T^2}{3m^2} - \frac{(eB(2k+1))^2}{4m^4} \frac{2\alpha^2}{\pi} b\left(\frac{\beta eB(2k+1)}{2m}, \pm\mu\right) \quad (4.37)$$

$$+ \frac{2\alpha}{\pi m^2} \left[ \frac{c\left(\frac{\beta eB(2k+1)}{2m}, \pm\mu\right)}{\beta^2} + \frac{eB(2k+1)}{2m\beta} a\left(\frac{\beta eB(2k+1)}{2m}, \pm\mu\right) \right] \quad (4.38)$$

$$- \frac{(eB(2k+1))^2}{8m^2} b\left(\frac{\beta eB(2k+1)}{2m}, \pm\mu\right) \quad (4.39)$$

$$+ \frac{3(eB(2k+1))^4}{2^7 m^4} \beta^2 h\left(\frac{\beta eB(2k+1)}{2m}, \pm\mu\right) \quad (4.40)$$

The wave-function renormalization constant becomes, in the limit  $eB \gg m^2$ ,

$$Z_2^{-1}\left(\frac{\beta eB(2k+1)}{2m}, \mu\right) \simeq Z_2^{-1}(T = \mu = 0) \quad (4.41)$$

$$- \frac{(eB(2k+1))^2}{4m^4} \frac{2\alpha}{\pi} b\left(\frac{\beta eB(2k+1)}{2m}, \mp\mu\right) \quad (4.42)$$

$$- \frac{5\alpha}{\pi} \tilde{b}\left(\frac{\beta eB(2k+1)}{2m}, \mu\right) \quad (4.43)$$

$$- 2 \frac{\alpha T^2}{\pi E^2} \left[ \tilde{c}\left(\frac{\beta eB(2k+1)}{2m}, \mu\right) - \frac{\pi^2}{6} \right] \quad (4.44)$$

$$- m\beta\tilde{a}\left(\frac{\beta eB(2k+1)}{2m}, \mu\right) \quad (4.45)$$

Where the  $\tilde{a}\tilde{b}\tilde{c}$  give the net contributions of Masood's abc functions over the positron and electron,

$$\tilde{a}(\mathcal{M}\beta, \mu) = \frac{1}{2} \left[ a(\mathcal{M}\beta, \mu) - a(\mathcal{M}\beta, -\mu) \right] \quad (4.46)$$

$$\tilde{b}(\mathcal{M}\beta, \mu) = \frac{1}{2} \left[ b(\mathcal{M}\beta, \mu) - b(\mathcal{M}\beta, -\mu) \right] \quad (4.47)$$

$$\tilde{c}(\mathcal{M}\beta, \mu) = \frac{1}{2} \left[ c(\mathcal{M}\beta, \mu) - c(\mathcal{M}\beta, -\mu) \right] \quad (4.48)$$

The correction to  $Z_3$ , the electron charge renormalization constant [1] will become

$$Z_3 = 1 - \frac{8m^2e^2}{(eB(2k+1))^2\pi^2} \left[ \frac{1}{\beta^2} \tilde{c} \left( \frac{\beta eB(2k+1)}{2m}, \mu \right) \right] \quad (4.49)$$

$$- \frac{eB(2k+1)}{2m\beta} \tilde{a} \left( \frac{\beta eB(2k+1)}{2m}, \mu \right) \quad (4.50)$$

$$\left. - \frac{1}{4} \left( \frac{(eB(2k+1))^2}{4m^2} + \frac{\omega^2}{3} \right) \tilde{b} \left( \frac{\beta eB(2k+1)}{2m}, \mu \right) \right] \quad (4.51)$$

### 4.3 Renormalization Constants for Various B Ranges

However, in order to fully understand neutron stars, we must incorporate density effects such that  $\mu > T$  and examine  $\frac{eB}{m} > \mu > T > m$ , as well as  $\mu > T > m > \frac{eB}{m}$ . Estimates suggest  $T \sim 70$  MeV and  $\mu \sim 300$  MeV in certain circumstances, so these are physically relevant parameters estimated from observation. For the magnetic field, we could have anywhere from  $\frac{eB}{m} \sim 1 - 500$  MeV, so these calculations might apply to some of the most magnetic objects in the universe. Recall from the previous chapter that [35] we use the  $I$  and  $\mathcal{J}$  integrals in the limit  $\mu > T$  ( $I'_1, I'_2, I'_3$  for the electron,

and unprimed  $I$  for the positron),

$$\frac{\delta m}{m}(T, \mu) \simeq \frac{\pi\alpha T^2}{3m^2} - \frac{2\alpha}{\pi}I_2 + \frac{2\alpha}{\pi m^2} \left[ I_1 - \frac{m^2}{2}I_2 - \frac{m^4}{8}I_3 \right] \quad (4.52)$$

$$Z_2^{-1}(T, \mu) = Z_2^{-1}(T = \mu = 0) - \quad (4.53)$$

$$\frac{\alpha}{4\pi} \left[ I_A - \frac{I^0}{E} - \frac{4\pi}{E^2}I_1 - 12\pi I_2 - \frac{\pi E^2}{2}I_3 \right] \quad (4.54)$$

$$Z_3(T, \mu) \cong 1 + \frac{2e^2}{m^2\pi^2} \left[ \mathcal{J}_1 + \frac{1}{4} \left[ m^2 + \frac{\omega^2}{3} \right] \mathcal{J}_2 - \frac{1}{4}m^4 \mathcal{J}_3 \right] \quad (4.55)$$

Now we modify the  $I$  and  $\mathcal{J}$  integrals to support a magnetic field  $B$ , where  $\frac{eB}{m} \gg m$  and  $\mathcal{M} \simeq \frac{eB(2k+1)}{2m}$  in this limit

$$I'_1(T, \mu, B) = \frac{\mu^2}{2} \left( 1 - \frac{(eB(2k+1))^2}{4m^2\mu^2} \right) - \frac{a'(\mathcal{M}\beta, \mu)}{\beta} - \frac{c'(\mathcal{M}\beta, \mu)}{\beta^2} \quad (4.56)$$

$$I'_2(T, \mu, B) = \ln \left( \frac{2m\mu}{eB(2k+1)} \right) + b'(\mathcal{M}\beta, \mu) \quad (4.57)$$

$$I'_3(T, \mu, B) = \frac{2m^2}{(eB(2k+1))^2} \left( 1 - \frac{(eB(2k+1))^2}{4m^2\mu^2} \right) - \quad (4.58)$$

$$\frac{1}{4\mu^2} + \frac{4m^2 n_F(\mu - \frac{eB(2k+1)}{2m})}{(eB(2k+1))^2} + \quad (4.59)$$

$$\frac{2m\beta}{eB(2k+1)} \frac{e^{-\beta(\mu-\mathcal{M})}}{(1 + e^{-\beta(\mu-\mathcal{M})})^2} + d'(\mathcal{M}\beta, \mu) \quad (4.60)$$

The corresponding  $a'b'c'd'$  functions in this limit are given as

$$a'(\mathcal{M}\beta, \mu) = \mu \ln 2 - \frac{eB(2k+1)}{2m} \ln \left( 1 + e^{-\beta(\mu - \frac{eB(2k+1)}{2m})} \right) \quad (4.61)$$

$$b'(\mathcal{M}\beta, \mu) = \sum_{n=1}^{\infty} (-1)^n e^{-n\beta\mu} Ei\left(n \frac{eB(2k+1)}{2m} \beta\right) \quad (4.62)$$

$$c'(\mathcal{M}\beta, \mu) = \frac{\pi^2}{12} + \sum_{n=1}^{\infty} (-1)^n e^{-n\beta(\mu - \frac{eB(2k+1)}{2m})} \quad (4.63)$$

$$d'(\mathcal{M}\beta, \mu) = \sum_{n=1}^{\infty} (-1)^n \frac{(n\beta)^2}{2} \left( \ln \left[ \frac{2m\mu}{eB(2k+1)} \right] - \right. \quad (4.64)$$

$$\left. \frac{1}{2n\beta\mu} + Ei \left[ n \frac{eB(2k+1)}{2m} \beta \right] \right) \quad (4.65)$$

and  $I_1, I_2, I_3$  for the positron,

$$I_1(T, \mu) = \frac{a''(\mathcal{M}\beta, \mu)}{\beta} - \frac{c''(\mathcal{M}\beta, \mu)}{\beta^2} \quad (4.66)$$

$$I_2(T, \mu) = b''(\mathcal{M}\beta, \mu) \quad (4.67)$$

$$I_3(T, \mu) = \frac{4m^2 n_F(\mu - \frac{eB(2k+1)}{2m})}{(eB(2k+1))^2} + \quad (4.68)$$

$$\frac{2m\beta}{eB(2k+1)} \frac{e^{-\beta(\mu + \frac{eB(2k+1)}{2m})}}{(1 + e^{-\beta(\mu + \frac{eB(2k+1)}{2m})})^2} + d''(\mathcal{M}\beta, \mu) \quad (4.69)$$

The corresponding  $a''b''c''d''$  functions in this limit are given as

$$a''(\mathcal{M}\beta, \mu) = \frac{eB(2k+1)}{2m} \ln \left( 1 + e^{-\beta(\mu + \frac{eB(2k+1)}{2m})} \right) \quad (4.70)$$

$$b''(\mathcal{M}\beta, \mu) = \sum_{n=1}^{\infty} (-1)^n e^{-n\beta\mu} Ei\left(-n \frac{eB(2k+1)}{2m} \beta\right) \quad (4.71)$$

$$c''(\mathcal{M}\beta, \mu) = \sum_{n=1}^{\infty} (-1)^n e^{-n\beta(\mu + \frac{eB(2k+1)}{2m})} \quad (4.72)$$

$$d''(\mathcal{M}\beta, \mu) = \sum_{n=1}^{\infty} (-1)^n \frac{(n\beta)^2}{2} e^{-n\beta\mu} Ei\left(-n \frac{eB(2k+1)}{2m} \beta\right) \quad (4.73)$$

Where  $Ei(x)$  is the exponential integral,  $Ei(x) = \int_{-\infty}^x \frac{dt e^{-t}}{t}$ , as before. The  $\mathcal{J}_i$  become

$$\mathcal{J}_1(T, \mu, B) = \frac{1}{2} \left[ \frac{\mu^2}{2} \left( 1 - \frac{(eB(2k+1))^2}{4m^2\mu^2} \right) - \frac{a''(\mathcal{M}\beta, \mu) + a'(\mathcal{M}\beta, \mu)}{\beta} \right] \quad (4.74)$$

$$\left. \frac{c''(\mathcal{M}\beta, \mu) + c'(\mathcal{M}\beta, \mu)}{\beta^2} \right] \quad (4.75)$$

$$\mathcal{J}_2(T, \mu, B) = \frac{1}{2} \left[ \ln \frac{2m\mu}{eB(2k+1)} + b''(\mathcal{M}\beta, \mu) + b'(\mathcal{M}\beta, \mu) \right] \quad (4.76)$$

$$\mathcal{J}_3(T, \mu, B) = \frac{1}{2} \left[ \frac{2m^2}{(eB(2k+1))^2} \left( 1 - \frac{(eB(2k+1))^2}{4m^2\mu^2} \right) - \frac{1}{4\mu^2} + \right. \quad (4.77)$$

$$\left. \frac{n_F(\mu + \frac{eB(2k+1)}{2m}) + n_F(\mu - \frac{eB(2k+1)}{2m})}{m^2} + \right. \quad (4.78)$$

$$\left. \frac{2m\beta}{eB(2k+1)} \left[ \frac{e^{-\beta(\mu - \frac{eB(2k+1)}{2m})}}{(1 + e^{-\beta(\mu - \frac{eB(2k+1)}{2m})})^2} + \frac{e^{-\beta(\mu + \frac{eB(2k+1)}{2m})}}{(1 + e^{-\beta(\mu + \frac{eB(2k+1)}{2m})})^2} \right] + \right. \quad (4.79)$$

$$\left. d'(\mathcal{M}\beta, \mu) + d''(\mathcal{M}\beta, \mu) \right] \quad (4.80)$$

For  $\mu \gg T > m > \frac{eB}{m}$  the classical limit is obtained, so we do not discuss it too deeply. Simulations will suggest whether  $\frac{eB}{m} > \mu > T > m$  or  $\mu > \frac{eB}{m} > m > T$  is the more significant limit, which is the subject of the next section.

## 4.4 Calculation of QED Renormalization Constants

For convenience we review the limits in which discussion is most relevant to our work.

**The Superdense Limit ( $\mu > T$ )** The next limit we must discuss is the superdense limit, where  $\mu > T > m \gg \frac{eB}{m}$ , where density and temperature are high and the

electron mass low.

$$\frac{\delta m}{m}(T, \mu) \simeq \frac{\pi\alpha T^2}{3m^2} - \frac{2\alpha}{\pi} I_2^\pm + \frac{2\alpha}{\pi m^2} \left[ I_1^\pm - \frac{m^2}{2} I_2^\pm - \frac{m^4}{8} I_3^\pm \right] \quad (4.81)$$

$$Z_2^{-1}(T, \mu) = Z_2^{-1}(T = \mu = 0) - \quad (4.82)$$

$$\frac{\alpha}{4\pi} \left[ 8\pi \int_0^\infty \frac{dk}{k} n_B(k) + \frac{4}{3} \frac{\pi^3 T^2}{E^2} - \frac{4\pi}{E^2} I_1^\pm - 12\pi I_2^\pm - \frac{\pi E^2}{2} I_3^\pm \right] \quad (4.83)$$

$$Z_3(T, \mu) \cong 1 + \frac{2e^2}{m^2 \pi^2} \left[ \mathcal{J}_1 + \frac{1}{4} \left[ m^2 + \frac{\omega^2}{3} \right] \mathcal{J}_2 - \frac{1}{4} m^4 \mathcal{J}_3 \right] \quad (4.84)$$

The functions  $I_{1,2,3}^\pm$  and  $\mathcal{J}_{1,2,3}$  are given in the appendix of [35]. The magnetic field in this limit,  $\mu > \frac{eB}{m} > T \gg m$ , and  $\mu > T > \frac{eB}{m} \gg m$  for high density and temperature with non-negligible magnetic field B, have results of which were given and discussed in Section 4.3.

**The Classical Limit** ( $\mu > m$ ) The limit  $\mu > m > T$  is as mentioned the classical limit, the regime of our lab frame, where temperature is less than the electron mass but overall density is still high, and the magnetic field effects are negligible. In this limit the electron mass, wavefunction and charge renormalization constants [33] [35]

are

$$\frac{\delta m^+}{m}(T, \mu) \approx \frac{\alpha \pi T^2}{3m^2} \quad (4.85)$$

$$\frac{\delta m^-}{m}(T, \mu) \approx \frac{\alpha \pi T^2}{3m^2} - \frac{2\alpha}{\pi} \ln(\mu/m) \quad (4.86)$$

$$+ \frac{2\alpha}{\pi m^2} \left[ \frac{\mu^2}{2} \left[ 1 - \frac{m^2}{\mu^2} \right] - \frac{m^2}{2} \ln(\mu/m) - \frac{m^4}{8} \frac{1}{2m^2} (1 - m^2/\mu^2) \right] \quad (4.87)$$

$$Z_{2+}^{-1}(T, \mu) = Z_2^{-1}(T = \mu = 0) - \frac{\alpha}{4\pi^2} \left[ 8\pi \int_0^\infty \frac{dk}{k} n_B(k) + \frac{4}{3} \frac{\pi^3 T^2}{E^2} \right] \quad (4.88)$$

$$Z_{2-}^{-1}(T, \mu) = Z_2^{-1}(T = \mu = 0) \quad (4.89)$$

$$- \frac{\alpha}{4\pi^2} \left[ 8\pi \int_0^\infty \frac{dk}{k} n_B(k) + \frac{4}{3} \frac{\pi^3 T^2}{E^2} - \frac{4\pi}{E^2} \frac{\mu^2}{2} \left[ 1 - \frac{m^2}{\mu^2} \right] \right] \quad (4.90)$$

$$- 12\pi \ln(\mu/m) - \frac{\pi E^2}{2} \frac{1}{2m^2} (1 - m^2/\mu^2) \quad (4.91)$$

$$Z_3(\mu) \approx 1 - \frac{e^2}{2\pi m^2} \left[ \frac{\mu^2 - 2m^2}{8} \left[ 1 - \frac{m^2}{\mu^2} \right] \right] \quad (4.92)$$

Where the  $+/-$  is for the positron/electron. Where in all limits we have the renormalized values as

$$m_R = m_0(1 + \delta m) \quad (4.93)$$

$$\psi_R = Z_2^{-1} \psi_0 \quad (4.94)$$

$$e_R = Z_3^{1/2} e_0 \quad (4.95)$$

$$\alpha_R = Z_3 \alpha_0 \quad (4.96)$$

**The Early Universe Limit ( $T > m$ )** The next limit we must discuss is the early universe limit, where  $T \gg m$ , and the converse,  $m \gg T$ , where  $\mu$  and  $B$  are

ignored [3]. This limit corresponds to the early universe, since  $m \sim 10^9 \text{ K}$  this is approximately one second after the Big Bang.

$$\frac{\delta m}{m}(T) \simeq \frac{\pi\alpha T^2}{3m^2} \left[ 1 - \frac{6}{\pi^2} c(m\beta) \right] + \frac{2\alpha T}{\pi m} a(m\beta) - \frac{3\alpha}{\pi} b(m\beta) \quad (4.97)$$

$$Z_2^{-1}(T) = Z_2^{-1}(T = \mu = 0) - \frac{2\alpha}{\pi} \int_0^\infty \frac{dk}{k} n_B(k) + \quad (4.98)$$

$$\frac{2\alpha}{\pi} \frac{1}{E^2 \beta^2} \left[ \frac{\pi^2}{6} - c(m\beta) + m\beta a(m\beta) \right] - \frac{5\alpha}{\pi} b(m\beta) \quad (4.99)$$

$$Z_3 = 1 - \frac{2e^2}{m^2 \pi^2} \left[ \frac{\tilde{c}}{\beta^2} - \frac{m\tilde{a}}{\beta} - \frac{1}{4} \left( m^2 + \frac{\omega^2}{3} \right) \tilde{b} \right] \quad (4.100)$$

Where the  $\tilde{a}\tilde{b}\tilde{c}$  functions are given in [1] [2]. The charge renormalization constant is not modified when  $m > T$ .

**The Very Early Universe Limit ( $T > \mu$ )** The final limit we must discuss is the very early universe limit, where  $T > \mu > m$ , since temperature and density are high, and comparatively the electron mass is low.

$$\frac{\delta m}{m}(m\beta, \mu) \simeq \frac{\pi\alpha T^2}{3m^2} \left[ 1 - \frac{6}{\pi^2} \tilde{c}(m\beta) \right] + \frac{2\alpha T}{\pi m} \tilde{a}(m\beta) - \frac{3\alpha}{\pi} \tilde{b}(m\beta) \quad (4.101)$$

$$Z_2^{-1}(m\beta, \mu) = Z_2^{-1}(T = \mu = 0) - \frac{2\alpha}{\pi} \int_0^\infty \frac{dk}{k} n_B(k) - \quad (4.102)$$

$$\frac{5\alpha}{\pi} \tilde{b}(m\beta, \mu) - \frac{2\alpha T^2}{\pi E^2} \left[ -\frac{\pi^2}{6} + \tilde{c}(m\beta, \mu) - m\beta \tilde{a}(m\beta, \mu) \right] \quad (4.103)$$

Where the  $\tilde{a}\tilde{b}\tilde{c}$  functions are the abc functions averaged over the positron and electron contributions. The full abc expressions are located in [3]. The results including a non-negligible magnetic field  $T > \mu > \frac{eB}{m} \gg m$ , and  $T > \frac{eB}{m} > \mu \gg m$  are included in Section 4.2.1.

## 4.5 Results and Discussions

Using computational techniques, we graph and analyze data from Python code that approximate the values of Masood's **abc** functions at the superdense limit  $\mu > T > \frac{eB}{m}$  and for ultra-strong magnetic fields  $\frac{eB}{m} > \mu > T$ , as well as the early universe limit  $T > m_e > \frac{eB}{m}$  and  $\frac{eB}{m} > T > m_e$ . The **abc** functions give contributions to the self energy constant for the electron as well as  $Z_2^{-1}$  and  $Z_3$ , the wavefunction renormalization constant and electron charge renormalization constant. We also graph these constants and analyze the results. Here we will assume  $m = m_e$  the mass of the electron.

At low to zero magnetic field contribution, we find that in the limit  $T$  large relative to the bare electron mass  $T \gg m > \frac{eB}{m}$  we find Masood's function **a** approaches the limit  $\ln(2)$  (Figure 4.3, top), which is sensible, as **a** is defined as  $\ln(1+e^{-f(1/T)})$ , a large  $T$  implies the exponential argument approaches zero, and thus  $\ln(1+e^0) = \ln(2)$ . Masood's **c** function approaches  $-\pi/12$ , which can be seen in Figure 4.3 (middle). In this figure the blue line (hidden by the orange line) is the case where  $B$  is essentially zero.

We wish to investigate non-zero magnetic fields  $B$ , so we run simulations of the magnetic field for the case  $eB/m \sim m$  and  $eB/m \gg m$ . The case  $eB/m \sim m$  corresponds to a neutron star with magnetic field on the order of  $B = 10^{10}$  T, and for  $eB/m \gg m$  we have a field on the order of  $B = 10^{14}$  T, which corresponds to an energy of around 75 MeV.

In order to convert from  $eB/m$  to units of energy we introduce a conversion factor  $F = 3.7 * 10^{20} \frac{eV^2}{T \cdot C}$  to move from Tesla Coulumb ( $T \cdot C$ ) to electronVolt (eV) or

$F^{-1} = 3.7 * 10^{-22} \frac{\text{T}\cdot\text{C}}{\text{eV}^2}$  to move the opposite direction. In this way we can see,

$$B \sim \frac{m^2}{eF} \quad (4.104)$$

$$B \sim \frac{0.5^2 * 10^{12}}{1.6 * 10^{-19} * 3.7 * 10^{20}} \frac{\text{eV}^2(\text{T} * \text{C})}{\text{C} * \text{eV}^2} = 4.2 * 10^9 \text{T} \sim 10^{10} \text{T} \quad (4.105)$$

which is assumed to be a reasonable value for the magnetic field of a neutron star, also. We ultimately find negligible effects in the  $eB/m \sim m$  limit and significant deviation from the usual  $B=0$  case when  $eB/m \gg m$ , however this is for fields around 4 orders of magnitude stronger than physically observed.

As mentioned for  $T > \frac{eB}{m} \sim m$  we find an almost negligible effect, although the  $\mathbf{b}$  function appears to show some significant changes (See Figure 4.3, bottom). However, this does not translate into a meaningful change in the renormalization constants, as can be seen in Figure 4.4 where the renormalization constants are virtually identical to their  $B=0$  counterparts.

**Behavior of Masood's abc functions** For the nonphysical case, when  $eB/m \gg T > m$ , things are more interesting, despite being at magnetic field strengths that have not been observed. Considering a similar analysis for the  $\mathbf{abc}$  functions (Figure 4.5), when a magnetic field is turned on, we find that the magnetic field tends to "pull the contribution" of all the  $\mathbf{abc}$  functions closer to zero, essentially suppressing the contribution for each. It is important to mention that the value used for the magnetic field,  $B = 10^{14} \text{T}$  is around ten thousand times an upper limit on the magnetic field found in nature. Most likely, this kind of field would be found in only the most compact of stellar objects, such as neutron stars and magnetars, if at all. The analysis is relevant in the event such a extreme object is found.

Examining Masood's  $\mathbf{b}$  function with this in mind, the proportional dependence on the exponential integral  $Ei$ , which itself depends on  $B$ , suggests a possible cause for

the suppression due to ultra-high magnetic field  $B$ , since the exponential term in the function is parameterized by  $T$ ,  $e^{\mp n\mu/T}$ , it seems this could be the only reason for the suppressive effect of the magnetic field on Masood's  $b(\mu, T, B)$  function contribution (Figure 4.5).

We see a similar story when graphing Masood's  $c$  with and without the ultra-high magnetic field. Clearly we see a similar effect in  $a$  where the contribution is "pulled closer" to zero due to  $B$ , thereby reducing and countering in some sense the effect of an extremely high temperature. The shape of the graph under high magnetic field is similar but less pronounced than the  $B=0$  counterpart.

Analyzing the data resulting from simulations, the data show the effect of ultra-high magnetic field  $B$  (where  $T > m$ , Figure 4.5) is possibly non-negligible. Although the overall behavior of these functions is similar, the specific suppressive effect of a reduction of contribution from  $a, b, c$ , suggests scientifically relevant interpretation may be useful here.

**Renormalization parameters** After simulating renormalized constants at finite temperature, we find a predictable, non-negligible difference between constants at a ultra-strong, unrealistic, ( $B=1.00E14$  T) magnetic field, and no real difference at typical neutron star magnetic fields ( $B=1.00E10$  T), as can be seen in Figures 4.1 and 4.2 for the  $\mu > T$  limit and Figures 4.4 and 4.6 for the limit  $T > m$ .

Most apparent in this data is in the electron mass, computed as a correction to  $m_e = m_0 + \delta m$ . By graphing the related quantity  $\delta m/m$  which is unitless, we find that a strong magnetic field arcs the change in electron mass upwards, *above* the regular  $B = 0$  line, in both the limit  $T > m$  (Figure 4.6, top) and  $\mu > T$  (Figure 4.2, top). This is significant and may imply either the rebalanced contribution proportion

of  $\mathbf{a/b/c}$  has generated what could be a measurable effect in extremely high dense, compact, stellar systems.

A somewhat similar picture emerges for the inverse of  $Z_2$ , the wave normalization constant. In this case we plotted terms proportional to temperature and found a reduced contribution when simulated against high magnetic fields. An even greater reduction in significance was found for  $Z_3$ , the electron charge renormalization constant, which contributes to the coupling constant of QED, all of which can be seen in Figure 4.6, middle and bottom diagrams. All of this data suggest that at ultra-high magnetic fields there are some non-negligible physical effects that may be measurable, which cannot be discounted, while at high magnetic field  $B$ , effects could be negligible.

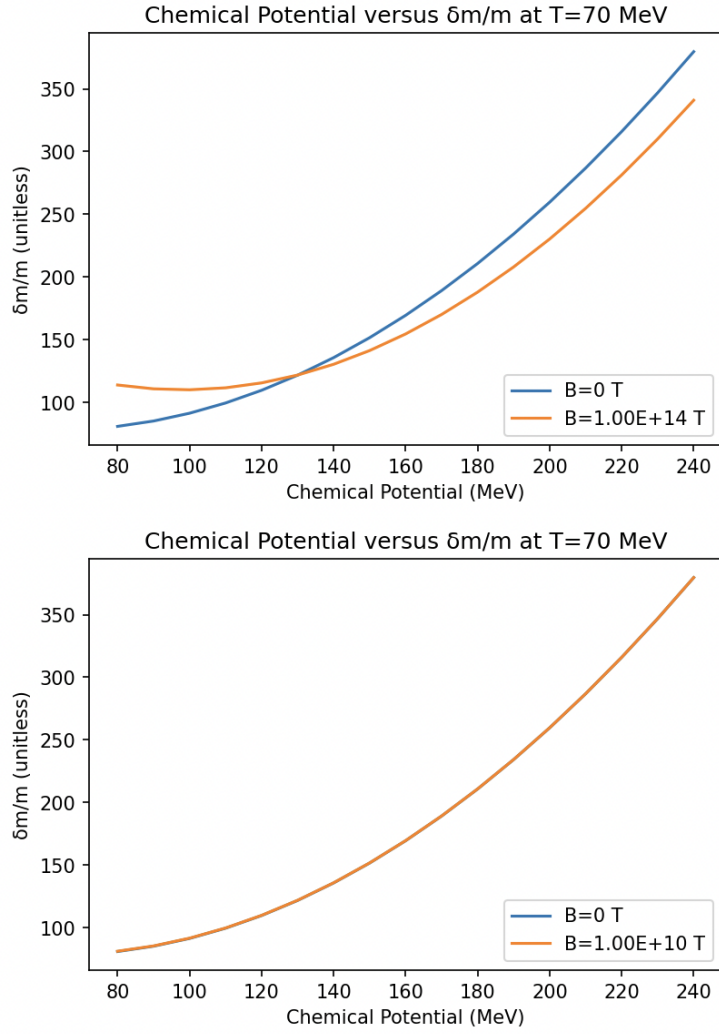


**Figure 4.1.** Renormalization constant  $\delta m/m$  compared when ( $B=1.00E+14$  T)  $eB/m \gg m$  and ( $B=1.00E+10$  T)  $eB/m \sim m$  in the limit  $\mu > T$ . In the  $eB/m \sim m$  case there is a negligible change and the two graphs are overlaid thus  $B$  has almost no effect on electron mass.

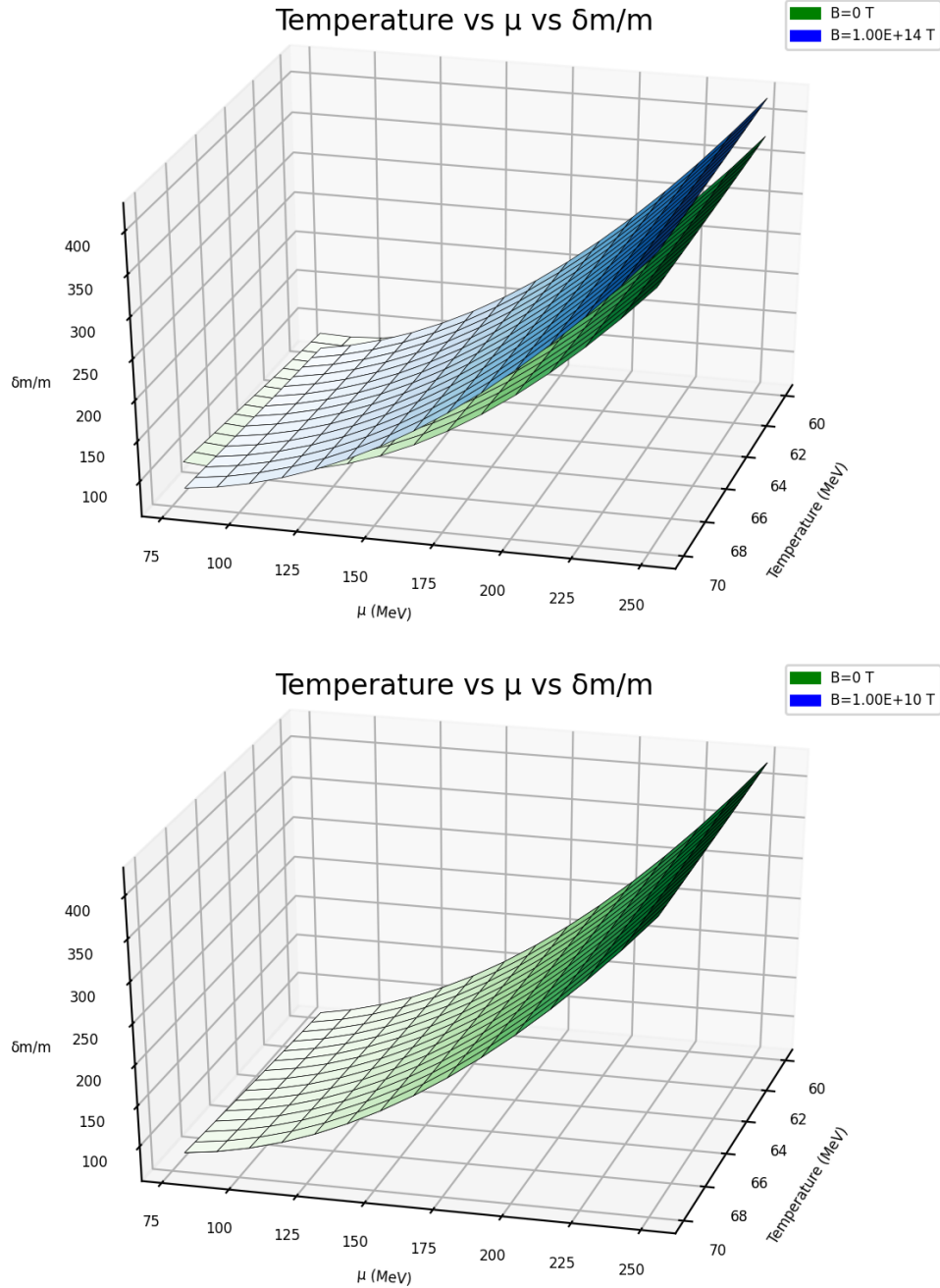


**Figure 4.2.** Renormalization constant  $\delta m/m$  compared when ( $B=1.00E+14$  T)  $eB/m \gg m$  and ( $B=1.00E+10$  T)  $eB/m \sim m$  in the limit  $\mu > T$ . We graph chemical potential versus temperature versus the value of  $\delta m/m$ . We observe a virtually identical result as in Figure 4.1. There is a negligible change for a typical neutron star magnetic field ( $B=1.00E+10$  T) and the two graphs are overlaid thus  $B$  has almost no effect on electron mass.

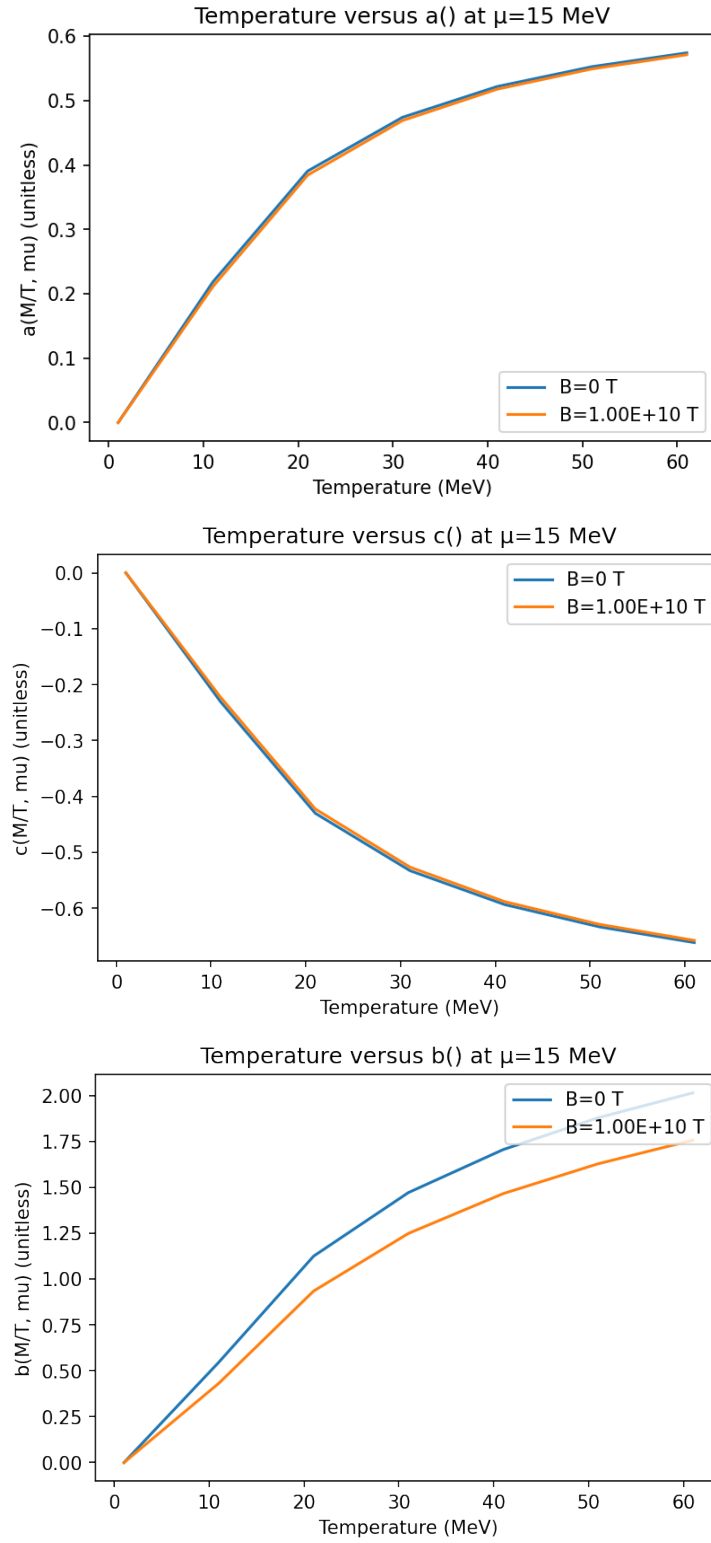


**Figure 4.3.** Masood's abc functions compared when ( $B=1.00E+10$  T)  $eB/m \sim m$  in the limit  $T > m$ . The functions **a** and **c** show almost no change, while **b** does change a small amount, by comparison.

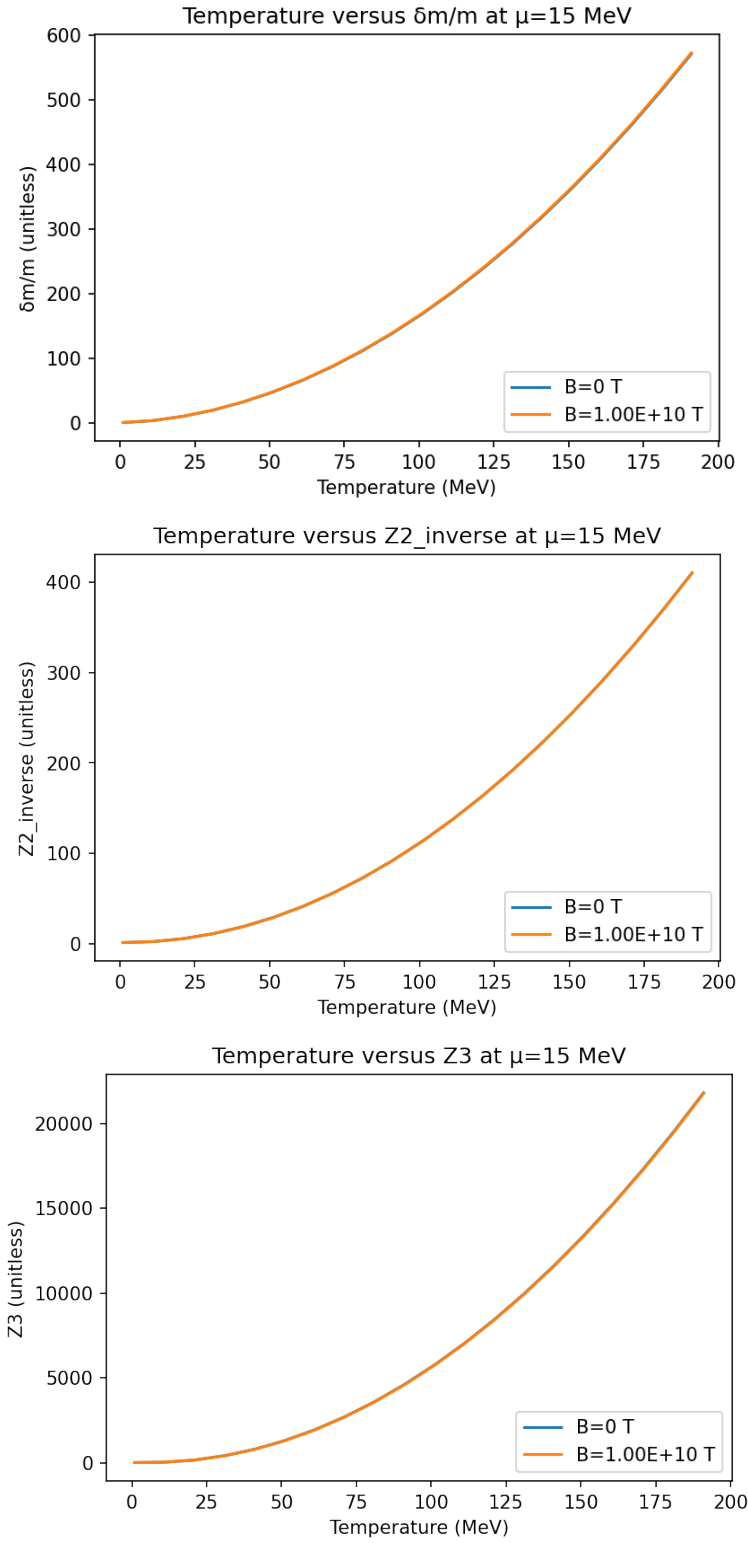


**Figure 4.4.** Renormalization constants compared when ( $B=1.00E+10$  T)  $eB/m \sim m$ . In these graphs, there is a negligible change and the two graphs are virtually identical, and overlaid, in the limit  $T > m$ .

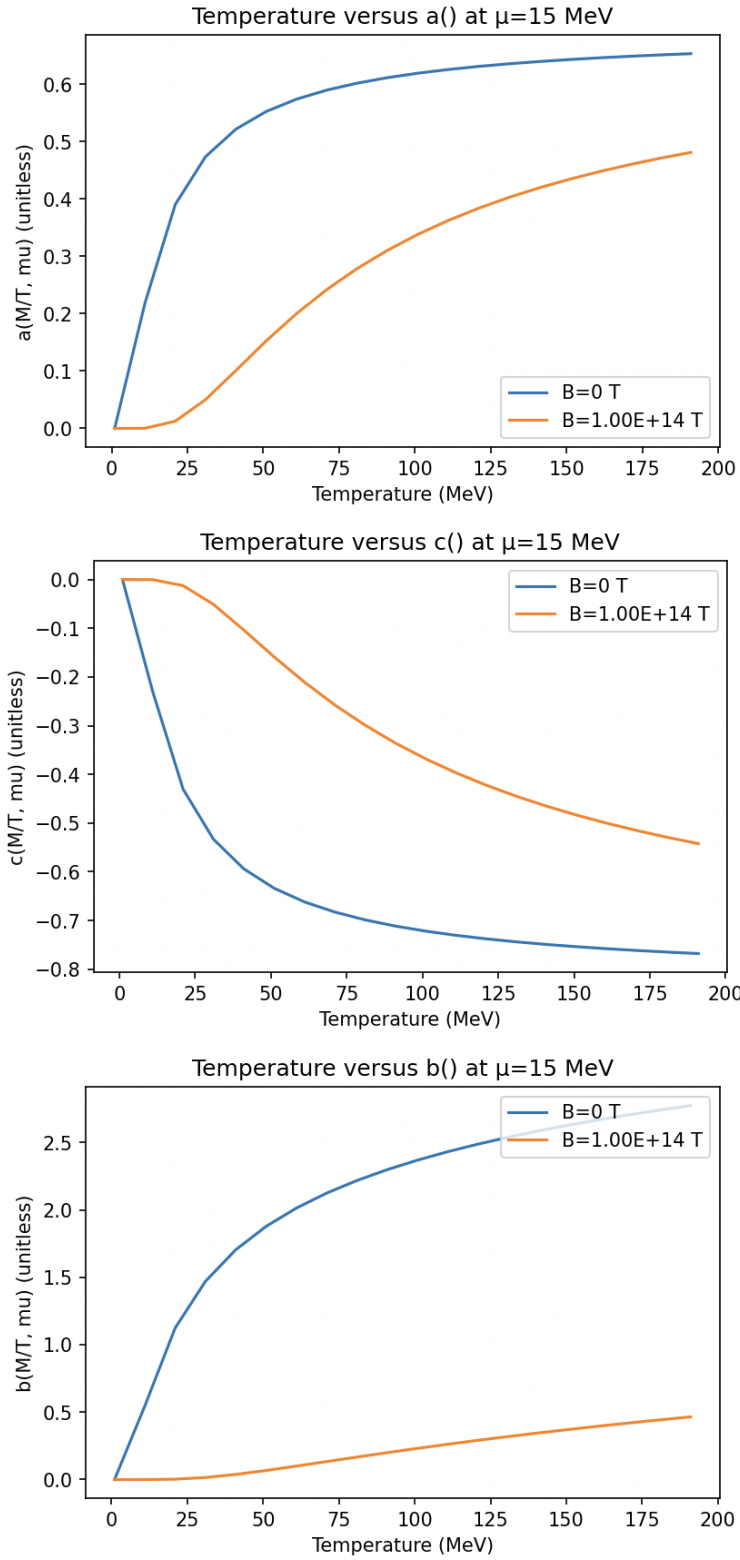


**Figure 4.5.** Masood's abc functions compared when  $(B=1.00E+14 \text{ T}) eB/m \gg m$  in the limit  $T > m$ . Compared with Figure 4.3, we see dramatic changes due to the magnetic field, and the contribution of all functions is reduced in this magnetic field.

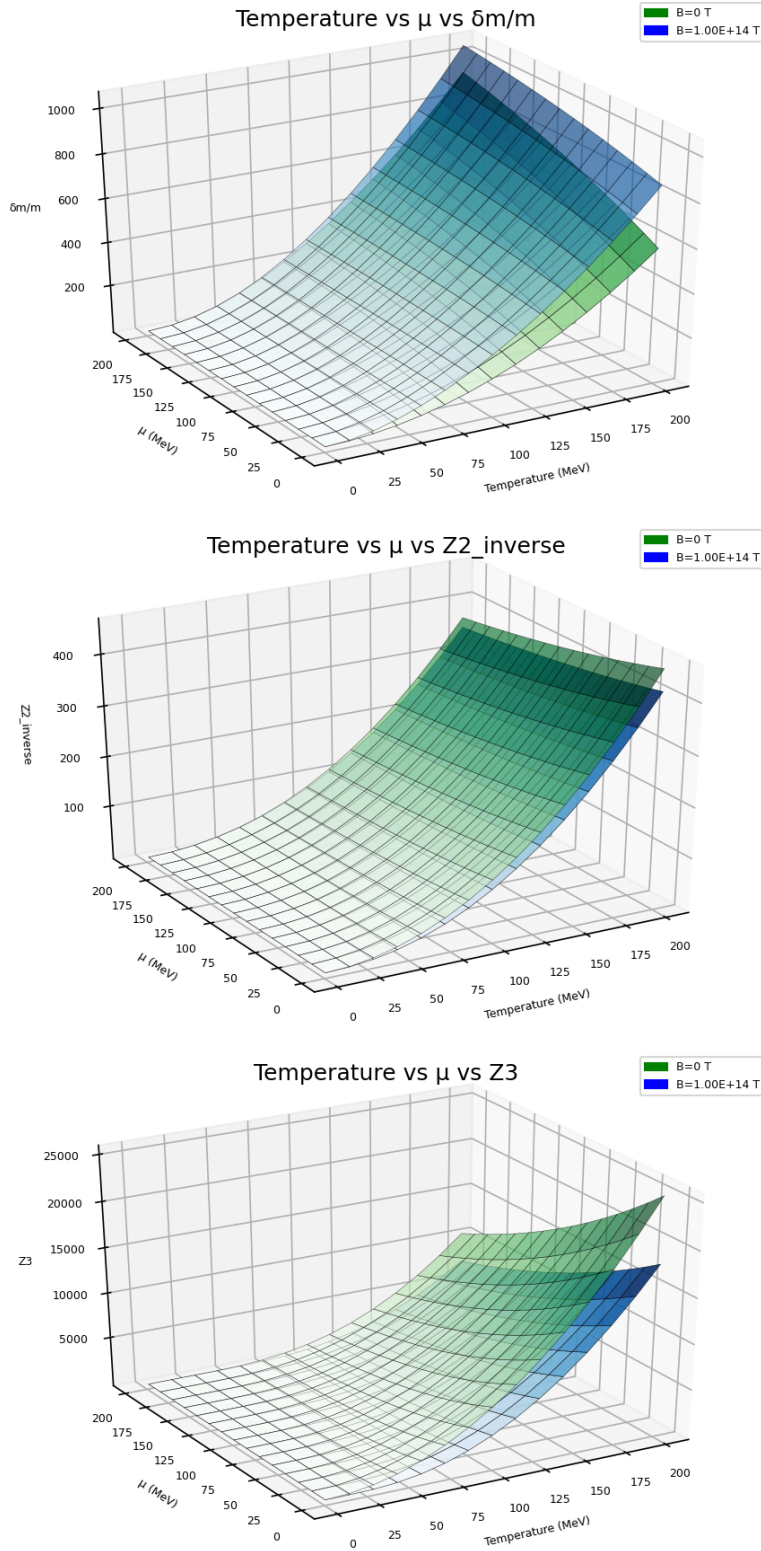


**Figure 4.6.** Renormalization constants compared when  $(B=1.00E+14 \text{ T}) eB/m \gg m$  in the limit  $T > m$ . Compared with Figure 4.4 we see dramatic differences as the high magnetic field reduces the renormalization constants  $Z_2^{-1}$  and  $Z_3$  while increasing  $\delta m/m$ .

## 4.6 Applications, Future Work and Conclusions

In neutron stars we have a relatively unknown core of very high density, on the order of some of the most dense objects in the universe. In these cores, we must conjecture the composition in order to have a better idea of observational results. The above analysis shows that we not only have potential changes that occur in the cores of such compact stellar objects like supernovae and neutron stars, but perhaps that these changes are observable, given the right compact object. Despite there being little to no change in a typical neutron star, there is still room for observations to change our understanding of the extremes of the universe. Under these conditions, we can make inferences due to the drastic difference in curve data comparing the unchanged renormalization constants at finite temperature to one at ultra-high magnetic fields, that are at least a few orders of magnitude above what is to be expected inside some of the most compact objects in the known universe.

Considering the changes to the electron mass in these stellar environments, it is worthwhile to investigate the medium effect on other particle propagation processes such as beta decay in these conditions. Any resulting changes may lead to dramatically different observations by astronomers, and our work provides a baseline for understanding these observations in the context of finite temperature field theory as one possible valid model. Subsequent results using a similar approach might then produce related changes and the potential for more validation of observations that do not meet current expectations.

Furthermore, because of the state of the early universe, which is hot, dense, and compact, similar to a stellar compact object, we should expect modifications of the same type in any plasma that is necessarily dense and hot enough. Thus, the applications of this work are not simply to compact objects, but the early universe, which

may imply different rates of free streaming or nucleosynthesis ratios that may not necessarily agree with current, established theory. It is worth noting, while we have specifically focused on the renormalization constants of the electron, necessarily these calculations can be performed on other particles, which may or may not necessarily produce a measurable, or observable result.

It is here that we champion other particles to be studied under similar conditions, as the possible utility of this model to observational astronomers could be quite large. In conclusion, we must continue to probe the deepest regions of spacetime in order to better understand our current universe, and the mathematical model described here, finite temperature field theory, certainly allows for researchers to keep leading ideas relevant by being able to express them in the language of finite temperature field theory (FTD).

## BIBLIOGRAPHY

- [1] K. Ahmed and Samina S. Masood. Vacuum polarization at finite temperature and density in qed. *Annals of Physics*, 207(2):460–473, 1991. ISSN 0003-4916. doi: [https://doi.org/10.1016/0003-4916\(91\)90066-H](https://doi.org/10.1016/0003-4916(91)90066-H). URL <https://www.sciencedirect.com/science/article/pii/000349169190066H>.
- [2] K. Ahmed and Samina Saleem. Renormalization and radiative corrections at finite temperature reexamined. *Phys. Rev. D*, 35:1861–1871, Mar 1987. doi: 10.1103/PhysRevD.35.1861. URL <https://link.aps.org/doi/10.1103/PhysRevD.35.1861>.
- [3] K. Ahmed and Samina Saleem. Finite-temperature and -density renormalization effects in qed. *Phys. Rev. D*, 35:4020–4023, Jun 1987. doi: 10.1103/PhysRevD.35.4020. URL <https://link.aps.org/doi/10.1103/PhysRevD.35.4020>.
- [4] CE Alvarez-Salazar. About the influence of the density profile on neutron star cooling by neutrino emission. 2018. <https://doi.org/10.1016/j.astropartphys.2018.07.007>.
- [5] P.D. Beale. *Statistical Mechanics*. Elsevier Science, 2011. ISBN 9780123821898. URL <https://books.google.com/books?id=KdbJJAXQ-RsC>.
- [6] V.B. Berestetskii, L.P. Pitaevskii, and E.M. Lifshitz. *Quantum Electrodynamics: Volume 4*. Number v. 4. Elsevier Science, 2012. ISBN 9780080503462. URL <https://books.google.com/books?id=Tpk-lqyr3GoC>.
- [7] H.A. Bethe. Energy Production in Stars. *Physical Review*, 55(5):434–456, March 1939. doi: 10.1103/PhysRev.55.434.

- [8] D. Blaschke, N.K. Glendenning, and A. Sedrakian. *Physics of Neutron Star Interiors*. Lecture Notes in Physics. Springer Berlin Heidelberg, 2008. ISBN 9783540445784. URL [https://books.google.com/books?id=t\\_hqCQAAQBAJ](https://books.google.com/books?id=t_hqCQAAQBAJ).
- [9] D.A. Bromley and W. Greiner. *Classical Electrodynamics*. Classical Theoretical Physics. Springer New York, 2012. ISBN 9781461205876. URL <https://books.google.com/books?id=acjcBwAAQBAJ>.
- [10] M. Camenzind. *Compact Objects in Astrophysics: White Dwarfs, Neutron Stars and Black Holes*. Astronomy and Astrophysics Library. Springer Berlin Heidelberg, 2016. ISBN 9783662500323. URL <https://books.google.com/books?id=-WK1DAEACAAJ>.
- [11] Carroll and Ostlie. *An introduction to modern astrophysics*. 2017.
- [12] M. Chaichian, S. S. Masood, C. Montonen, A. Pérez Martínez, and H. Pérez Rojas. Quantum magnetic collapse. *Phys. Rev. Lett.*, 84:5261–5264, Jun 2000. doi: 10.1103/PhysRevLett.84.5261. URL <https://link.aps.org/doi/10.1103/PhysRevLett.84.5261>.
- [13] Arnab Rai Choudhuri. *Astrophysics for physicists*. 2010.
- [14] Piers Coleman. *Introduction to Many-Body Physics*. Cambridge University Press, 2015. doi: 10.1017/CBO9781139020916.
- [15] M.G. Cottam and Z. Haghshenasfard. *Many-Body Theory of Condensed Matter Systems: An Introductory Course*. Cambridge University Press, 2020. ISBN 9781108488242. URL <https://books.google.com/books?id=3PXvDwAAQBAJ>.

- [16] L. Dolan and R. Jackiw. Symmetry behavior at finite temperature. *Phys. Rev. D*, 9:3320–3341, Jun 1974. doi: 10.1103/PhysRevD.9.3320. URL <https://link.aps.org/doi/10.1103/PhysRevD.9.3320>.
- [17] W.H. Donahue and O. Gingerich. *Johannes Kepler New Astronomy*. Cambridge University Press, 1992. ISBN 9780521301312. URL <https://books.google.com/books?id=RCZpQgAACAAJ>.
- [18] John F. Donoghue and Barry R. Holstein. Renormalization and radiative corrections at finite temperature. *Phys. Rev. D*, 28:340–348, Jul 1983. doi: 10.1103/PhysRevD.28.340. URL <https://link.aps.org/doi/10.1103/PhysRevD.28.340>.
- [19] John F. Donoghue and Barry R. Holstein. Renormalization and radiative corrections at finite temperature. *Phys. Rev. D*, 28:340–348, Jul 1983. doi: 10.1103/PhysRevD.28.340. URL <https://link.aps.org/doi/10.1103/PhysRevD.28.340>.
- [20] John F. Donoghue, Barry R. Holstein, and R.W. Robinett. Quantum electrodynamics at finite temperature. *Annals of Physics*, 164(2):233–276, 1985. ISSN 0003-4916. doi: [https://doi.org/10.1016/0003-4916\(85\)90016-8](https://doi.org/10.1016/0003-4916(85)90016-8). URL <https://www.sciencedirect.com/science/article/pii/0003491685900168>.
- [21] Lyn Evans. Particle accelerators at cern: From the early days to the lhc and beyond. *Technological Forecasting and Social Change*, 112:4–12, 2016. ISSN 0040-1625. doi: <https://doi.org/10.1016/j.techfore.2016.07.028>. URL <https://www.sciencedirect.com/science/article/pii/S0040162516301858>.
- [22] Carlo Giunti. Theory of neutrino oscillations. 2004. <https://arxiv.org/pdf/hep-ph/0409230.pdf>.

- [23] H. Goldstein, C.P. Poole, and J.L. Safko. *Classical Mechanics*. Addison Wesley, 2002. ISBN 9780201657029. URL <https://books.google.com/books?id=tJCuQgAACAAJ>.
- [24] P. Haensel, A.Y. Potekhin, and D.G. Yakovlev. Neutron stars 1: Equation of state and structure. 2006.
- [25] K Huang. Statistical mechanics. 1987. URL <https://books.google.com/books?id=M8PvAAAAAMAAJ>.
- [26] J.D. Jackson. *Classical Electrodynamics*. Wiley, 1998. ISBN 9780471309321. URL <https://books.google.com/books?id=FOBBEAAAQBAJ>.
- [27] Rudolf Kippenhahn, Alfred Weigert, and Achim Weiss. Stellar structure and evolution. 2012. Chapters 7,27,30,18.
- [28] L.D. Landau and E.M. Lifshitz. *Statistical Physics: Volume 5*. Number v. 5. Elsevier Science, 2013. ISBN 9780080570464. URL <https://books.google.com/books?id=VzgJN-XPTRsC>.
- [29] N.P. Landsman and Weert. Real and imaginary-time field theory at finite temperature and density. *Physics Reports*, 145(3), 1987. doi: [https://doi.org/10.1016/0370-1573\(87\)90121-9](https://doi.org/10.1016/0370-1573(87)90121-9). URL <http://www.sciencedirect.com/science/article/pii/0370157387901219>.
- [30] Samina Masood. Electromagnetic properties of a hot and dense medium, 2016.
- [31] Samina Masood and Iram Saleem. Propagation of electromagnetic waves in extremely dense media. *International Journal of Modern Physics A*, 32(15): 1750081, 2017. doi: 10.1142/S0217751X17500816. URL <https://doi.org/10.1142/S0217751X17500816>.

- [32] Samina S. Masood. Neutrino physics in hot and dense media. <https://doi.org/10.1103/PhysRevD.48.3250>.
- [33] Samina S. Masood. Photon mass in the classical limit of finite-temperature and -density qed. *Phys. Rev. D*, 44:3943–3948, Dec 1991. doi: 10.1103/PhysRevD.44.3943. URL <https://link.aps.org/doi/10.1103/PhysRevD.44.3943>.
- [34] Samina S. Masood. Neutrino physics in hot and dense media. *Phys. Rev. D*, 48:3250–3258, Oct 1993. doi: 10.1103/PhysRevD.48.3250. URL <https://link.aps.org/doi/10.1103/PhysRevD.48.3250>.
- [35] Samina S. Masood. Renormalization of qed in superdense media. *Phys. Rev. D*, 47:648–652, Jan 1993. doi: 10.1103/PhysRevD.47.648. URL <https://link.aps.org/doi/10.1103/PhysRevD.47.648>.
- [36] Mikhail M. Meskhi, Noah E. Wolfe, Zhenyu Dai, Carla Frohlich, Jonah M. Miller, Raymond K. W. Wong, and Ricardo Vilalta. A new constraint on the nuclear equation of state from statistical distributions of compact remnants of supernovae, 2021.
- [37] Jonah M. Miller, Ben. R. Ryan, and Joshua C. Dolence. Radiation GRMHD for neutrino-driven accretion flows. 241(2):30, apr 2019. doi: 10.3847/1538-4365/ab09fc. URL <https://doi.org/10.3847/1538-4365/ab09fc>.
- [38] Jonah M. Miller, Benjamin R. Ryan, Joshua C. Dolence, Adam Burrows, Christopher J. Fontes, Christopher L. Fryer, Oleg Korobkin, Jonas Lippuner, Matthew R. Mumpower, and Ryan T. Wollaeger. Full transport model of gw170817-like disk produces a blue kilonova. *Phys. Rev. D*, 100:023008, Jul 2019. doi: 10.1103/PhysRevD.100.023008. URL <https://link.aps.org/doi/10.1103/PhysRevD.100.023008>.

- [39] Jonah M. Miller, Trevor M. Sprouse, Christopher L. Fryer, Benjamin R. Ryan, Joshua C. Dolence, Matthew R. Mumpower, and Rebecca Surman. Full transport general relativistic radiation magnetohydrodynamics for nucleosynthesis in collapsars. 902(1):66, oct 2020. doi: 10.3847/1538-4357/abb4e3. URL <https://doi.org/10.3847/1538-4357/abb4e3>.
- [40] J. R. Oppenheimer and G. M. Volkoff. On massive neutron cores. *Phys. Rev.*, 55:374–381, Feb 1939. doi: 10.1103/PhysRev.55.374. URL <https://link.aps.org/doi/10.1103/PhysRev.55.374>.
- [41] M.E. Peskin and D.V. Schroeder. *An Introduction To Quantum Field Theory*. Frontiers in Physics. Avalon Publishing, 1995. ISBN 9780813345437. URL <https://books.google.de/books?id=EVeNNcslvX0C>.
- [42] David Pines. Pulsars and compact x-ray sources: Cosmic laboratories for the study of neutron stars and hadron matter. *Le Journal de Physique Colloques*, 41 (C2):C2–111, 1980.
- [43] Samantha López Pérez, Daryl Manreza Paret, Gretel Quintero Angulo, Aurora Pérez Martínez, and Diana Alvear Terrero. Modeling anisotropic magnetized strange quark stars. *Astronomische Nachrichten*, 340(9-10):1013–1017, 2019. doi: <https://doi.org/10.1002/asna.201913721>. URL <https://onlinelibrary.wiley.com/doi/abs/10.1002/asna.201913721>.
- [44] L. Rezzolla, P. Pizzochero, D.I. Jones, N. Rea, and I. Vidaña. *The Physics and Astrophysics of Neutron Stars*. Astrophysics and Space Science Library. Springer International Publishing, 2019. ISBN 9783319976150. URL <https://books.google.com/books?id=OXTvuAEACAAJ>.

- [45] Henry Norris Russell. Relations Between the Spectra and Other Characteristics of the Stars. *Popular Astronomy*, 22:275–294, May 1914.
- [46] F. Scheck. *Electroweak and Strong Interactions: Phenomenology, Concepts, Models*. Graduate Texts in Physics. Springer Berlin Heidelberg, 2013. ISBN 9783642269516. URL [https://books.google.com/books?id=a\\_YlngEACAAJ](https://books.google.com/books?id=a_YlngEACAAJ).
- [47] Matthew D. Schwartz. Quantum field theory and the standard model, 2013.
- [48] Silvan S Schweber. Physics, community and the crisis in physical theory. *physics today*, 46:34–34, 1993.
- [49] Peter S. Shternin, Dmitry G. Yakovlev, Craig O. Heinke, Wynn C. G. Ho, and Daniel J. Patnaude. Cooling neutron star in the Cassiopeia A supernova remnant: evidence for superfluidity in the core. *Monthly Notices of the Royal Astronomical Society: Letters*, 412(1):L108–L112, 03 2011. ISSN 1745-3925. doi: 10.1111/j.1745-3933.2011.01015.x. URL <https://doi.org/10.1111/j.1745-3933.2011.01015.x>.
- [50] Saul A. Teukolsky Stuart L. Shapiro. Black holes, white dwarfs, and neutron stars, 2007.
- [51] M. Tuckerman. *Statistical Mechanics: Theory and Molecular Simulation*. Oxford Graduate Texts. OUP Oxford, 2010. ISBN 9780198525264. URL <https://books.google.com/books?id=UNqmCAAQBAJ>.
- [52] Steven Weinberg. Gauge and global symmetries at high temperature. *Phys. Rev. D*, 9:3357–3378, Jun 1974. doi: 10.1103/PhysRevD.9.3357. URL <https://link.aps.org/doi/10.1103/PhysRevD.9.3357>.

- [53] H. Arthur Weldon. Covariant calculations at finite temperature: The relativistic plasma. *Phys. Rev. D*, 26:1394–1407, Sep 1982. doi: 10.1103/PhysRevD.26.1394. URL <https://link.aps.org/doi/10.1103/PhysRevD.26.1394>.
- [54] Kenneth G. Wilson. The renormalization group and critical phenomena. *Rev. Mod. Phys.*, 55:583–600, Jul 1983. doi: 10.1103/RevModPhys.55.583. URL <https://link.aps.org/doi/10.1103/RevModPhys.55.583>.
- [55] Dmitrii G Yakovlev, Pawel Haensel, Gordon Baym, and Christopher Pethick. Lev Landau and the concept of neutron stars. *Physics-Uspekhi*, 56(3):289–295, Mar 2013. ISSN 1468-4780. doi: 10.3367/ufne.0183.201303f.0307. URL <http://dx.doi.org/10.3367/UFNe.0183.201303f.0307>.
- [56] A. Zangwill. *Modern Electrodynamics*. Modern Electrodynamics. Cambridge University Press, 2013. ISBN 9780521896979. URL <https://books.google.com/books?id=tEYSUegp9WYC>.
- [57] Anthony Zee. Quantum field theory in a nutshell: 2nd ed., 2010.